7-3-2012

Characterizing and modeling the hydrologic properties of coal combustion by-products in landfills

Ryan Webb

Ryan William Webb

Department of Civil Engineering

This thesis is approved, and it is acceptable in quality and form for publication:

Approved by the Thesis Committee:

Dr. John Stormont, Chairperson

Dr. Mark Stone

Dr. Bruce Thomson

CHARACTERIZING AND MODELING THE HYDROLOGIC PROPERTIES OF COAL COMBUSTION BYPRODUCTS (CCBs) IN LANDFILLS

BY

Ryan William Webb

Bachelor of Science in Construction Engineering

THESIS

Submitted in Partial Fulfillment of the Requirements for the Degree of

Master of Science

Civil Engineering

The University of New Mexico

Albuquerque, New Mexico

May, 2012

ACKNOWLEDGMENTS

I would like to acknowledge Dr. John Stormont, my advisor and committee chair, for the continued guidance and teachings throughout the writing of these chapters.

I would also like to thank my other committee members, Dr. Mark Stone, and Dr. Bruce Thomson, for their valuable recommendations and helpful guidance to this study as well as my academic career. Daniel B Stephens and Associates deserves acknowledgement and gratitude for assistance and guidance in laboratory testing methods of materials. Gratitude is extended to the New Mexico Mining and Minerals Division and bhpbilliton for the funding and support to pursue this research.

Also of importance is to mention is the work of undergraduate research assistance from Meghan Wilson that I received on this project.

Characterizing and Modeling the Hydrologic Properties of Coal Combustion By-Products in Landfills

by

Ryan William Webb

B.S., Construction Engineering, University of New Mexico, 2010

ABSTRACT

Coal combustion byproducts (CCBs) disposed of in unlined landfills can impact the quality of adjacent water resources. In previous studies, CCBs have been found to leach toxic heavy metals such as arsenic, mercury, and lead into groundwater. CCBs include fly ash, bottom ash, and flue gas desulfurization product (FGD gypsum). This investigation focused on determination of the saturated and unsaturated hydraulic properties of fly ash and bottom ash to then be used in order to develop a 1-dimensional unsaturated flow model.

Ash samples from a power plant as well as core samples from buried CCB pits were collected for laboratory analysis. Saturated hydraulic conductivity was measured using falling head tests. Moisture characteristic curves were developed from hanging column tests, pressure plate tests, dew point potentiometer measurements and relative humidity measurements. Hydraulic properties were measured at various densities to simulate a range of conditions expected in the deep disposal pits.

The measured hydraulic properties were utilized in a saturated/unsaturated hydrologic water movement model of flow through disposal pits containing natural overburden and buried CCBs. The model used historical climatic conditions at the ground surface, and estimated water infiltration through the CCB pits. Results display infiltration from surface water into CCB pits is most likely to occur in areas where ponding occurs. These results can be coupled with information about the chemical quality of CCB leachates to estimate the impact of landfill disposal of CCBs on the underlying ground water quality.

TABLE OF CONTENTS

CHARACTERIZING AND MODELING THE HYDROLOGIC PROPERTIES OF COAL COMBUSTION BYPRODUCTS (CCBs) IN LANDFILLS

Objective: To determine, through laboratory testing, the saturated and unsaturated hydraulic properties of fly ash and bottom ash as a function of dry density and, utilizing numerical modeling, determine potential infiltration of surface water into CCB pits in an arid environment.

1. INTRODUCTION

Background

Millions of tons of coal combustion bi-products (CCBs) are produced every year by coal burning power plants. The American Coal Ash Association (ACAA) reported over 118 million metric tons were produced in the year 2010, making CCBs one of the most predominant forms of waste related to energy production (Yeboah and Burns, 2011). Three major types of CCBs are fly ash, bottom ash, and flue-gas desulfurization gypsum (FGD gypsum). In 2010 fly ash made up 63% of these major CCBs by weight, bottom ash 17%, and FGD gypsum 20% (ACAA, 2010).

Fly ash is the CCB made up of finer particles which rise with the flue gas stream and is collected by air quality control devices prior to entering the atmosphere. Fly ash generally ranges in particle size from 0.01 to 100 µm (Adriano et al., 1980). Bottom ash is the material that remains in the furnace after the coal combustion process is complete. Bottom ash generally consists of angular, porous particles that range in particle size from 0.1 to 10 mm (Seals et al., 1972). FGD gypsum, generally ranging in sizes less than 45 µm (Miller, 2007), is produced from the removal of sulfur oxide from the flue gas and is often extracted by scrubbers (Adriano et al., 1980; Kumar and Stewart, 2003).

One of the most common methods for CCB disposal in the western US is landfilling. The other common disposal methods include stockpiling and settling ponds. During the landfill process, materials are generally placed back into the pits and ramps used to mine the parent coal. Ash materials can contain every naturally existing chemical element. Trace elements have been shown to increase in concentration with decreasing particle sizes of ash materials (Adriano et al., 1980; El-Mogazi et al. 1988).

The major concern of landfills containing CCBs is the potential leaching of trace elements to adjacent water resources. Leachability of potentially toxic elements from CCB deposits depends on a number of different factors such as solubility of the element, interstitial flow rate, and the pH of water (Adriano et al., 1980; El-Mogazi et al., 1988; Joshi et al., 1994; Palmer et al., 2000; Mudd, 2000). Each of these factors can be associated specifically to source coal, CCB collection methods, and setting of disposal site. The hydraulic properties of the

CCBs will control the rate at which water moves through the buried material and potentially leaches elements from the pit.

Because of potential environmental impacts from trace elements, federal and state regulations are in place for the disposal of CCBs. Most landfill pits are lined with engineered material considered to be impermeable by standard practices (Huang et al, 1998; Ferraiolo et al., 1990). There are, however, some landfill sites that remain unlined.

As CCBs are disposed of in a landfill, effective stress can increase considerably as the depth of a pit increases. As stress increases, particles will rearrange themselves into a higher density configuration with a corresponding decrease in porosity and void ratio. The manner in which a material's density changes in response to changes in stress is known as the material's compressibility. Changes in porosity can have a significant impact on both saturated and unsaturated hydraulic properties of a material (Lu and Likos, 2004) as flow though a porous material depends largely upon the size and distribution of pores within the material at any given time. Studies have found that for clay soils and silty soils, both saturated hydraulic conductivity and unsaturated hydraulic properties are impacted by compaction and variations in void ratio (Zeng et al., 2011; Richard et al., 2001).

Compressibility of CCBs

Previous research concerning the compressibility of CCBs is focused largely upon using ash materials to produce hydraulic barriers for use as landfill covers and liners. The concept stems from the fact that the majority of CCBs are fine grained particles that can be used to produce low permeable materials. Such studies use standard and modified proctor tests to determine theoretical maximum dry densities at optimum water contents and often use various admixtures along with the CCBs (Campbell et al., 1983; Martin et al., 1990; Prashanth et al., 1998; Prashanth et al., 2001; Kumar and Stewart, 2003).

Results from these studies showed proctor maximum dry densities for fly ash ranging, for the most part, from 980 to 1280 kg/m^3 with a small percentage of the results reaching as high as 1880 kg/m^3 (Campbell et al., 1983; Martin et al., 1990; Prashanth et al., 1998; Prashanth et al., 2001). Bottom ash results show a range of proctor maximum densities from 1050 to 1670 kg/m^3 (Martin et al., 1990; Kumar and Stewart, 2003). Optimum gravimetric water contents for these proctor densities were reported from a range of 25 to 33% with one bottom ash having an optimum moisture content of 15% (Kumar and Stewart, 2003).

Admixtures such as bentonite and lime are commonly used in combination with fly ash and bottom ash for compressibility. Bentonite has characteristically low hydraulic conductivity, which is beneficial for hydraulic barriers, but it tends to crack as it dries. Fly ash and bentonite mixtures are an attempt to reduce the cracking behavior of bentonite liners. Lime is often mixed

with fly ash in order to create liner in which particles chemically react and cement together over time. Combinations of fly ash and bottom ash with bentonite or lime have been shown to create low permeable materials on the order of 10^{-7} cm/s or less. (Campbell et al., 1983; Martin et al., 1990; Prashanth et al., 1998; Prashanth et al., 2001; Kumar and Stewart, 2003).

Edil and Berthouex (cited by Palmer et al., 2000) found that, for fly ash without any admixtures, increasing the water content and compactive effort increased the dry unit weight. Sivapullaiah and Lakshmikantha investigated the relative deformation vs. pressure for fly ash response, showing similar results. Seals (1972) found bottom ash to have compressibility characteristics similar to that of sand. Because CCBs are subjected to a range of stresses corresponding to their depth of burial, it is important to determine the compressibility of CCBs.

Saturated Hydraulic Conductivity of CCBs

There has been some measurements of the saturated hydraulic conductivity of CCBs principally to support investigations of the use of fly ash and bottom ash in the construction of landfill covers and liners. These studies often use a single dry unit weight for testing, usually the theoretical maximum, and often incorporate various admixtures such as lime or bentonite (Campbell et al., 1983; Joshi et al., 1994; Prashanth et al., 2001; Kumar and Stewart, 2003; Mudd et al., 2000). Of these tests in which pure fly ash samples were tested, hydraulic

conductivities ranging from 10^{-6} to as high as 10^{-3} cm/s were measured (Campbell et al., 1983; Joshi et al., 1994; Prashanth et al., 2001).

Sivapullaiah and Lakshmikantha showed a change in hydraulic conductivity with a change in void ratio for fly ash. In this study, the range in void ratios was from 1.12 -1.15, this is near the proctor maximum density, and hydraulic conductivities were on the order of 10^{-7} cm/s. Edil and Berthouex (cited by Palmer et al., 2000) found that increasing the water content and compactive effort not only increases the dry unit weight, it also decreases the saturated hydraulic conductivity. These studies cover only a narrow range of dry unit weights near the theoretical maximum for fly ash. For bottom ash, Seals (1972) found the hydraulic conductivity to be similar to sand (10^{-2} cm/s) when the void ratio was approximately that of 50% of maximum relative density, no other densities or void ratios were tested. FGD gypsum has been shown, in one study, to have a low hydraulic conductivity (exact numbers not reported) when compacted (Rudisell et al., 2001).

For clay materials, saturated hydraulic conductivity steadily decreases as void ratio decreases (e.g., Zeng et al., 2011). Because CCBs in landfill sites are experiencing various overburden conditions creating a range of dry densities, it is important to determine variations to the hydraulic conductivity changes associated with decreases in dry density.

Unsaturated Hydraulic Properties of CCBs

There has been limited research has investigated the unsaturated hydraulic properties of CCBs. Truman et al. (2010) found that amending soils with amounts of FGD gypsum can increase water retention. Pathan et al. (2003) conducted research investigating the use of fly ashes to amend soils to increase plant available water, assuming the fine particle sizes of fly ash will assist in the retention of water. The water retention characteristics, however, were of samples at a single density not necessarily representative of any particular field conditions, aiming only to be indicative of relative differences between ash samples. Results showed that all fly ashes used retain more water than the sandy soils investigated. Mudd et al. (2007) studied numerous ash and soil samples for various geotechnical properties, including water retention characteristics. The 23 ash samples collected ranged from fly ash to bottom ash. Air entry pressures ranged from approximately -1 kPa (10 cm of water) for bottom ash to -100 kPa (1000 cm of water) for fly ash. Each sample was tested only at its proctor maximum dry density. In another study conducted by Chakrabarti et al. (2005), unsaturated properties of ash were incorporated into a water balance model to predict leaching behaviors. This study concluded that a thorough understanding of the unsaturated moisture characteristics of coal ash is essential to accurately predict moisture behavior in disposal sites.

Although there is no direct data regarding the change in unsaturated properties of CCBs due to compaction, testing on soils reveals that changes in porosity due to compaction have an impact on their unsaturated hydraulic

properties (Richard et al., 2001; Assouline et al., 1997; Hill & Sumner, 1967). Therefore, it is expected that as dry density of CCBs increase, the unsaturated hydraulic properties have the potential to vary. These variations may be vital in understanding the possible behavior of water in landfill sites.

CCBs can vary significantly depending upon the source coal and collection method. Disposal methods in landfill sites create a profile of varying overburden pressures and a potential range of hydraulic properties. Proper knowledge of the manner in which these properties vary with depth within a CCB landfill pit are essential in analyzing the potential impact on local water resources.

2. MATERIALS

Source of Samples

The majority of fly and bottom ash samples for this study were received from the San Juan Power Generating Station in northwestern New Mexico. These samples were taken directly from the collection units prior to transport to the landfill site, and are subsequently referred to as fresh samples. The samples were received by mail in June of 2011 and were contained in plastic bags specific to each of the 4 burning units. Approximately 10 kg were received for each unit. All samples used for this study were taken from unit 4.

The San Juan Mine (SJM), located on the same property as the power generating station, is the location in which the coal is mined and CCBs are placed back into the mined pits. The SJM is located approximately 15 miles west of Farmington, NM (figure 1) in the San Juan Basin bound by a geologic feature known as the Hogback Monocline on the west, northwest, and north. Coal in the San Juan Basin is of the late-Cretaceous age and characterized as ranging from sub-bituminous A to high volatile bituminous C. The Fruitland Formation, mined at SJM is primarily sub-bituminous coal consisting of <1% sulfur. Production rates at the SJM reach approximately 7 million tons of coal mined each year and 2.7 million tons of CCBs backfilled into the mine pits and ramps. The CCBs produced consist of approximately 70% fly ash, 15% bottom ash, and 15% FGD gypsum. Silica, alumina, oxides of calcium, magnesium, and iron are the principle components of the CCBs disposed of at SJM with secondary elements consisting of carbon and other trace elements (Luther et al., 2009).

In addition to the fresh samples, geo-probe samples were also collected in the Summer of 2010 in order to obtain the physical and hydraulic properties of in situ soils at the SJM (Chan, 2010). Also, in the Spring of 2011, observation wells were being installed at the SJM using a sonic drilling rig and samples were collected at a range of depths for analysis (Parker, 2011).

Figure 1: Location of San Juan Mine and Power Generating Station

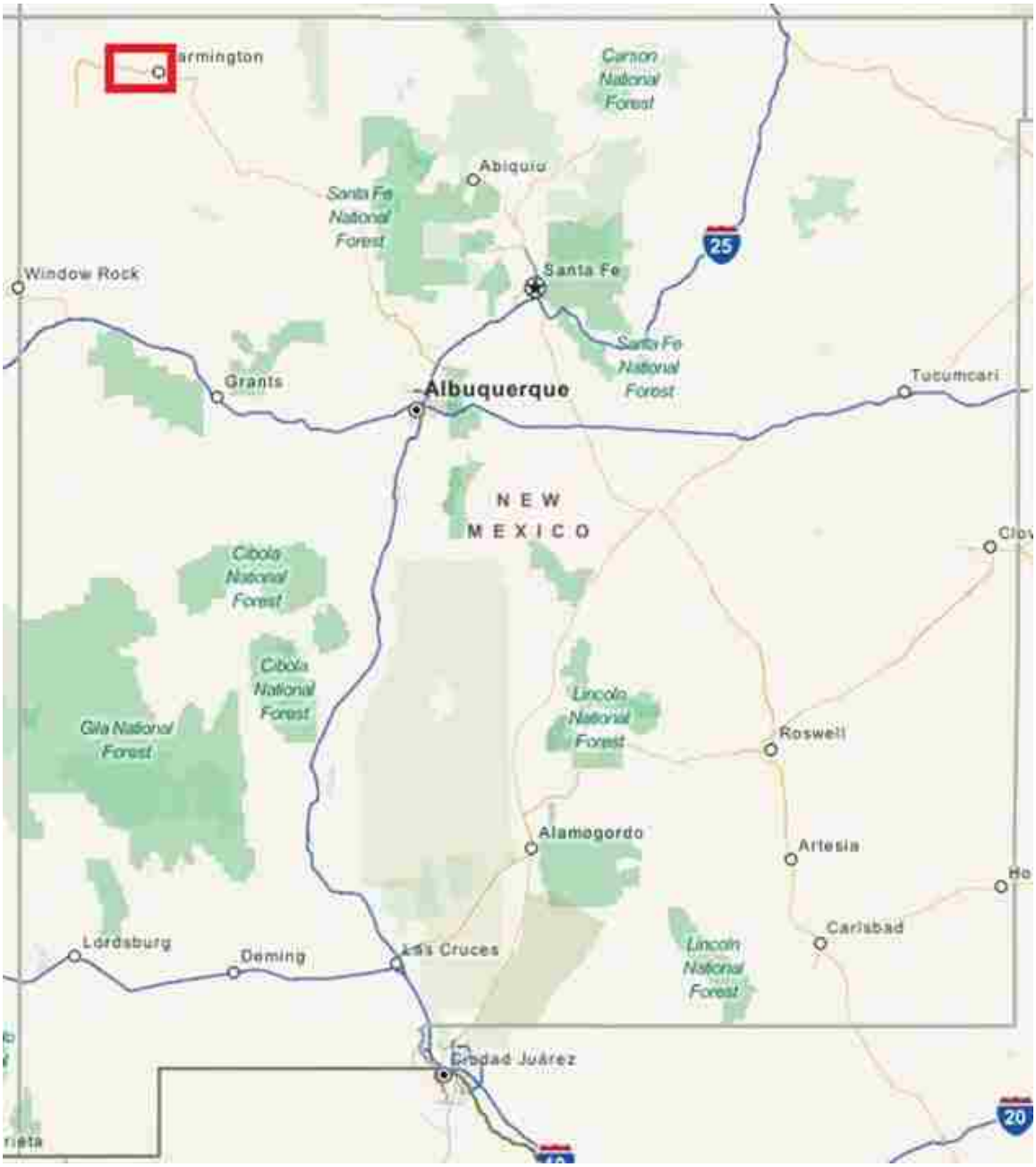

3. LABORATORY TESTING METHODS

Physical Properties

Grain size distributions were determined for a sample mass of approximately 100 g of oven-dry fly ash and approximately a 230 g sample of oven-dry bottom ash following the methods of ASTM D422 (2007). The sample materials were washed through a #200 sieve, and a hydrometer test was conducted for the material passing through and a sieve analysis conducted for the retained material.

Specific gravity testing was conducted following the methods described by ASTM D854 (2009). Three tests were conducted on fly ash and three tests on bottom ash.

Relative density tests, as described by the Department of the Army Office of the Chief of Engineers (1970), were also conducted on one oven-dry sample of fly ash and one oven-dry sample of bottom ash using a 15 cm diameter proctor mold.

In-situ samples were collected by means of a geo-probe to determine field conditions present at the SJM in a separate study (Chan, 2010). Moisture contents were determined by methods described in ASTM D-2216 (2010) and densities by ASTM D-7263 (2009), method B. The known volume from the

density tests and mass of water from moisture content were then used to produce volumetric water contents.

Clod density tests were performed with methods similar to ASTM D-7263 (2009) method B. Copper rings measuring approximately 16 mm in diameter and 29 mm in length were sharpened on one end and inserted into the clods to collect samples of a known volume. Excess material was removed with a razorblade from either end of the rings to ensure the soil was level with the edges of the ring. Only two clods were large enough to be tested. Two samples were collected from one clod and one sample from the other.

Compressibility

Compressibility curves were developed for 4 samples of fly ash and 4 samples of bottom ash. Tests provided one-dimensional pressure loading on samples at gravimetric moisture contents consistent with field conditions at the SJM. The moisture content present at the SJM was determined to be 20% (Chan, 2010). Samples were contained in brass rings on top of a porous stone. The ring diameter was 60 mm with a height of 25 mm; samples filled the ring to a height of 22 mm. Each sample's initial dry density was the minimum dry density determined by relative density tests. Samples were compacted in a series of 4 lifts on top of the porous stone. Marks were made on the inside of the sample rings as well as on the tamper to ensure the sample was compacted to the proper height.

A series of 10 loadings, using a consolidometer, ranging from 50 to 1000 kPa were applied to prepared samples. The applied loads were approximately (in kPa): 50, 100, 165, 230, 330, 410, 555, 655, 885, and 985. Loads were selected on a basis of weights available in a manner to gradually increase pressure differences between loading increments. Dial gages with 0.025 mm precision were zeroed before the first applied load and used to measure changes in sample height for each loading cycle. Loads were applied for a period of one hour, after which a measurement was taken recording the change in height for each sample. It was observed that, for these particular materials, most of the volume change occurred in the first 15-30 minutes; there were no measurable sample height changes that occurred following 1 hour of load being applied.

Saturated Hydraulic Conductivity

Fly and bottom ash samples were tested for the coefficient of saturated hydraulic conductivity (K_{sat}) in accordance to ASTM D5856 (2007), method B (constant tail water). Porous stones were used on the bottom and top of each sample within a rigid-walled permeameter. Each compacted sample measured 76 mm in diameter and 25 mm in height. University of New Mexico tap water was used as the permeant liquid. Saturation of samples was done by allowing constant flow of water through the compacted sample for at least 16 hours. Hydraulic gradients across each sample ranged from 4 to 25.

Fly ash and bottom ash samples were tested at three different dry densities. Two compacted samples at each dry density were tested.

Moisture Characteristic Curve (MCC) Measurements

Moisture characteristic curves during desorption were developed for three dry densities for both fly and bottom ash samples. Testing methods used to collect data for the MCCs are similar to those described in ASTM D6836 (2008) for hanging column and pressure plate tests, Klute (1986) for relative humidity box measurements, and Decagon Devices (2010) for chilled mirror hygrometer readings.

For the hanging column and pressure plate tests, three samples at each of the three specified dry densities were prepared and tested for both fly and bottom ash, producing a total of 18 samples tested (9 fly ash and 9 bottom ash). Each sample was compacted to a target dry density so as to completely fill a brass ring of 60 mm diameter and 25 mm height. Synthetic nylon screening with openings measuring 25 microns were attached to the top and bottom of each sample ring by a hose clamp to contain the sample while allowing free movement of water. Each sample was saturated in de-aired de-ionized water with an applied negative pressure of 80 kPa for at least 24 hours.

Saturated samples were placed directly into saturated Buchner funnels connected to reservoirs/burettes by flexible tubing. The Buchner funnels were saturated in de-aired de-ionized water with an applied negative pressure of 80

kPa for at least 24 hours. A thin layer of a diatomaceous earth was spread on each porous plate to improve the hydraulic contact with the sample. Negative pressures were then introduced to each of the samples by raising the Buchner funnel and/or lowering the reservoir/burette. Samples were allowed to equilibrate at 6 different negative pressure heads ranging from 5 cm to 160 cm of water, at which point the mass of each sample was taken to the nearest 0.01 g and subsequently used to determine volumetric water content. Equilibration at each pressure, determined by water ceasing to move from the sample to the burette for at least 24 hours, took 6 to 7 days for most samples.

After the final measurement in the hanging column, the samples were moved to the pressure plate apparatus. The porous plate was saturated in de-aired de-ionized water for a period of at least 24 hours with an applied negative pressure of 80 kPa. A thin layer of a diatomaceous earth was spread on the plate to improve the hydraulic contact with the sample. The pressure plate test was used to produce negative pressure heads of 510 and 1275 cm of water. Pressures were introduced by sealing the samples on a porous plate in a pressure chamber and applying gas pressure to the chamber using compressed nitrogen gas. The porous plate has an outflow tube to a reservoir at atmospheric pressure at the bottom of each sample. Readings were taken from the pressure plate test by allowing the samples to equilibrate for 14 days at each pressure at which point the samples would be removed and masses measured to the nearest 0.01 g in order to determine the volumetric water content.

A chilled mirror hygrometer was used to collect data for the MCC at negative pressure heads ranging from 7,600 cm to 15,000 cm of water. A WP4 dew point potentiometer from Decagon Devices, Inc. was used as the testing apparatus. It was determined that, for values of negative pressure head less than 7,600 cm of water for bottom ash and 9,900 cm of water for fly ash, the WP4 readings were outside the range of accuracy (Decagon Devices, Inc., 2010). 5 readings were taken for fly ash and 3 for bottom ash. Large amounts of ash (~200 g) were brought to target moisture contents and at least 25 g of moist sample was placed in a stainless steel WP4 sample cup. Plastic lids were used to seal the cups and allow samples to equilibrate for at least 16 hours. Following equilibration, water potential was read immediately upon removing the lid from the sample cup. The samples were then weighed immediately following the potential reading and removal from the WP4 apparatus. A drying oven was used for at least 16 hours to dry the samples. Once dry, samples were allowed to cool in a desiccator for 10 to 15 minutes and masses were measured to calculate the moisture content of each sample. Gravimetric water contents and water potentials were converted to volumetric water contents and negative pressure heads, respectively, for each specified density.

A relative humidity box was used to measure 2 final readings for the MCC. Saturated solutions of NaCl and LiCl were used to achieve negative pressure head equivalents of over 4×10^5 cm and 3×10^6 cm of water respectively (Lu and Likos, 2004). The saturated solutions were placed in the bottom of a desiccator. Fly and bottom ash samples (~10 g) were then placed directly above the salt

solution atop a plastic grate and allowed 7 days for equilibration, after which masses were measured and converted to volumetric water contents.

4. LABORATORY RESULTS

Physical Properties

Grain size distributions tests determined fly ash to be 85.4% finer than a #200 sieve (0.075 mm diameter) and bottom ash was 22.3% finer (table 1). Grain size distribution curves are shown in figure 2.

Results for the average specific gravity testing are shown in table 1, fly ash was found to have an average specific gravity of 2.00 and bottom ash had 2.06 by these methods.

Relative density testing showed oven-dry fly ash to have a loose dry density of 1007.4 kg/m^3 and a maximum dry density of 1184.4 kg/m^3. Oven-dry bottom ash had a loose dry density of 692.2 kg/m^3 and a maximum dry density of 813.8 kg/m^3. Results of the relative density test are summarized in table 1.

Table 1: Material Physical Properties

Property	Fly Ash	Bottom Ash
% finer #200 sieve (0.075 mm)	85.4	22.3
% larger #200 sieve (0.075 mm)	14.6	77.7
Minimum Relative Density (kg/m^3)	1007.4	692.2
Maximum Relative Density (kg/m^3)	1184.4	813.8
Average Specific Gravity	2.00	2.06

Figure 2: Grain Size Distribution for Fly Ash (above) and Bottom Ash (below)

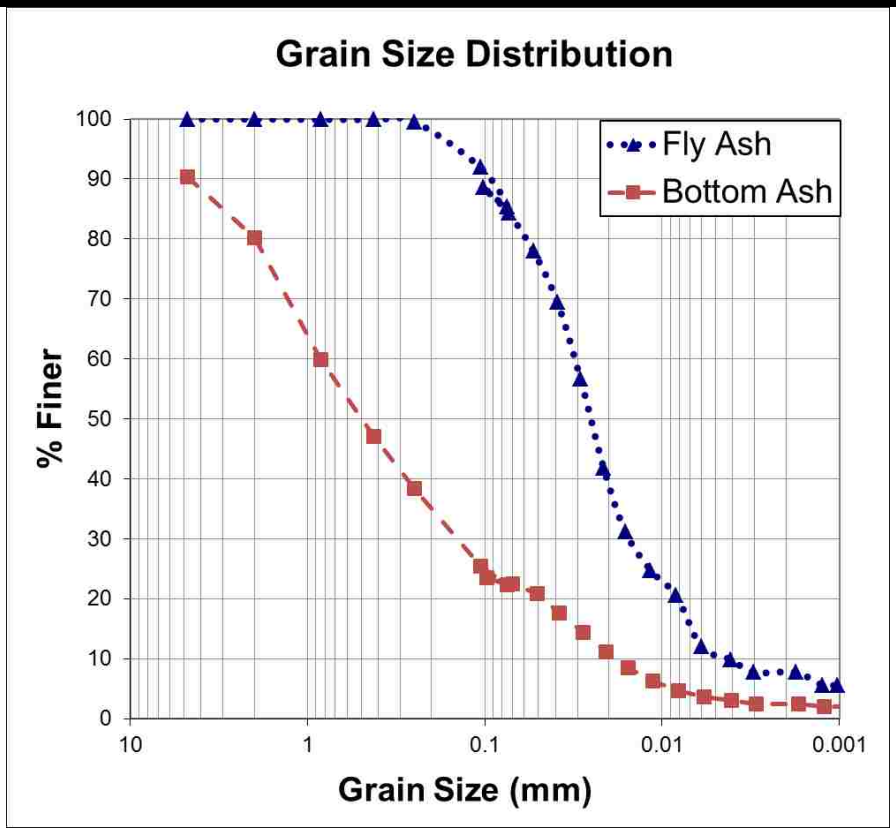

Results of the geo-probe investigation by Chan (2010) are given in table 2. These results, including samples from three different locations, show the average gravimetric moisture content of the soil to be 19%.

Clod density tests performed on clods collected at 38 m below the ground surface show an average dry density at this depth and location to be 1028.8 kg/m^3 (table 3). This material was determined to be bottom ash through a separate study (Parker, 2011).

Table 2: Water Contents from Geo-Probe Samples

Sample	Gravimetric Water Content	Volumetric Water Content	Depth of Sample (m)	Comments
1	24%	25%	4.2	Traces of ash (Yucca Ramp 1)
2	20%	18%	7.0	Traces of ash (Yucca Ramp 1)
3	22%	21%	6.7	Traces of ash (West Yucca Pit)
4	12%	18%	2.7	Layered core w/ clay (Juniper Pit)
5	19%	31%	4.9	Layered mostly clay (Juniper Pit)
6	19%	31%	9.4	Layered mostly clay (Juniper Pit)
Average	19%	24%		**Top-soils not included**

Table 3: Clod Density Results of Sample from Juniper Pit 04 at 42 m depth

	Volume (cm^3)	Dry Sample Mass (g)	Dry Density (kg/m^3)
Ring 1	561.9	5.69	1012.66
Ring 2	564.1	6.06	1074.21
Ring 3	566.3	5.66	999.43
		Average:	**1028.76**

Compressibility

Results of the compressibility tests and curve fitting parameters are summarized in table 4 and presented graphically in figure 3, it is important to note the differences in the vertical axis values between graphs. Fly ash and

bottom ash samples experienced maximum changes in height ranging from 2.2 to 3.4 mm and 5.1 to 6.1 mm, respectively. These values represent a 10.0 to 15.3% and 23.0 to 27.5% change in sample height for fly ash and bottom ash, respectively. All samples experienced the largest deformation occurring at a pressure of 985 kPa. The maximum dry densities occurring under this pressure ranged from 1119.5 to 1189.0 kg/m^3 for fly ash and 898.2 to 954.8 kg/m^3 for bottom ash.

Data was fit to the following empirical equation:

$$\rho = r \cdot (1 - n^{-s\sigma_v}) + \rho_I \quad (1)$$

Where:

r = total range of densities for curve (kg/m^3)

n = steepness of the curve (dimensionless)

s = sharpness of curvature (kPa^{-1})

σ_v = overburden pressure (kPa)

ρ_I = Initial dry density of the material (kg/m^3)

The R^2 values for curves fit to the data using equation (1) range from 0.97 to 0.99. Selection of the equation was based upon the asymptotic approach towards a theoretical maximum dry density (r-ρ_I) and a predetermined vertical axis intercept for the loose dry density (ρ_I). Variations in the n and s parameters

fit the curve to the data. A summary of the parameters used to fit equation (1) is given in table 4.

Three selected dry densities to further test hydraulic properties are represented by the horizontal dashed lines in figure 3. For fly ash, the selected values of dry density (in kg/m^3) are 1028.4, 1113.3, and 1169.3. For bottom ash, the selected dry densities (in kg/m^3) are 727.2, 800.9, and 913.1. The lowest density was chosen specifically to be near the initial uncompacted density but slightly greater than since it is unexpected for any material to be found without experiencing some compaction. The highest density was selected to be near the higher end of the density curves. The third density to be tested was arbitrarily chosen in between the selected maximum and minimum dry densities to be tested.

Table 4: Summary of Compressibility Results and Parameters to Eq. 1

Sample	Initial ρ_d (kg/m^3)	Total ΔH (mm)	Final ρ (kg/m^3)	r (kg/m^3)	n	s (kPa^{-1}x10^{-4})	R^2
Fly Ash A	1006.9	3.4	1189.0	193	3200	3.1	0.980
Fly Ash B	1006.9	2.2	1119.5	123	1580	2.9	0.974
Fly Ash C	1006.9	3.1	1168.5	173	700	3.5	0.974
Fly Ash D	1006.9	2.5	1136.9	141	500	3.4.	0.979
Bottom Ash E	691.8	5.5	920.0	258	400	4.0	0.989
Bottom Ash F	691.8	5.1	898.2	236	1000	3.0	0.993
Bottom Ash G	691.8	6.1	954.8	283	800	4.0	0.981
Bottom Ash H	691.8	6.0	945.9	284	5000	2.8	0.981

Figure 3: Compressibility Data with Fitted Curves for Fly Ash (top) and Bottom Ash (bottom)

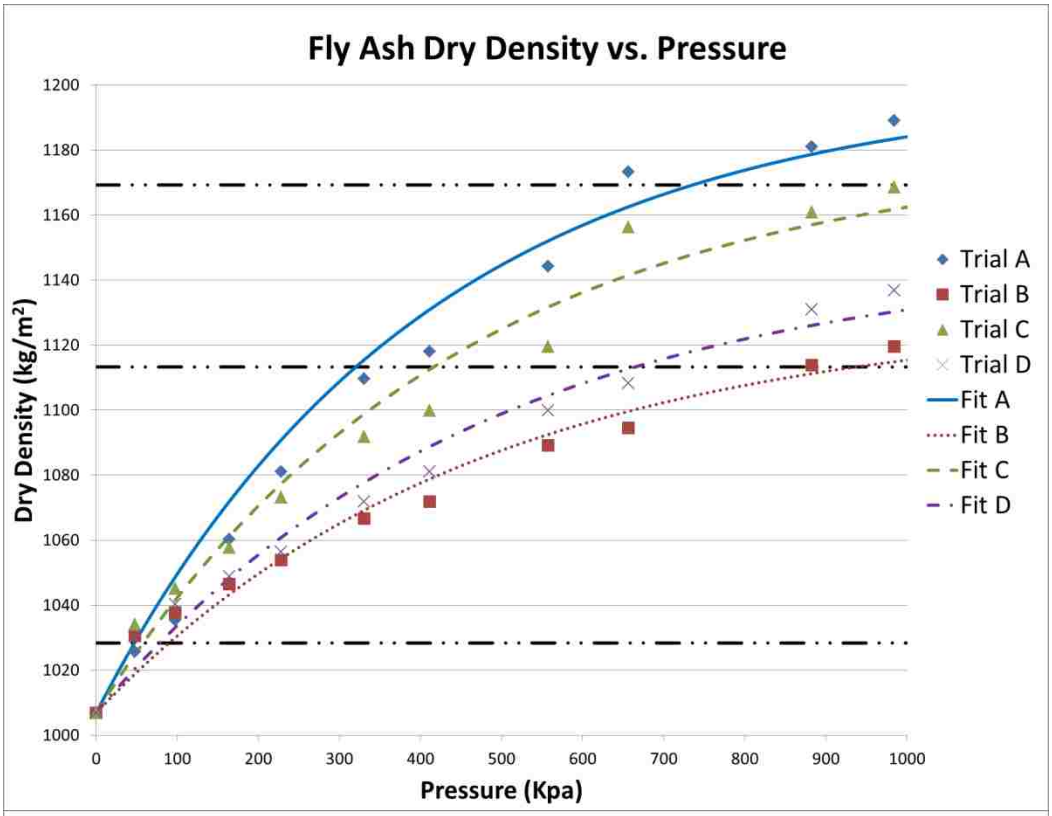

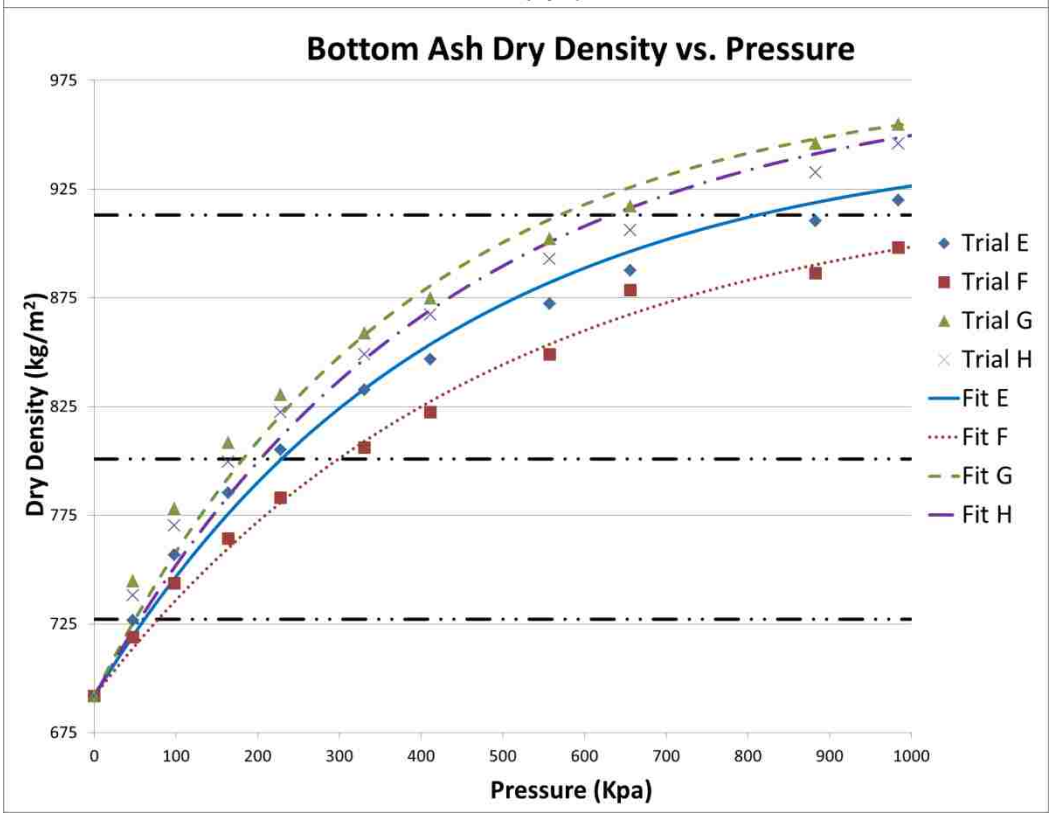

Saturated Hydraulic Conductivity

Results from the falling head permeability tests, constant tail water method, are presented in table 5. Fly ash samples yielded K_{sat} values ranging on the order of 10^{-4} to 10^{-5} cm/s while bottom ash samples yielded values on the order of 10^{-3} cm/s. The highest K_{sat} values measured were 1.3×10^{-4} cm/s and 6.5×10^{-3} cm/s for fly ash and bottom ash, respectively. These values were achieved at dry density values of 1024.0 kg/m^3 for fly ash and 724.4 kg/m^3 for bottom ash, which were the lowest dry density values that were tested for each material. The lowest K_{sat} values measured were 5.5×10^{-5} cm/s for fly ash and 1.5×10^{-3} cm/s for bottom ash. These values were measured at the highest densities tested for both fly ash (1163.0 kg/m^3) and bottom ash (910.4 kg/m^3). Graphical representation of K_{sat} vs. dry density is shown in figure 4. Trend lines were fit to the data displaying an R^2 value of 0.61 for fly ash and 0.27 for bottom ash.

Table 5: Saturated Hydraulic Conductivity Results

Material	Target Dry Density (kg/m^3)	Actual Dry Density (kg/m^3)	Sample 1 K_{SAT} (cm/s)	Sample 2 K_{SAT} (cm/s)
Fly Ash	1028.4	1024.0	7.81E-05	1.30E-04
Fly Ash	1113.3	1108.2	6.62E-05	8.10E-05
Fly Ash	1169.3	1163.0	5.45E-05	5.96E-05
Bottom Ash	727.2	724.4	3.53E-03	6.45E-03
Bottom Ash	800.9	796.9	2.27E-03	6.26E-03
Bottom Ash	913.1	910.4	1.48E-03	3.90E-03

Figure 4: Saturated Hydraulic Conductivity vs. Dry Density Results

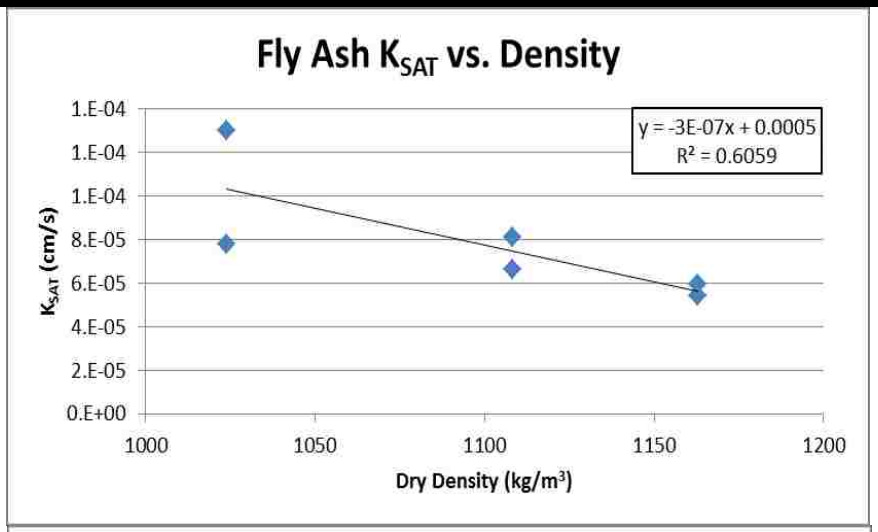

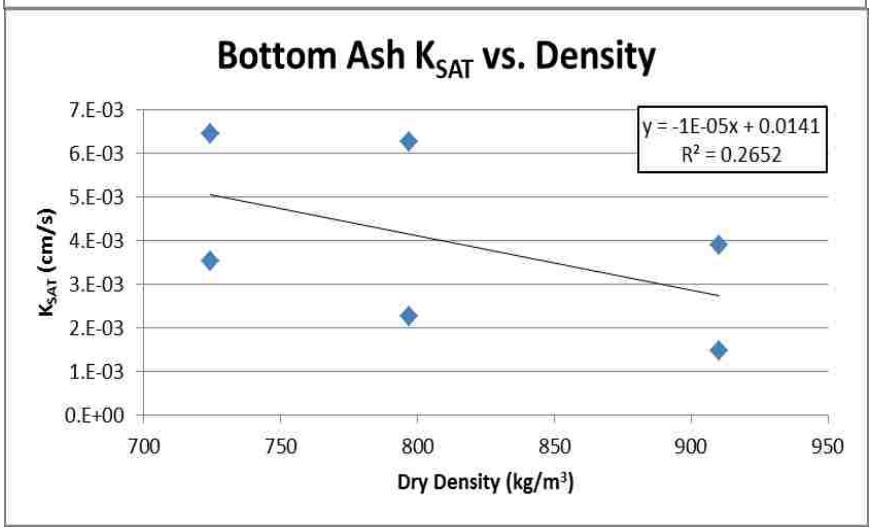

MCC

Measured data points were fit to the van Genuchten model for the MCC, which is given as (van Genuchten et al., 1991):

$$\theta = \theta_r + (\theta_s - \theta_r) \cdot (1 + (\alpha \cdot h)^n)^{-m} \quad (2)$$

Where:

θ = volumetric moisture content (dimensionless [L^3/L^3])

θ_r = retained volumetric moisture content (dimensionless [L^3/L^3])

θ_s = saturated volumetric moisture content (dimensionless [L^3/L^3])

α = curve fitting parameter representing the inverse of air-entry suction (1/L)

h = negative pressure head (L)

n = curve fitting parameter (dimensionless)

m = 1 – 1/n (dimensionless)

The Retention Curve (RETC) Program for Unsaturated Soils (van Genuchten et al., 1991) was used to fit the data to the van Genuchten model for MCCs. The model can be adjusted to observed data points by altering the weight of each measured value. Weighted values for this study were chosen in a manner such that all weighted values for a particular testing method are the same. Weighted values were altered, based upon accuracy of testing method for

each data point, within the RETC program until an acceptable curve was observed through the data points. Weighted values ranged between one and three in increments of 0.5.

Once MCCs had been produced for each individual sample of CCBs, MCCs were created using RETC to be representative of each target dry density of material. This was done by including all of the data from the 3 samples at each respective dry density to create a single MCC for that dry density. The input data for RETC used the same calibrated weights for each data point as determined by MCC curve creation for individual samples.

MCC COMPARISONS

Van Genuchten model parameters obtained using RETC are presented in table 6. Graphical representation of the MCCs for the materials at their respective target densities are shown in figures 5 - 10. MCCs were then plotted as l saturation instead of volumetric water content for comparison purposes. Saturation values (S) were calculated as follows:

$$S = {}^{\theta}/_{\theta_s} \qquad (3)$$

Best fit MCCs for each target dry density are displayed graphically in figure 11, and the parameters summarized in table 7. Each best fit curve uses the data from all three samples of the same target dry density. The three fly ash

best fit curves are displayed on the same graph to compare differences between dry densities; the same is done with bottom ash.

Van Genuchten model parameters are plotted vs. dry densities in figure 12. Linear trend lines have been fitted with the data for θ_s, α, and n values. Fly ash shows a strong linear trend, with R^2 values of .59 and .94 for θ_s and α, respectively, where bottom ash does not, with R^2 values of .17 and .38 for θ_s and α, respectively. Values of n show low R^2 values for both fly ash and bottom ash, the values are 0.1 and 0.27, respectively.

Table 6: Van Genuchten Model Parameters for Fly Ash (FA) and Bottom Ash (BA) Samples

Sample	Target Dry Density (kg/m^3)	Actual Dry Density (kg/m^3)	Θ_r (cm^3/cm^3)	Θ_s (cm^3/cm^3)	α (1/cm)	n
FA A	1028.4	1030.83	0.00	0.52	4.0E-03	1.59
FA B	1028.4	1033.12	0.00	0.57	3.9E-03	1.64
FA C	1028.4	1034.74	0.02	0.56	3.7E-03	1.97
FA D	1113.3	1,113.3	0.00	0.51	2.4E-03	1.66
FA E	1113.3	1,113.3	0.00	0.49	2.4E-03	1.67
FA F	1113.3	1,118.8	0.00	0.57	2.8E-03	1.60
FA G	1169.3	1172.19	0.00	0.47	1.3E-03	1.80
FA H	1169.3	1173.41	0.00	0.46	7.3E-04	1.99
FA I	1169.3	1,175.2	0.00	0.49	1.4E-03	1.77
BA A	727.2	729.21	0.00	0.51	2.6E-02	1.51
BA B	727.2	726.52	0.00	0.58	4.6E-02	1.45
BA C	727.2	724.22	0.00	0.60	5.6E-02	1.44
BA D	800.9	795.18	0.00	0.66	5.4E-02	1.47
BA E	800.9	797.06	0.00	0.68	3.4E-02	1.61
BA F	800.9	798.68	0.00	0.64	4.6E-02	1.50
BA G	913.1	912.26	0.00	0.69	3.4E-02	1.51
BA H	913.1	913.47	0.00	0.60	2.4E-02	1.54
BA I	913.1	916.85	0.00	0.60	1.8E-02	1.57

Table 7: Van Genuchten Model Parameters for Best Fit Curves at each Dry Density

Material	Target Dry Density (kg/m^3)	Θ_r (cm^3/cm^3)	Θ_s (cm^3/cm^3)	α (1/cm)	n
Fly Ash	1028.4	0.003	0.55	3.9E-03	1.68
Fly Ash	1113.3	0.00	0.52	2.4E-03	1.66
Fly Ash	1169.3	0.00	0.47	1.1E-03	1.85
Bottom Ash	727.2	0.00	0.56	4.1E-02	1.46
Bottom Ash	800.9	0.00	0.66	4.3E-02	1.52
Bottom Ash	913.1	0.00	0.63	2.5E-02	1.54

Figure 5: Graphs of Fitted Data (top) and Saturation MCCs (bottom)

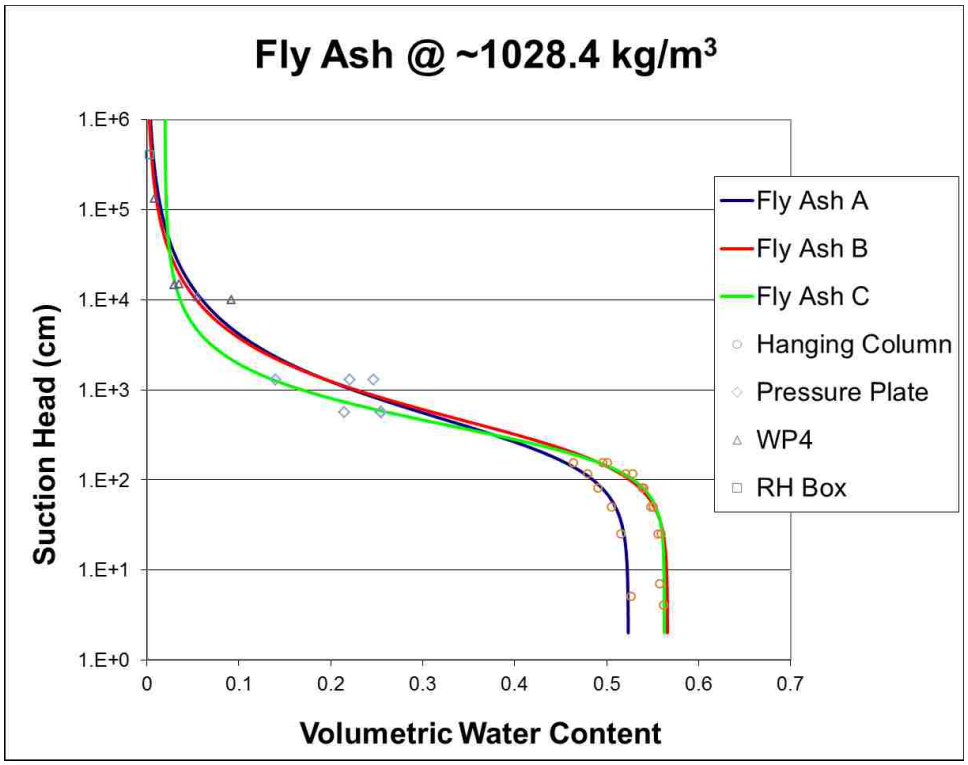

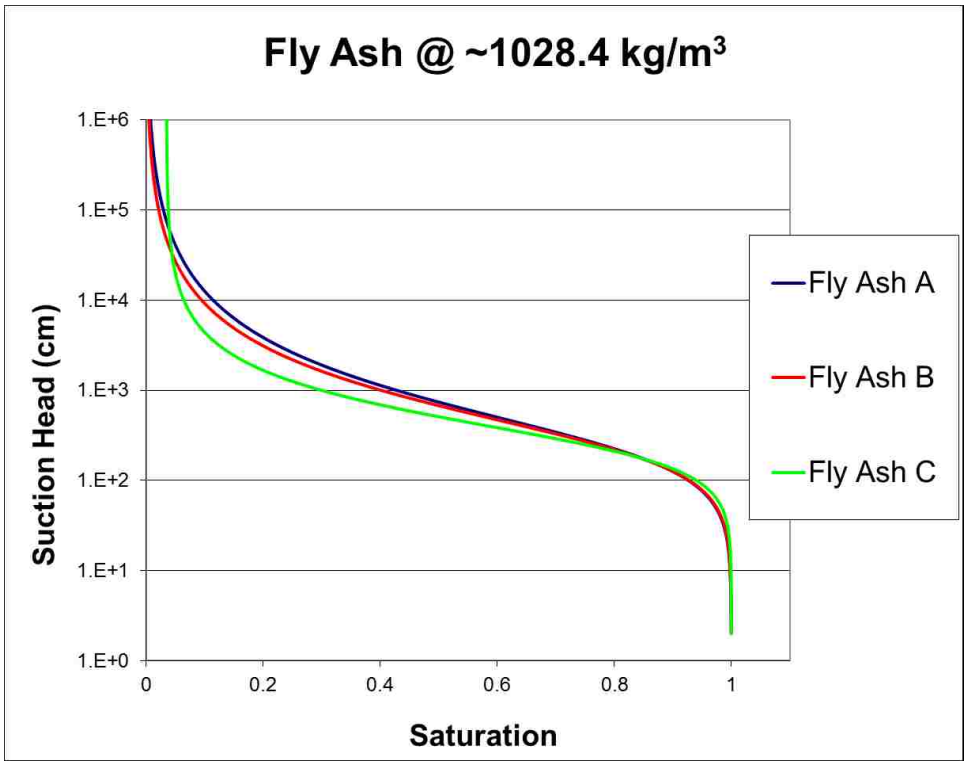

Figure 6: Graphs of Fitted Data (top) and Saturation MCCs (bottom)

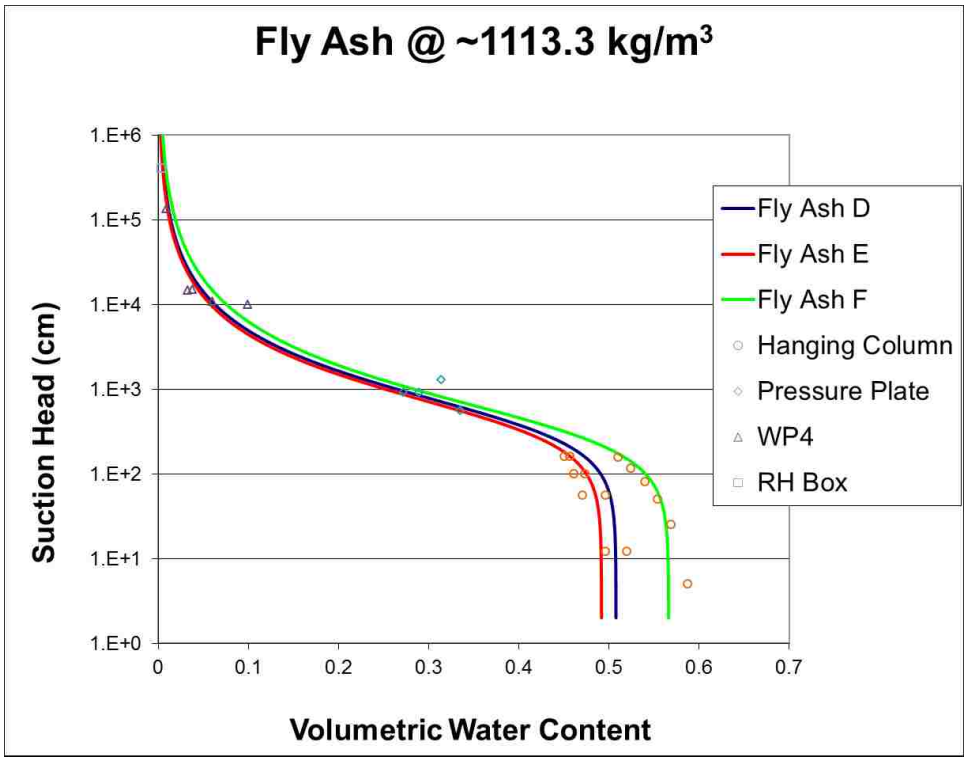

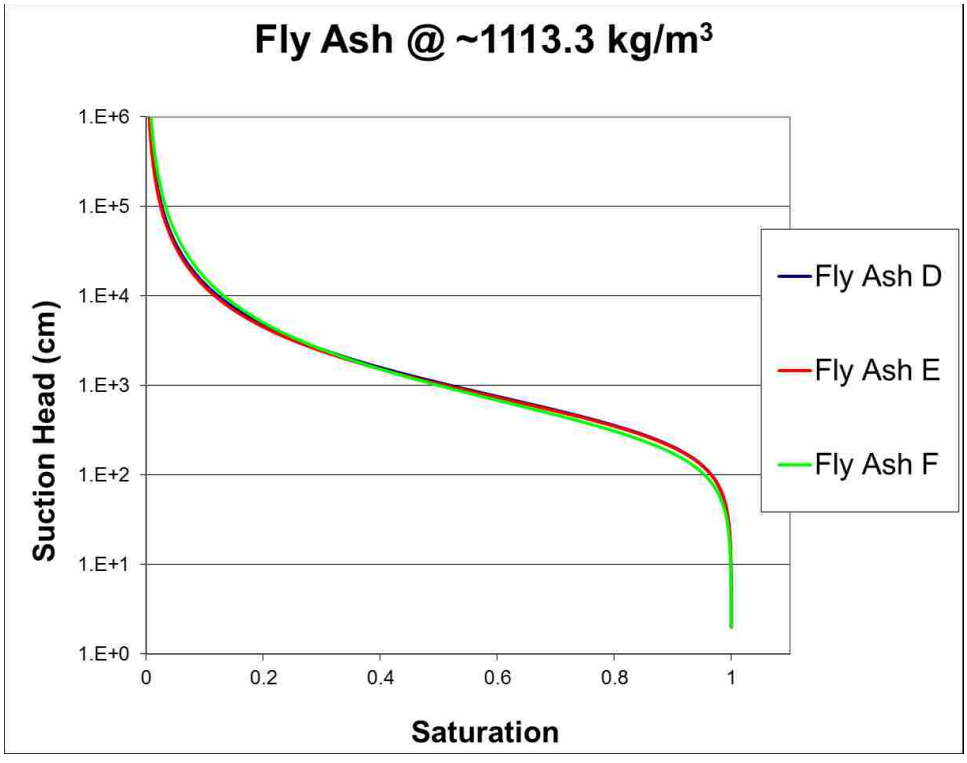

Figure 7: Graphs of Fitted Data (top) and Saturation MCCs (bottom)

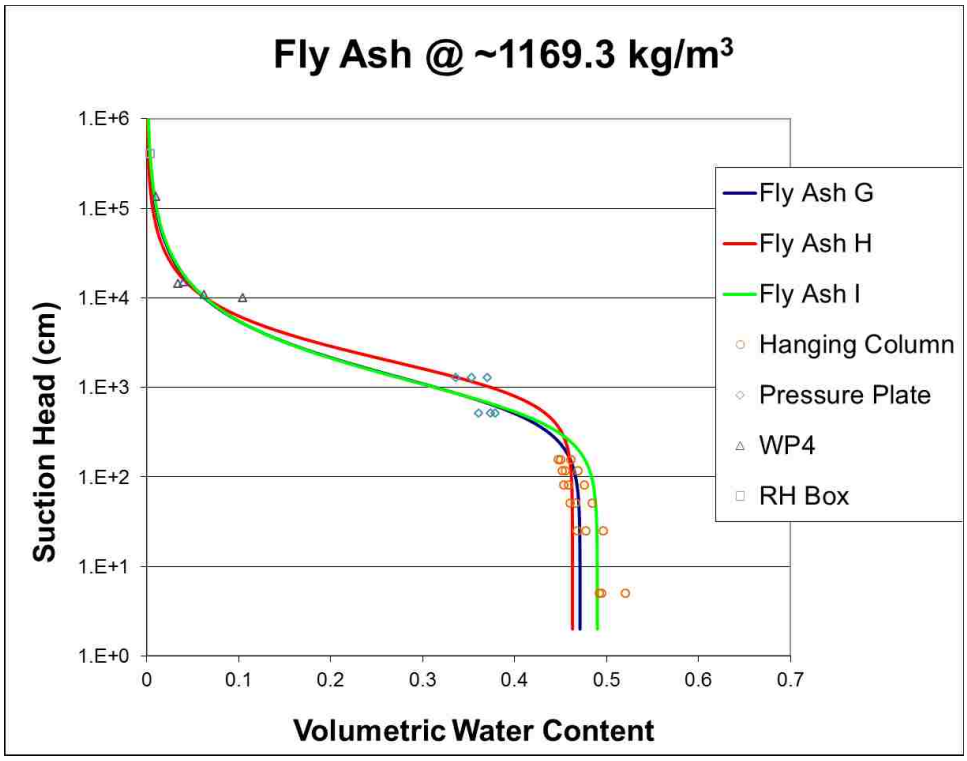

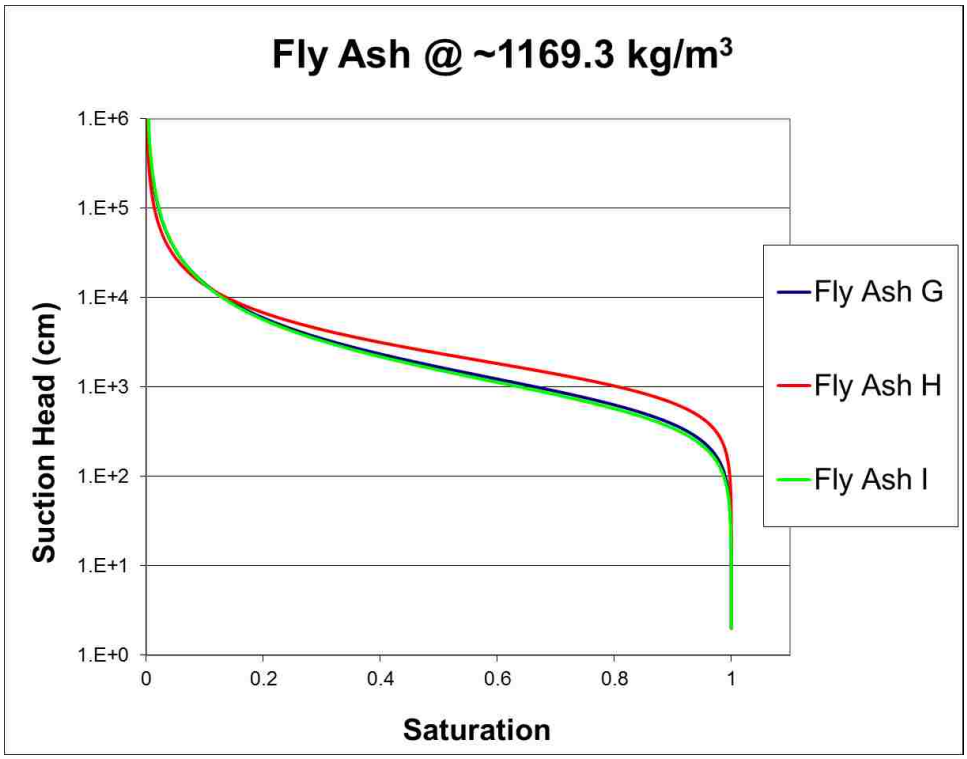

Figure 8: Graphs of Fitted Data (top) and Saturation MCCs (bottom)

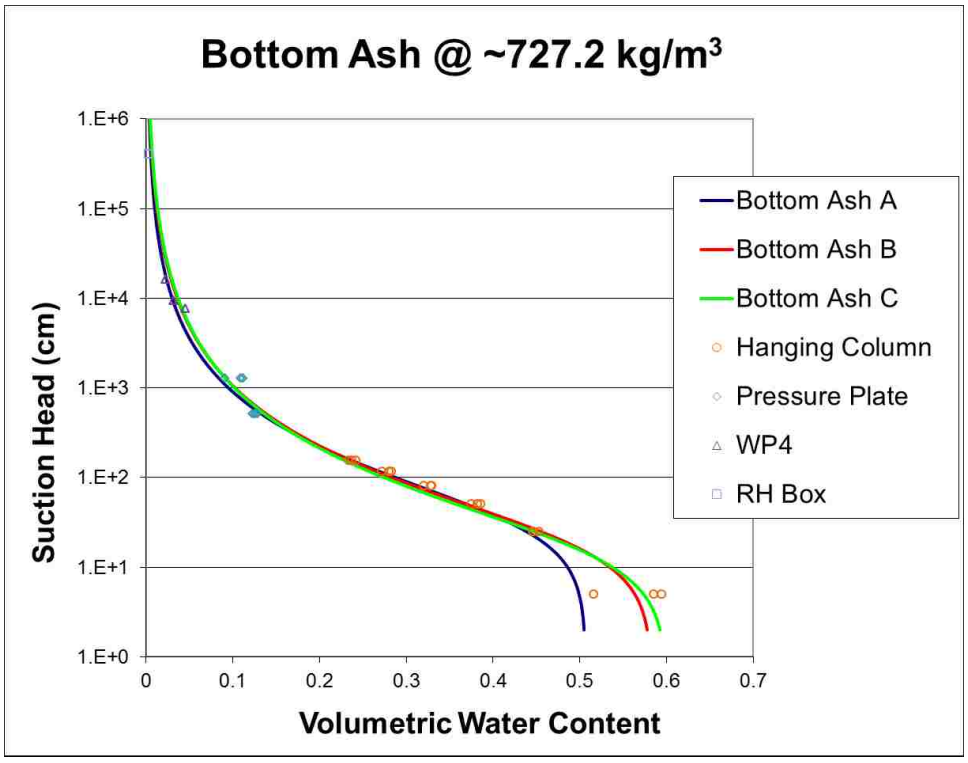

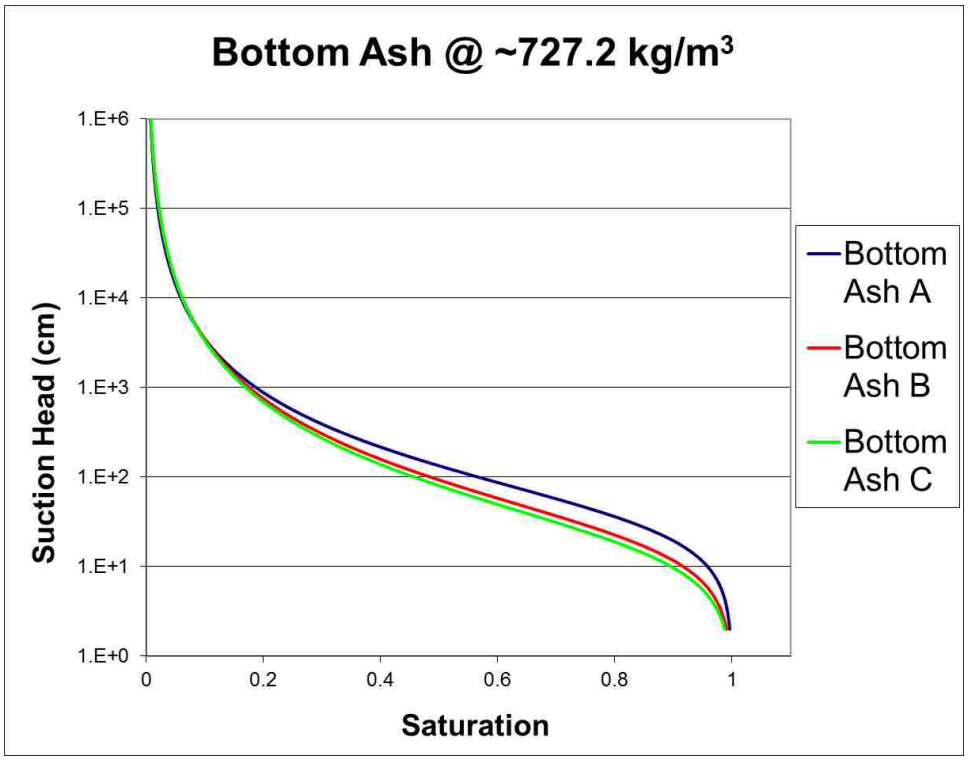

Figure 9: Graphs of Fitted Data (top) and Saturation MCCs (bottom)

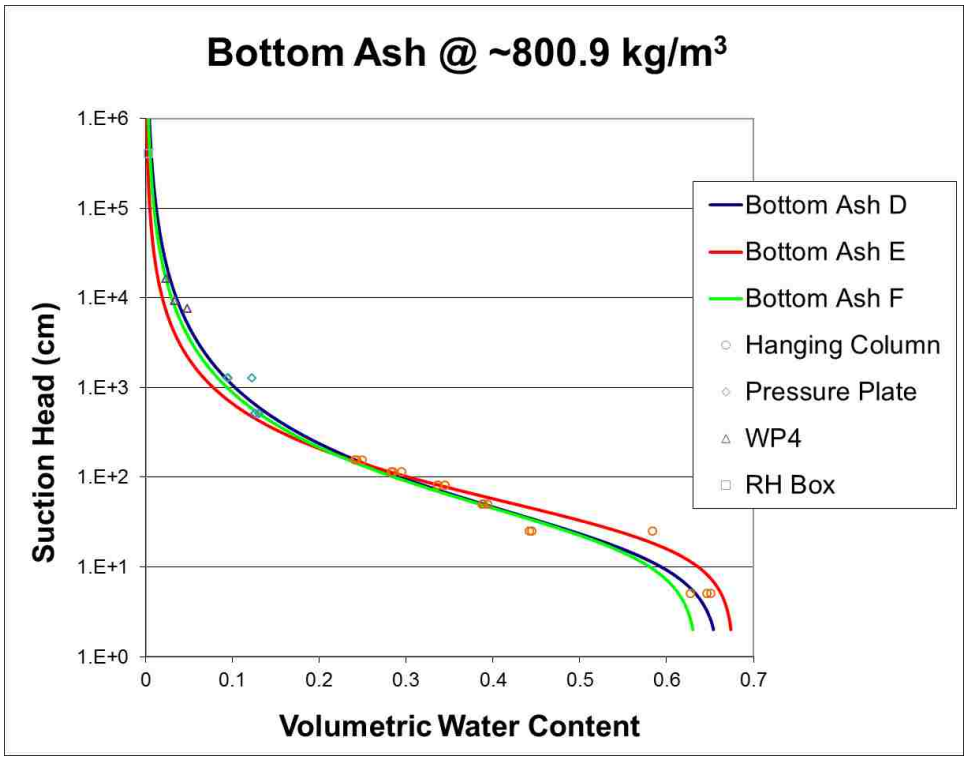

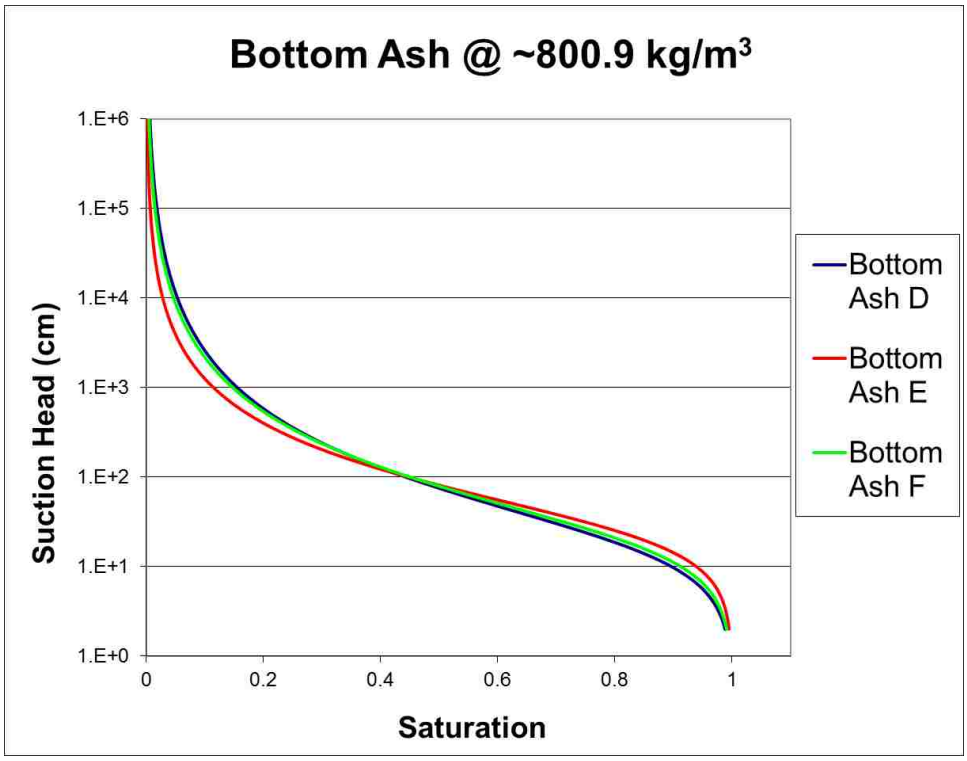

Figure 10: Graphs of Fitted Data (top) and Saturation MCCs (bottom)

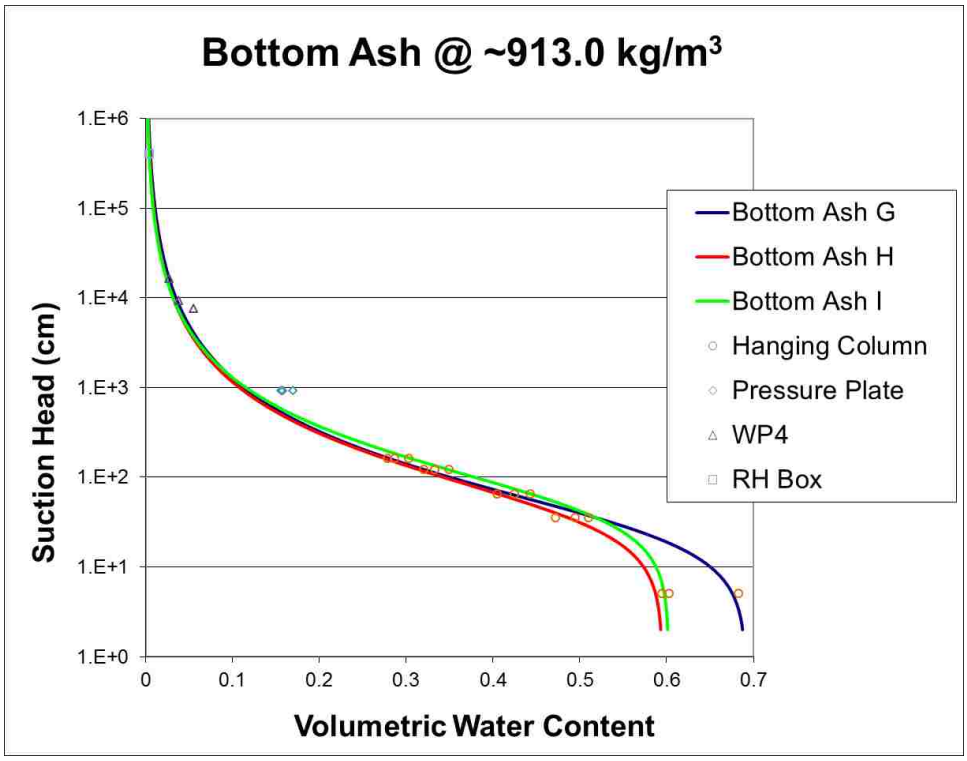

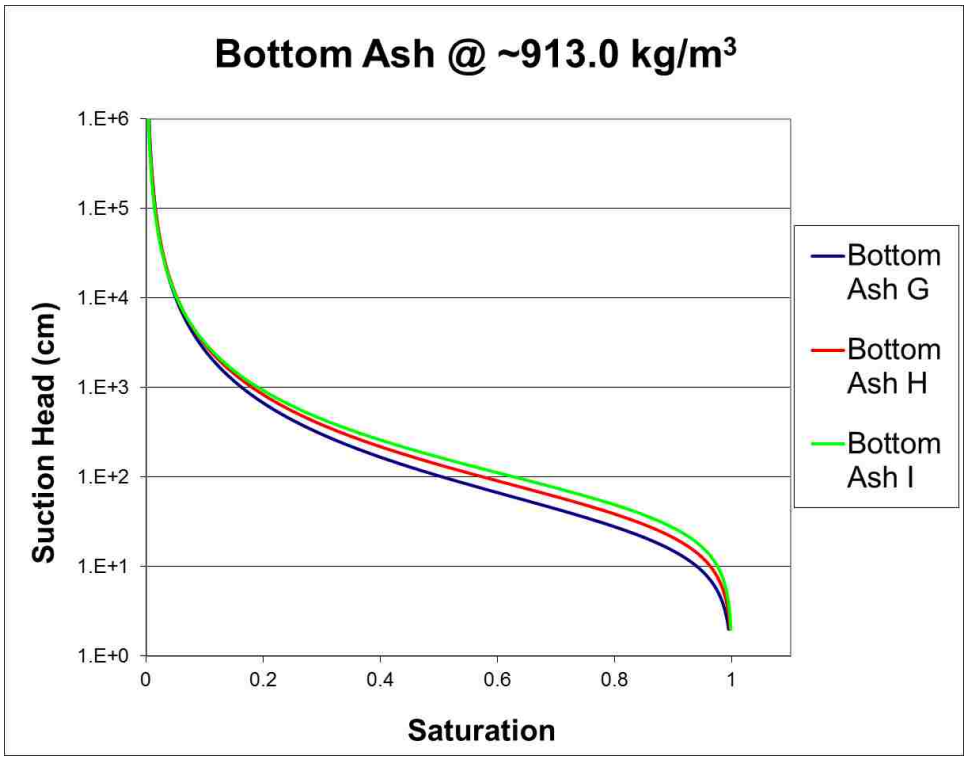

Figure 11: Graphs of Best Fit MCCs for each Dry Density

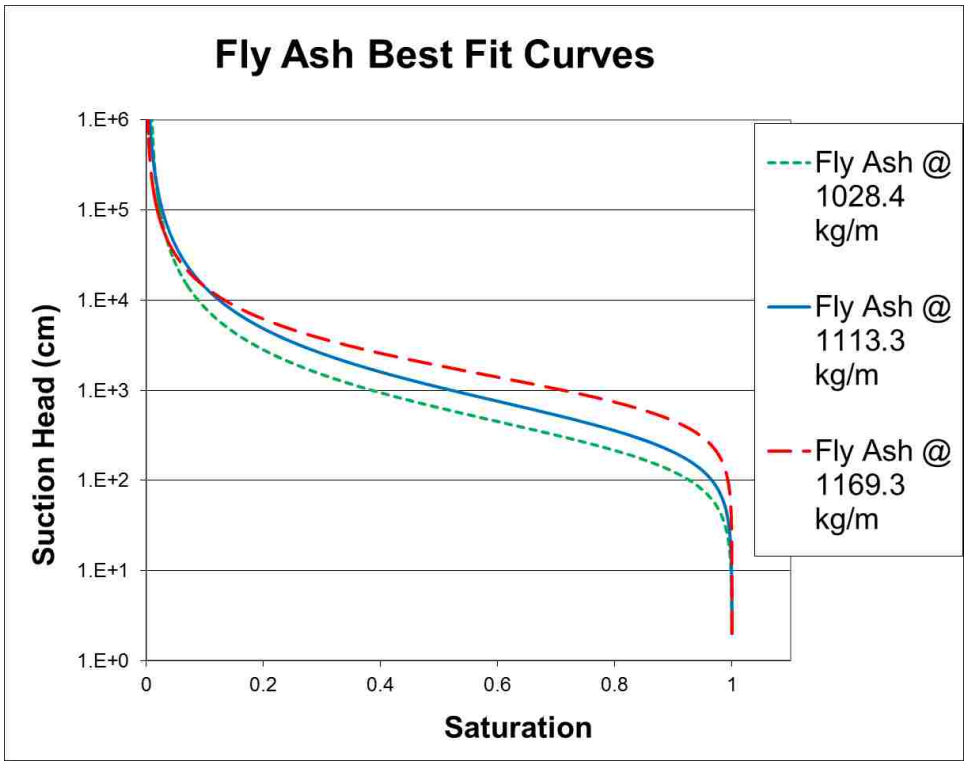

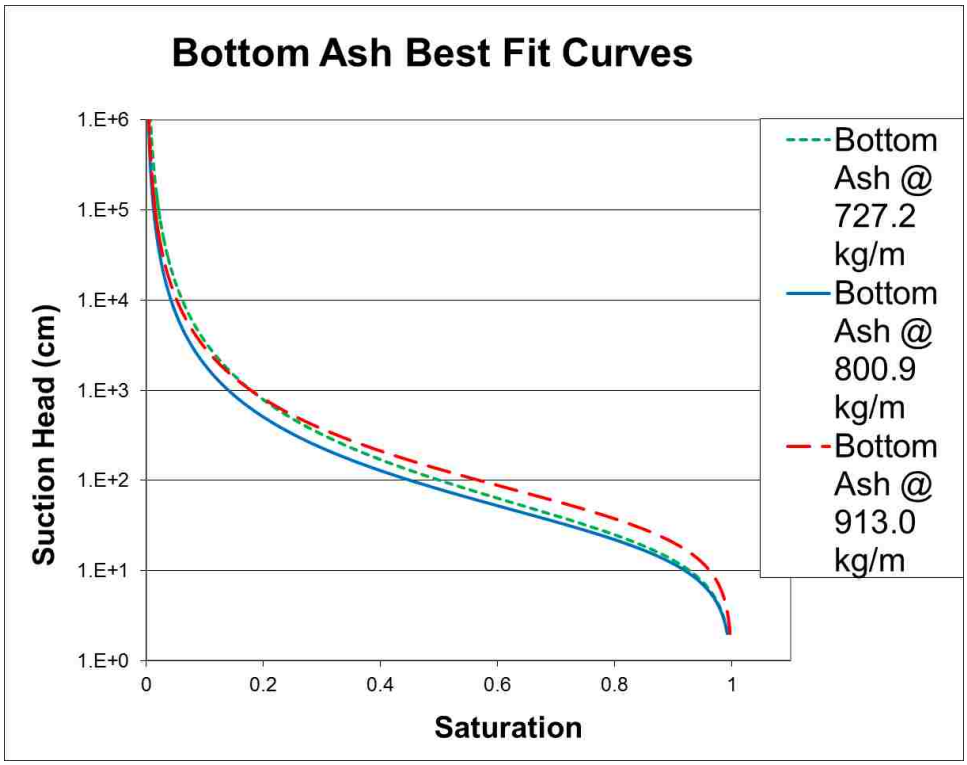

Figure 12: Graphs of Van Genuchten Parameters vs. Dry Densities

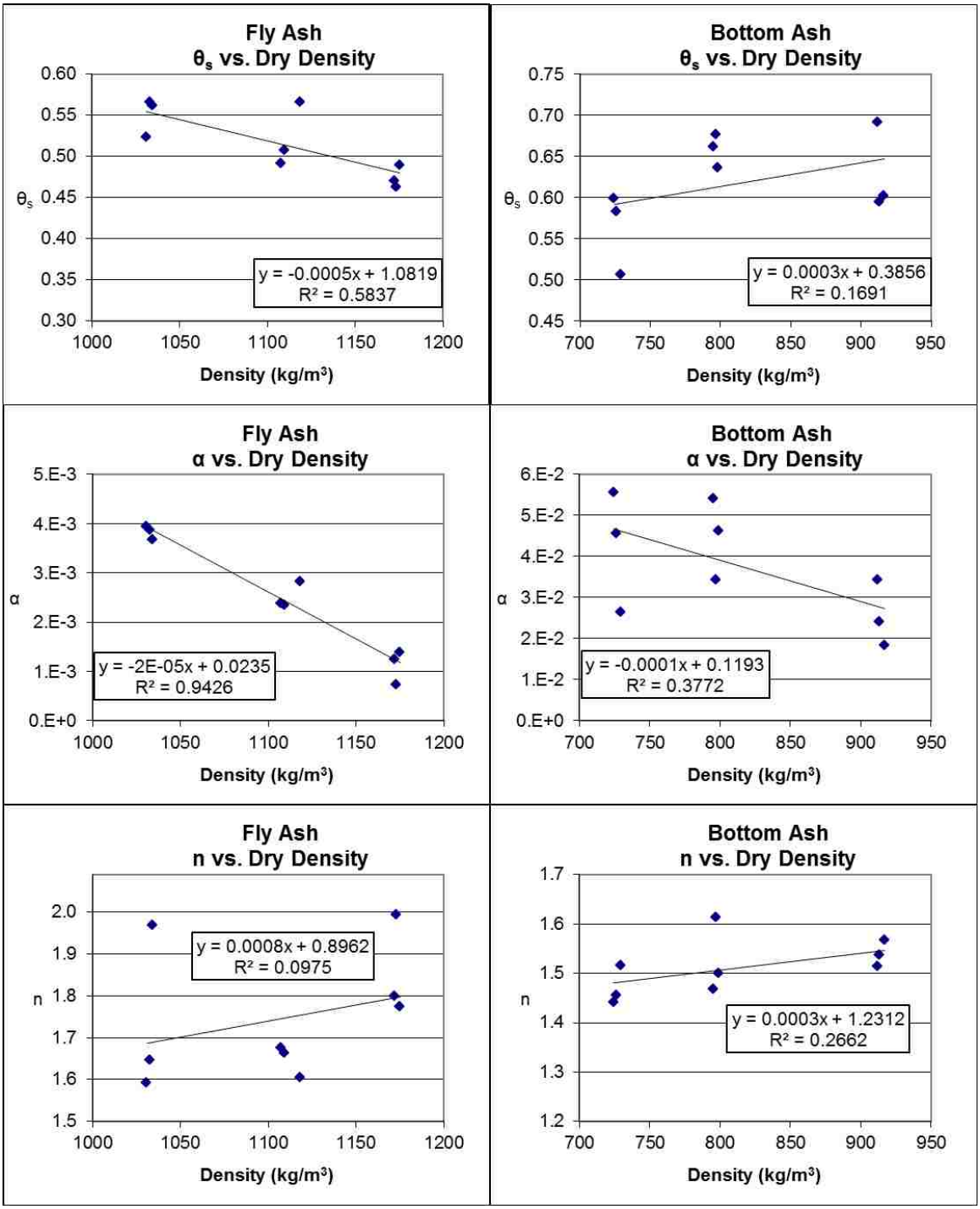

5. DISCUSSION OF LABORATORY RESULTS

Specific Gravity and Calculated Porosity of Fly Ash and Bottom Ash

Specific gravity tests resulted in an average specific gravity of 2.00 for fly ash and 2.06 for bottom ash. These results are within the range of results from other studies (El-Mogazi et al., 1988; Palmer et al., 2000; Prashanth et al., 1998; Seals et al., 1972). Porosity was calculated using the following equation:

$$porosity = 1 - {}^{\rho}/_{G_s} \quad (4)$$

Where:

ρ = sample density in g/cm^3

G_s = material specific gravity

When porosities are compared to fitted θ_s values, most samples appear to be over saturated. That is, the fitted θ_s is larger than the porosity calculated using the measured specific gravity (table 8). This result is consistent throughout all samples except for bottom ash samples with a target dry density of 727.0 kg/m^3.

It is highly unlikely that the samples were over saturated at the fitted θ_s values. It can be seen in the MCCs fitted with data (figures 5 - 10) that the fitted θ_s values (table 6) are often less than the volumetric water content measured at

-5 cm. Oversaturation is not likely to occur after equilibration at a negative pressure head of 5 cm.

A possible reason that some of the bottom ash samples appear under saturated may be that some of the particles have large hollow cores that are inaccessible to water. Attention was given during saturation to ensure fully saturated samples. There were no observations during testing to support that any of the samples were over or under saturated. Therefore, calculated porosities using specific gravity results are not used further.

Table 8: Calculated Porosity and Saturated Water Content Comparison

Sample	Target Dry Density (kg/m^3)	Actual Dry Density (kg/m^3)	G_s	calculated porosity (%)	Θ_s (cm^3/cm^3)	% saturated
FA A	1028.4	1030.8	2.00	48.5	0.52	108.0
FA B	1028.4	1033.1	2.00	48.3	0.57	117.1
FA C	1028.4	1034.7	2.00	48.3	0.56	116.6
FA D	1113.3	1,113.3	2.00	44.5	0.51	114.1
FA E	1113.3	1,113.3	2.00	44.6	0.49	110.2
FA F	1113.3	1,118.8	2.00	44.1	0.57	128.5
FA G	1169.3	1172.1	2.00	41.4	0.47	113.8
FA H	1169.3	1173.4	2.00	41.3	0.46	112.0
FA I	1169.3	1,175.2	2.00	41.2	0.49	118.8
BA A	727.2	729.2	2.06	64.6	0.51	78.5
BA B	727.2	726.5	2.06	64.7	0.58	90.1
BA C	727.2	724.2	2.06	64.8	0.60	92.5
BA D	800.9	795.2	2.06	61.4	0.66	107.8
BA E	800.9	797.1	2.06	61.3	0.68	110.5
BA F	800.9	798.7	2.06	61.2	0.64	103.9
BA G	913.1	912.3	2.06	55.7	0.69	124.1
BA H	913.1	913.5	2.06	55.7	0.60	106.9
BA I	913.1	916.9	2.06	55.5	0.60	108.6

Fly Ash

Equation (1) can be used to reasonably describe the load-dry density relationship of fly ash for the range of applied loads used. Similar results were shown for all four samples of fly ash that were subjected to one-dimensional loading for this study.

The results of the saturated hydraulic conductivity for fly ash show greater variability in the samples with lower dry densities. It can be speculated that this is caused by less uniform pore size distribution at lower densities which becomes more uniform with increasing dry density. Saturated hydraulic conductivity results between fly ash samples of the same dry densities are comparable with one another. These results provide a trend of K_{sat} decreasing as dry density increases, consistent with previous studies on fly ash. The values found in this study are comparable to what other studies have found. (Campbell et al., 1983; Joshi et al., 1994; Prashanth et al., 2001)

The van Genuchten model parameters of fly ash also display a trend in variation with density. Values of θ_s, which is related to the amount of pore space within the sample, are shown to decrease with increased density as expected. Values of α, commonly interpreted as the inverse of air entry pressure head (Mudd et al., 2007), also decrease with increases in dry density; this can be attributed to smaller pores in higher density materials being able to retain water at greater negative pressure heads. Values of air entry for fly ash are similar to what was found in previous studies (Mudd et al., 2007; Chakrabarti et al., 2005).

It is also important to note that, for fly ash, values of n show little variation with increasing density; all values are between 1.5 and 2.0. This result is reflected in the similar shapes of MCCs for all fly ash samples. All three samples at each dry density of fly ash provided similar results, indicating that the methods used to estimate unsaturated hydraulic properties are appropriate for fly ash materials.

Fly ash saturated and unsaturated hydraulic properties display similar results to that of a silty soil (Assouline, 1997; Lu and Likos, 2004; Richard et al., 2001).

Bottom Ash

Bottom ash compressibility results showed less variation between samples than fly ash. Equation (1) can be used to reasonably describe the load-dry density relationship of bottom ash for the range of applied loads used. Similar results were shown for all four samples of bottom ash that were subjected to one-dimensional loading for this study.

K_{sat} values measured for bottom ash samples showed a general linear trend of decreasing as density increases but with considerable variability.

Unsaturated properties of bottom ash show similar variability in the results. θ_s values show little linear trend as dry density increases, with a linear R^2 value of 0.17. θ_s values for bottom ash tend to increase slightly as density increases,

which conflicts with expectations. This may be attributed to lack of homogeneity in the material. The structure of the bottom ash has been observed to be heterogenous with pieces of unburned coal appearing at times and even larger pieces of gravel sized rocks. Lack of homogeneity within the bottom ash material brings complications in creating samples that have structures which are consistent with one another. The structure and porosity of a material has a strong impact on the saturated and unsaturated hydraulic properties of a material (Lu and Likos, 2004).

Values of α for bottom ash are similar to those found in other studies (Mudd et al., 2007; Chakrabarti et al., 2005). A linear trend line provides a relatively low R^2 value of 0.38; however, if the data is fit to a second order polynomial trend line, the R^2 value rises to 0.47 (figure 13). This suggests that, for bottom ash, unsaturated properties such as α may not be effected by increases in dry density until a threshold density is reached. Further testing would be required to support this speculation.

Values of n for bottom ash show less variation than fly ash values; all values are between 1.4 and ~1.6. This shows that the shapes of MCCs, for all bottom ash samples, are more similar relative to fly ash samples. The resulting MCCs for each dry density plot along similar curves providing further evidence that these methods are consistent in estimating unsaturated properties of bottom ash materials.

The variability in bottom ash properties compared to fly ash may be due to more heterogeneity in bottom ash. Larger sample volumes could provide less variability in results for K_{sat} and MCC measurements.

Bottom ash saturated and unsaturated hydraulic properties display similar results to that of a sandy soil (Assouline, 1997; Lu and Likos, 2004).

Figure 13: Comparison of Linear Trend Line and Parabolic Trend Line

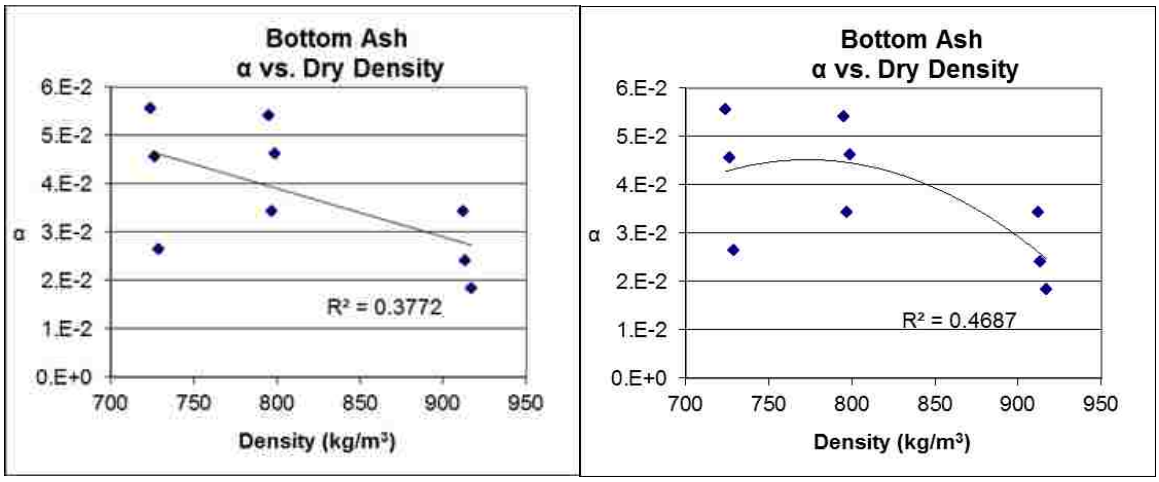

6. LABORATORY CONCLUSIONS

Fly ash K_{sat} values are shown to decrease as dry density increases. Unsaturated hydraulic properties, such as θ_s and α, for fly ash decrease with increases in dry density.

Bottom ash compressibility shows little variability whereas hydraulic properties have more variability relative to those of fly ash. K_{sat} values of bottom ash samples tend to decrease as dry density increases. Unsaturated properties of bottom ash show little trend in variations with changes in dry density. Test results may reflect the lack of homogeneity in bottom ash.

This study has shown that methods common to soil testing may be utilized to measure both saturated and unsaturated hydraulic properties of fly ash and bottom ash as a function of density.

7. ONE DIMENSIONAL WATER MOVEMENT MODEL

One-dimensional water movement modeling was conducted to simulate water movement in buried CCBs in a landfill in the arid climate of northwestern New Mexico. The modeling program used in this study was HYDRUS1D developed by Simunek et al. (2008). HYDRUS 1D is a software package designed for simulating the movement of water, heat, and multiple solutes in variably saturated media. Only water movement was simulated in this study. The program numerically solves Richards' equation for variably saturated water flow as well as a sink term to account for root water uptake. The program is capable of analyzing water and solute transport in unsaturated, partially saturated, as well as fully saturated porous media. The water flow portion of the model is capable of incorporating boundaries controlled by prescribed head and flux, atmospheric conditions, and free drainage. The governing flow and transport equations are solved numerically using Galerkin-type linear finite element schemes.

The developed model for this study represents a vertical profile form the ground surface, through 2m of top soil and 33m of buried CCBs to the underlying sandstone formation. For most simulations, the upper boundary was modeled using daily-varying climate data and the lower boundary was a no-flow boundary below the sandstone layer, a large distance from the CCB-sandstone contact. Additional simulations were conducted with focused recharge conditions on the surface and with a water table at the CCB-sandstone contact. The initial condition was an assumed water content, which was varied.

The model profile was created using 1001 nodes with a varying nodal density input values of 1 at the top of the profile and 50 at the bottom. These input values created a spacing of 0.33 cm at the top of the profile and 16.67 cm at the bottom. The nodal density represents the relative spacing between nodes, 1 being the default value in HYDRUS 1D and spacing becoming greater as the density value increases. The time units used for this study were days with an initial time step of 0.01, a minimum time step of 1e-6 and a maximum step of 1. A water content tolerance of 0.0001 was set with a maximum number of iterations of 200.

Profiles were 85 m in total depth with the top 2 m representing top soil, the next 33 m being held as the CCB pit, and the bottom 50 m being the pictured cliff sandstone. Initial volumetric moisture contents used were that of 20% throughout CCB materials and pictured cliffs, with 5% for the top soil. These initial moisture contents were chosen due to the results of the geo-probe sample results conducted at the SJM in 2010 (Chan, 2010). Observation points were placed in the model at depths of 2, 7, 12, 17, 22, 27, 32, and 35 m to collect data on fluxes, water content, and potential within the profile during simulations.

Profile Development

Ash disposal at the SJM involved the placement of different types of CCBs in the pits as they were produced at the generating station. Quarterly reports of ash disposal at the SJM (SJM, 2011) indicate a fairly constant ratio of fly ash to

bottom ash production (78 to 22), but there are no records as to the specific profile of landfill sites. Therefore, fifteen different profiles of landfill composition were developed in order to capture different possible landfill compositions. To create the different profiles, the total CCB pit depth (33m) was divided into 18 layers, each 1.83m thick. For a particular profile, each layer was randomly assigned the properties of fly ash or bottom ash while maintaining the overall ratio of fly ash to bottom ash in the profile. Each of these profiles was therefore different in the arrangement of fly ash and bottom ash layers.

Two additional profiles were also developed, one of which the CCB material is solely fly ash and another of solely bottom ash.

Material Properties

Top soil in situ density and hydraulic properties obtained from the investigation conducted by Chan (2010) were used for the model. Pictured cliff sandstone properties were those determined by other studies. The saturated hydraulic conductivity of the picture cliff sandstone was determined by Kernodle (1996). Unsaturated properties from a study conducted by Van Genuchten (1989) for hygiene sandstone formation located near Boulder, CO were used for the MCC fitting parameters. Both hygiene sandstone and pictured cliffs sandstone were formed in the late cretaceous period and have low permeability (Kernodle, 1996, Kiteley, 1977). A summary of the material properties for the top soil and the pictured cliff sandstone are given in table 9.

Table 9: Hydraulic Properties of Top Soil and Pictured Cliffs Sandstone

Material	Θ_r (cm^3/cm^3)	Θ_s (cm^3/cm^3)	α (1/cm)	n	K_S (cm/day)
Top Soil	.02018	0.44	0.0323	1.39	0.730
Pictured Cliffs	0.0	0.256	.00562	3.27	0.213

CCB densities were calculated using a weighted average curve from the compressibility results in chapter 4 (table 4). Parameters of equation 1 were weighted to the R^2 value of each fitted curve using the following equation:

$$FP = \frac{T_1 * R_1^2 + T_2 * R_2^2 + T_3 * R_3^2 + T_4 * R_4^2}{\sum R_n^2} \quad (5)$$

Where:

FP = fitting parameter being calculated

T_n = fitting parameter for trial number n

R^2_n = R^2 value for trial number n

Graphical representation of the weighted average density curve can be seen in figure 14.

Figure 15 shows one of the spreadsheets used to develop random profiles for the model. The top soil is highlighted in brown, the bottom ash in green, and the fly ash is not highlighted. Sandstone is not represented in this profile due to the fact that the properties of sandstone were constant and not dependent upon material densities above. Each segment of material had a calculated dry density from the weighted average density curves and a total density could then be

calculated by adding the appropriate mass associated with the gravimetric moisture content. The overburden is the total density multiplied by the depth of the segment (1.83 m for CCBs) and a total overburden pressure for each cell is the sum of pressures for all segments above the cell in question. Saturated and unsaturated properties of each material were then calculated using the trend lines calculated from the laboratory results as a function of dry density in chapter 4 (figures 4 and 12).

Figure 14: Fly Ash (top) and Bottom Ash (bottom) Dry Density vs. Pressure Curves

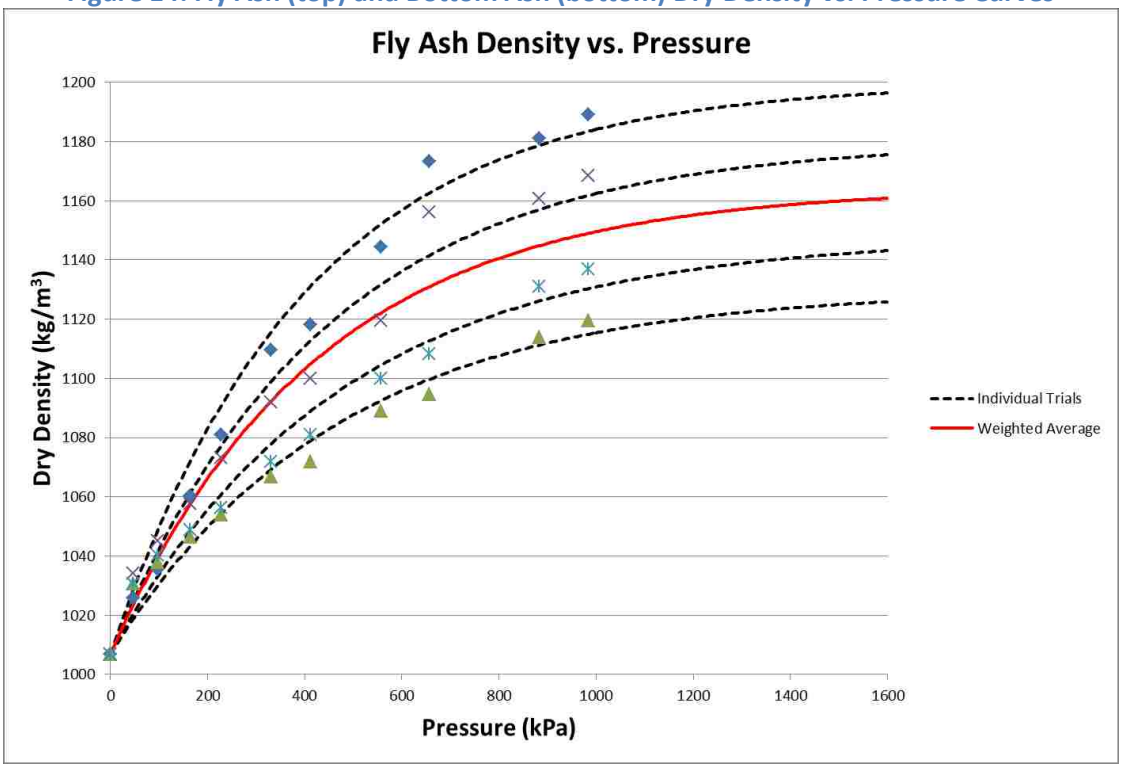

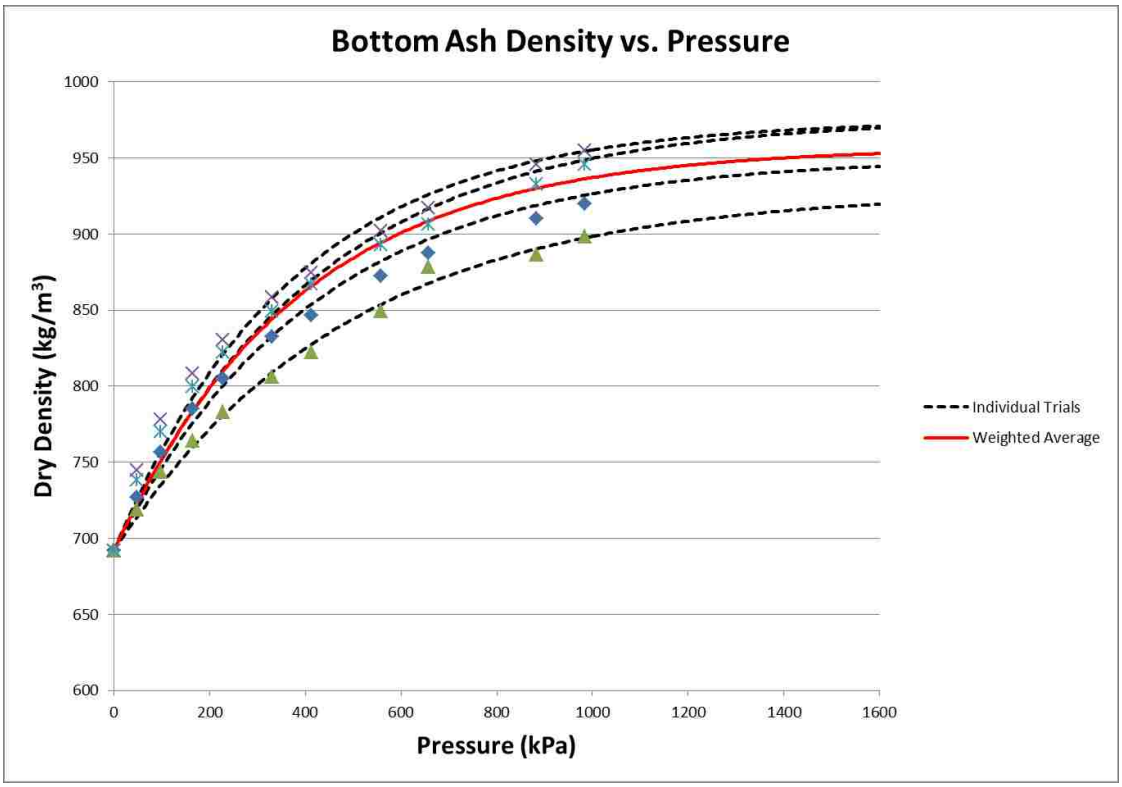

Figure 15: Example of Profile Spreadsheet

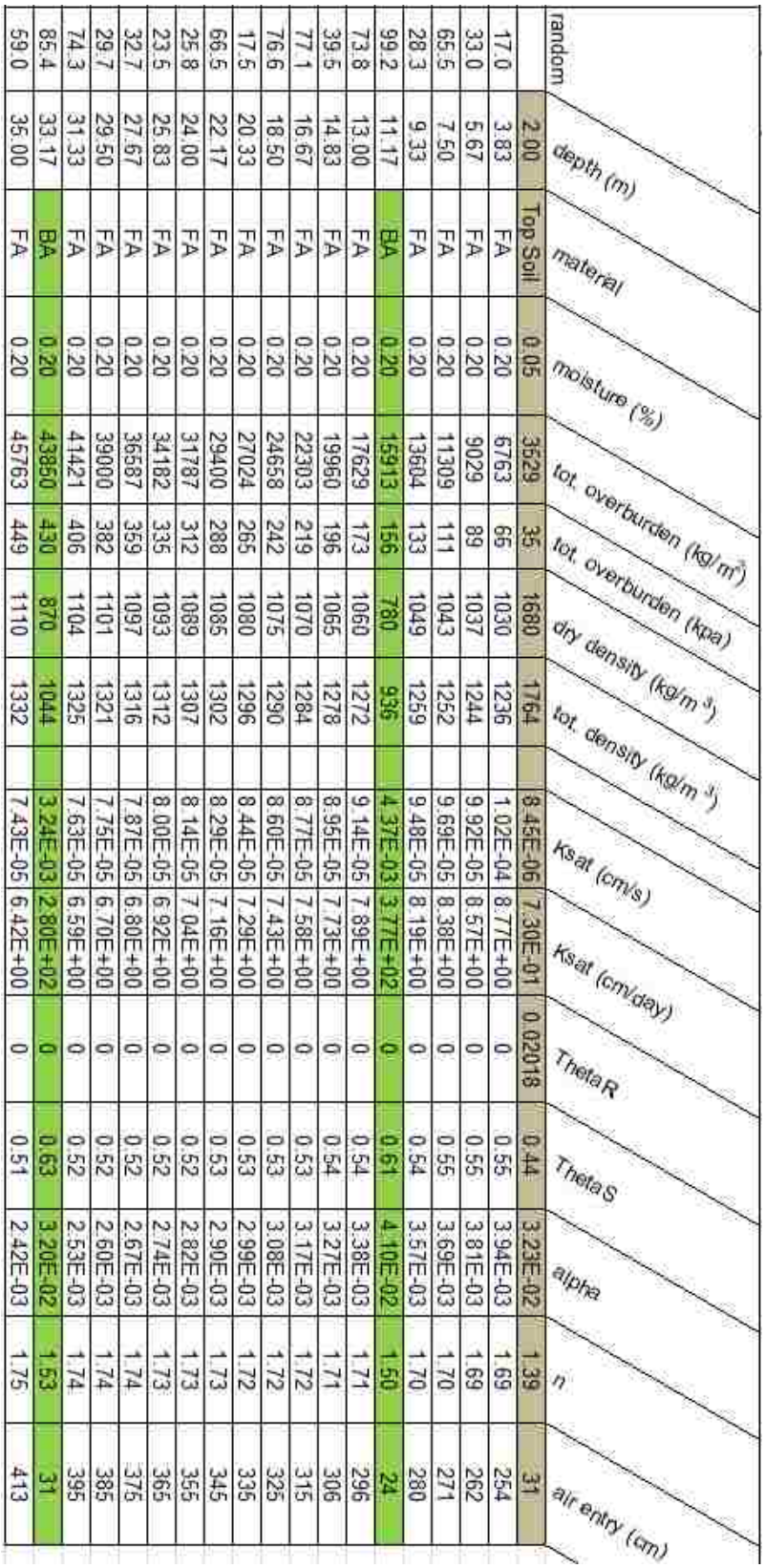

random	depth (m)	material	moisture (%)	tot. overburden (kg/m^2)	tot. overburden (kpa)	dry density (kg/m^3)	tot. density (kg/m^3)	Ksat (cm/s)	Ksat (cm/day)	ThetaR	ThetaS	alpha	n	air entry (cm)
	2.00	Top Soil	0.05	3529	35	1680	1764	8.45E-06	7.30E-01	0.02018	0.44	3.23E-02	1.39	31
17.0	3.83	FA	0.20	6763	66	1030	1236	1.02E-04	8.77E+00	0	0.55	3.94E-03	1.69	254
33.0	5.67	FA	0.20	9029	89	1037	1244	9.92E-05	8.57E+00	0	0.55	3.81E-03	1.69	262
65.5	7.50	FA	0.20	11309	111	1043	1252	9.69E-05	8.38E+00	0	0.55	3.69E-03	1.70	271
28.3	9.33	FA	0.20	13604	133	1049	1259	9.48E-05	8.19E+00	0	0.54	3.57E-03	1.70	280
99.2	11.17	BA	0.20	15913	156	780	936	4.37E-03	3.77E+02	0	0.61	4.10E-02	1.50	24
73.8	13.00	FA	0.20	17629	173	1060	1272	9.14E-05	7.89E+00	0	0.54	3.38E-03	1.71	296
39.5	14.83	FA	0.20	19960	196	1065	1278	8.95E-05	7.73E+00	0	0.54	3.27E-03	1.71	306
77.1	16.67	FA	0.20	22303	219	1070	1284	8.77E-05	7.58E+00	0	0.53	3.17E-03	1.72	315
76.6	18.50	FA	0.20	24658	242	1075	1290	8.60E-05	7.43E+00	0	0.53	3.08E-03	1.72	325
17.5	20.33	FA	0.20	27024	265	1080	1296	8.44E-05	7.29E+00	0	0.53	2.99E-03	1.72	335
66.5	22.17	FA	0.20	29400	288	1085	1302	8.29E-05	7.16E+00	0	0.53	2.90E-03	1.73	345
25.8	24.00	FA	0.20	31787	312	1089	1307	8.14E-05	7.04E+00	0	0.52	2.82E-03	1.73	355
23.5	25.83	FA	0.20	34182	335	1093	1312	8.00E-05	6.92E+00	0	0.52	2.74E-03	1.73	365
32.7	27.67	FA	0.20	36587	359	1097	1316	7.87E-05	6.80E+00	0	0.52	2.67E-03	1.74	375
29.7	29.50	FA	0.20	39000	382	1101	1321	7.75E-05	6.70E+00	0	0.52	2.60E-03	1.74	385
74.3	31.33	FA	0.20	41421	406	1104	1325	7.63E-05	6.59E+00	0	0.52	2.53E-03	1.74	395
85.4	33.17	BA	0.20	43850	430	870	1044	3.24E-03	2.80E+02	0	0.63	3.20E-02	1.53	31
59.0	35.00	FA	0.20	45763	449	1110	1332	7.43E-05	6.42E+00	0	0.51	2.42E-03	1.75	413

Baseline Upper Boundary Condition

The baseline model upper boundary condition incorporates climate data from the NMCC station located at the Farmington Agricultural Science Center, approximately 9 miles from the SJM. Meteorological data obtained from this site included daily temperature maximum and minimums, precipitation, and wind data. The climate data was used with the Penman Montheith equation to estimate evapotranspiration in HYDRUS 1D. Data used was between January, 1995 and December, 2004 was complete (no missing data) and was used for these simulations. For the simulations longer than 10 years, this 10 year period of data is repeated. The atmospheric boundary condition also allowed a maximum head of 5 cm to accumulate at the soil surface prior to runoff occurring.

Baseline Root Water Uptake

The root water uptake for this model was adopted from a study conducted by Garcia et al. (2011). Garcia et al. (2011) investigated the root water uptake for the creosote bush present in the Mojave Desert. The study uses HYDRUS 1D to simulate water movement in the root zone for this type of vegetation. The creosote bush study conducted by Garcia et al. (2011) displays similar transpiration as great basin shrubs present near the SJM (Steinwand et al., 2001).

The Feddes water uptake reduction model was used to represent the root water uptake in HYDRUS 1D. The leaf area index used for the simulation was set to a constant 0.38 according to Steinwand's study (2001), and a radiation extinction value of 0.6. The pressure head below which plants will begin to uptake water was set to 0; maximum water uptake was set to occur between -2,000 and -7,000 cm; water uptake rate decreases between -7,000 and -40,000 cm with a wilting point of -80,000 cm of root zone pressure head. The maximum transpiration rate was set to 0.5 cm/day and a lower rate of 0.1 cm/day. The root zone was set to 1 m in depth from the top of the soil profile. Table 10 shows root distribution input values.

Table 10: Root Distribution Input Values

Depth (cm)	Root Distribution
0-10	0
10-20	0.1
20-30	0.2
30-40	0.2
40-50	0.3
50-60	0.3
60-70	0.1
70-80	0.1
80-90	0.1
90-100	0.1

Baseline Lower Boundary Condition

The boundary condition at the bottom of the 85 m profile was a zero constant flux. It was determined by varying the bottom boundary condition and observing the water movement at the pictured cliffs sandstone- CCB interface

that alterations to the bottom boundary condition had no significant impact on water flow 50 m above. Figure 16 displays a diagram of the baseline profile.

Figure 16: Diagram of Baseline Model Materials and Boundary Conditions

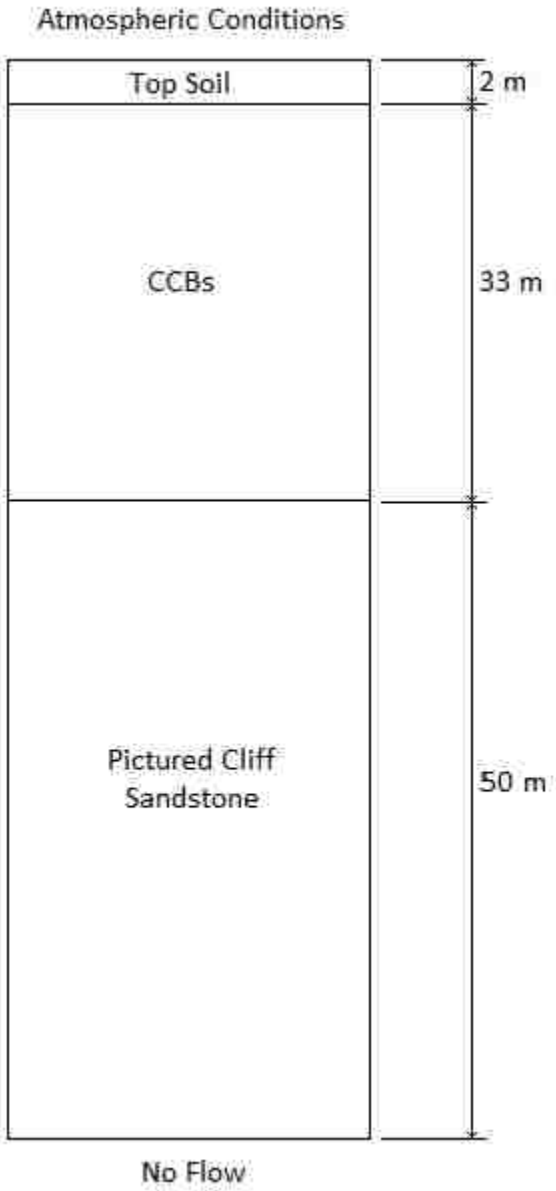

Initial Moisture Content

Four of the randomly generated profiles were selected, based on the number of and spacing between bottom ash materials in the profile, to investigate the sensitivity to the initial moisture content different from that of the baseline model. Also, fly ash only and bottom ash only profiles were used to investigate sensitivity to the initial moisture content. The initial moisture content of the top soil remained 5% for all simulations. The CCBs and picture cliffs sandstone initial moisture contents were changed from the baseline value of 20% to values of 10, 15, 25, 30, and 40%.

Root Water Uptake

Simulations were conducted without root water uptake to assess its impact on the model results for fly ash and bottom ash only profiles. All other aspects of the model were that of the baseline model.

Upper Boundary Condition

The upper boundary condition was changed from meteorological data to zero constant flux in order to analyze if any moisture was infiltrating through the top boundary of the baseline model, or if the observed fluxes at the interface between the topsoil and the CCB were due to initial conditions. Root water uptake was also not simulated during this analysis.

Extended Simulation Duration

The fly ash only and bottom ash only profiles of the baseline model were also simulated for 100 years. The upper boundary condition was set to zero constant flux and root water uptake was not simulated.

Focused Recharge on Surface

The topographic surface at the landfill site may provide natural sinks in which focused recharge may occur. In order to account for this, an analysis was conducted providing conditions under which focused recharge may occur for fly ash and bottom ash only Profiles.

The maximum allowed pressure head at the soil surface was changed from 5 cm to 0 cm to investigate how much runoff might occur under the given meteorological data. The graphs showing precipitation and surface runoff for this scenario can be viewed in figure 17. The amount of surface runoff for each precipitation event producing runoff was then multiplied by 10 to account for a watershed 10 times larger than the ponding area of the sink. The dates and magnitudes of runoff events can be seen in table 11. The calculated runoff of the watershed was then added to the precipitation occurring on the runoff dates in the meteorological input data for the baseline model. The maximum allowed pressure head at the soil surface was then changed from 0 to 100 cm to allow

focused recharge. This simulation was executed for a time period of 20 years on fly ash only and bottom ash only profiles.

Figure 17: Precipitation (left) and Surface Runoff (right)

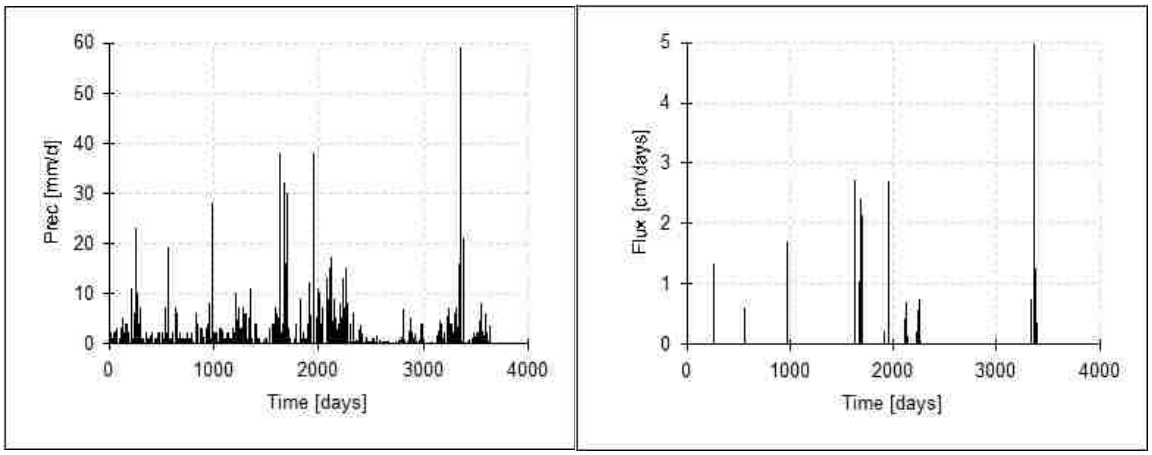

Table 11: Day and Magnitude of Runoff Events

Day in Model	Runoff (cm)	Excess for 10 m^2 (cm)
251	1.38	13.75
558	0.81	8.13
976	1.88	18.75
1622	2.81	28.13
1666	1.13	11.25
1671	2.50	25.00
1676	2.25	22.50
1914	0.31	3.13
1957	2.75	27.50
2108	0.50	5.00
2121	0.81	8.13
2231	0.56	5.63
2258	0.69	6.88
3342	0.75	7.50
3362	5.00	50.00
3381	1.25	12.50
3386	0.38	3.75

Presence of Water Table

Simulations that included the presence of a water table were conducted for the fly ash only and bottom ash only profiles. Alterations were made to the baseline model to create a scenario of a water table being located at 35 m in depth from the soil surface. The depth of the profile was changed from 85 to 35 m to remove the pictured cliff sandstone and the bottom boundary condition was set to a constant (saturated) water content; these water contents were 51% for fly ash only profile and 65% for bottom ash only.

Lowering of Water Table

The scenario in which the landfill pit equilibrates with the water table at 35 m depth and then the water table is significantly lowered was also simulated. The profile depth was kept at 85 m with the pictured cliff sandstone composing the lower 50 m. The upper boundary condition was set to a zero constant flux and the root water uptake simulation removed from the baseline model. This was done to eliminate outside influences other than the lowering of the water table. Initial conditions for the soil profile were also changed to represent an equilibrium condition with the water table at 35 m.

8. MODELING RESULTS

The fly ash only, bottom ash only, and two representative random profiles have been selected to display the results for the baseline model and moisture content sensitivity analyses. The random profiles are identified as profile numbers 3 and 8; these profiles were chosen because they represent the highest and least fluxes of the 15 random profiles at the observation points. Material discretization for profiles 3 and 8 can be seen in table 13. All other profiles show flux rates bounded by the two selected profiles. The figures display water flux for each observation point as a function of time and moisture content with depth at selected time steps.

Baseline Model Results

A summary of the value ranges for fluxes and water contents can be viewed in table 12. A positive flux value represents upward water movement and a negative flux represents downward movement. All baseline model simulations indicate the picture cliff sandstone becoming saturated at the bottom of the material and drying near the interface with the CCB pit. The top soil shows little change in moisture content over the duration of the simulations.

The fly ash only profile simulation displays the CCB pit wetting at the bottom, though not fully saturated, as the interface with top soil dries. The

bottom ash only profile simulation displays the CCB pit wetting at the bottom, though not fully saturated, with intermittent wetting and drying sections between the top soil and bottom of the pit. The profile 3 and 8 simulations display the CCB pit wetting at the bottom of fly ash sections, though not fully saturated, and drying within the bottom ash materials. No water infiltration is observed across the top soil and CCB pit interface for any of the basic models during the entire duration of the simulation. These results can be seen in figure 18, 19, 20, and 21.

Table 12: Range of Fluxes and Water Contents for the Baseline Model Simulation

Profile	Total Range of Observation Point Fluxes (cm/day)	Total Range of Water Contents (cm/cm)	CCB pit range of Water Contents (cm/cm)
FA only	-0.02 - 0.09	0.01 - 0.33	0.16 - 0.33
BA only	0.0 - 0.12	0.01 - 0.27	0.19 - 0.27
3	-0.03 - 0.02	0.08 - 0.32	0.08 - 0.32
8	-0.1 – 0.05	0.01 - 0.31	0.08 - 0.31

Table 13: Material Distribution for Profiles 3 and 8

Depth (m)	Profile 3 Material	Profile 8 Material
0-2	Topsoil	Topsoil
2-3.8	BA	FA
3.8-5.7	FA	FA
5.7-7.5	FA	FA
7.5-9.3	FA	BA
9.3-11.2	FA	FA
11.2-13.0	FA	BA
13.0-14.8	BA	FA
14.8-16.7	FA	BA
16.7-18.5	FA	FA
18.5 – 20.3	FA	FA
20.3 – 22.2	FA	BA
22.2 – 24.0	FA	FA
24.0 – 25.8	FA	FA
25.8 – 27.7	FA	FA
27.7 – 29.5	FA	FA
29.5 – 31.3	BA	BA
31.3 – 33.2	BA	FA
33.2 – 35.0	BA	FA
35.0 – 85.0	Sandstone	Sandstone

**Figure 18: Baseline Results: Flux for
Fly Ash Only Profile (top) and Bottom Ash Only Proflie (bottom)**

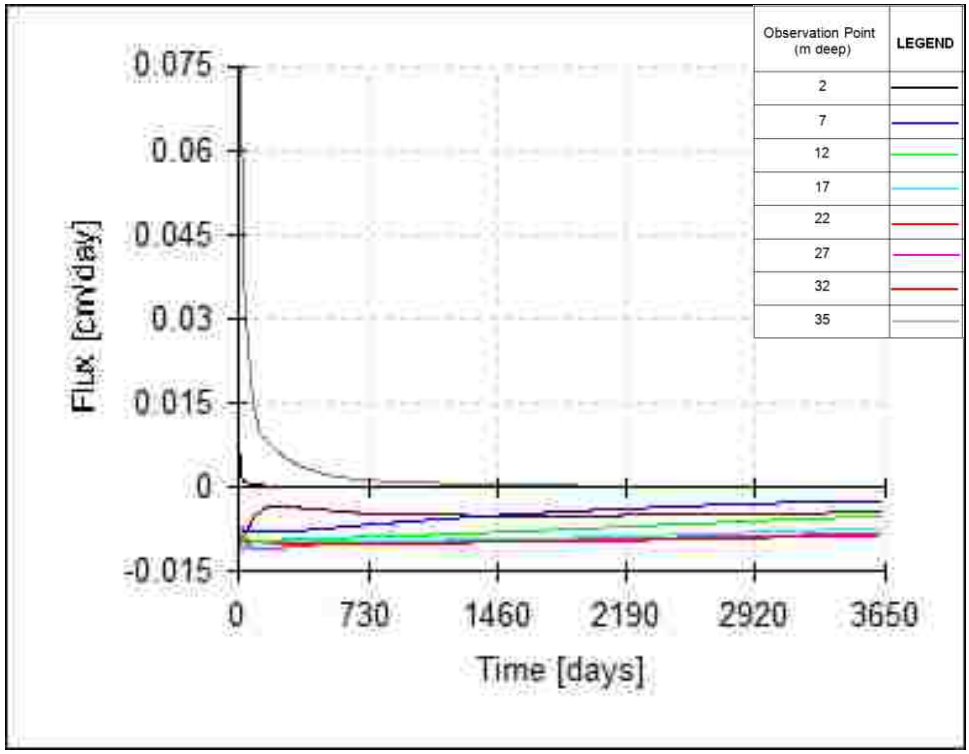

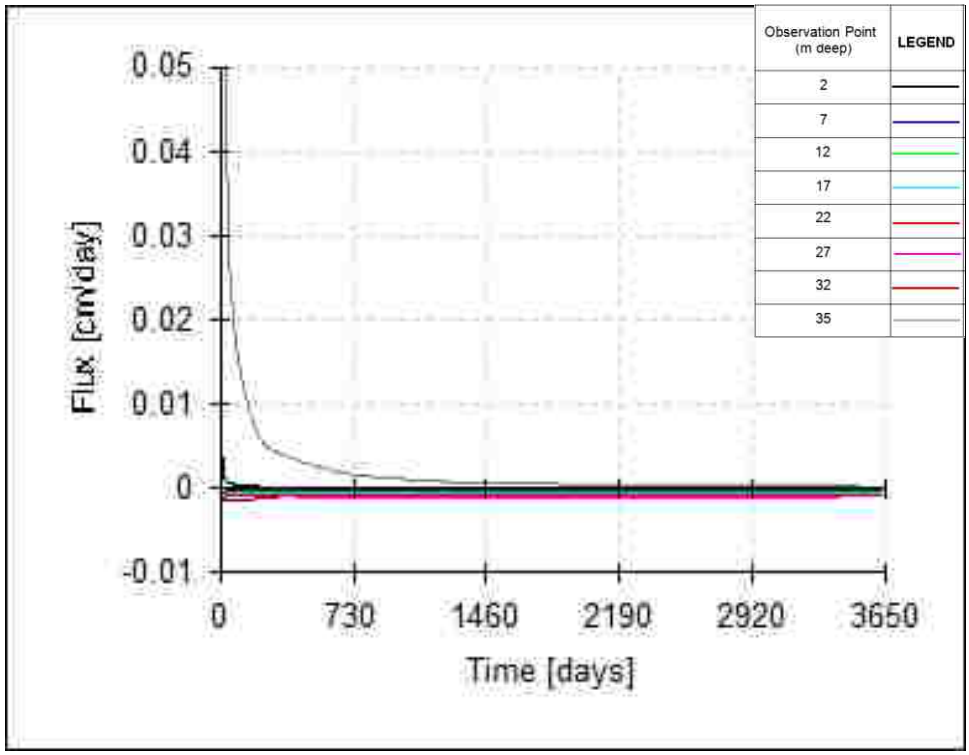

Figure 19: Baseline Results: Water Content vs Depth for Fly Ash (top) and Bottom Ash (bottom) Only Profiles

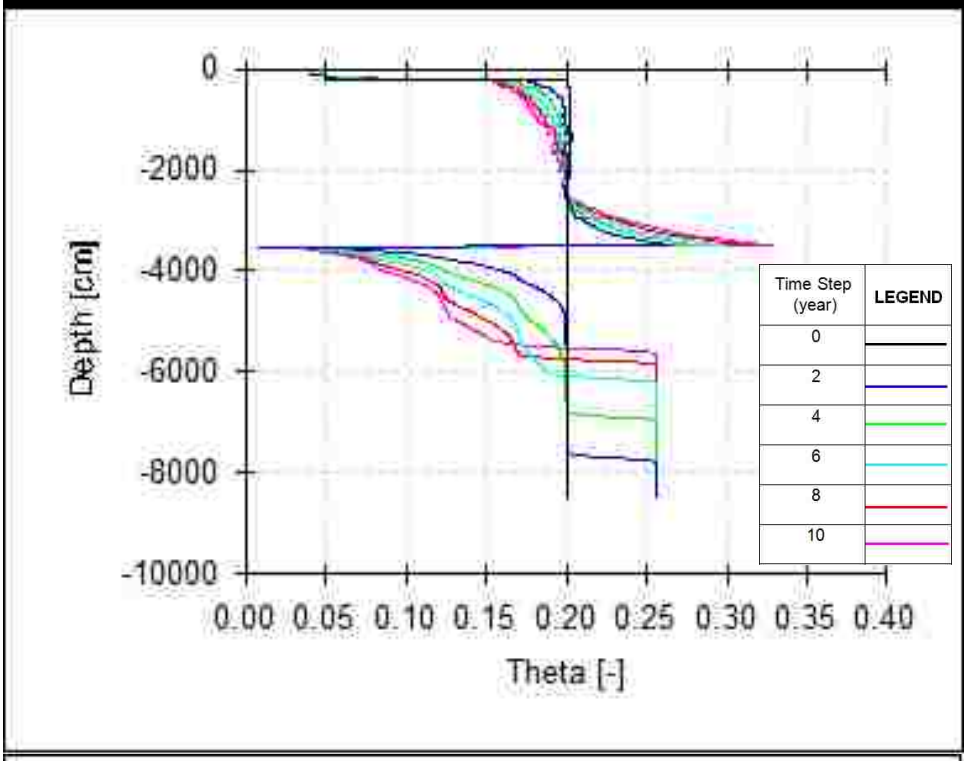

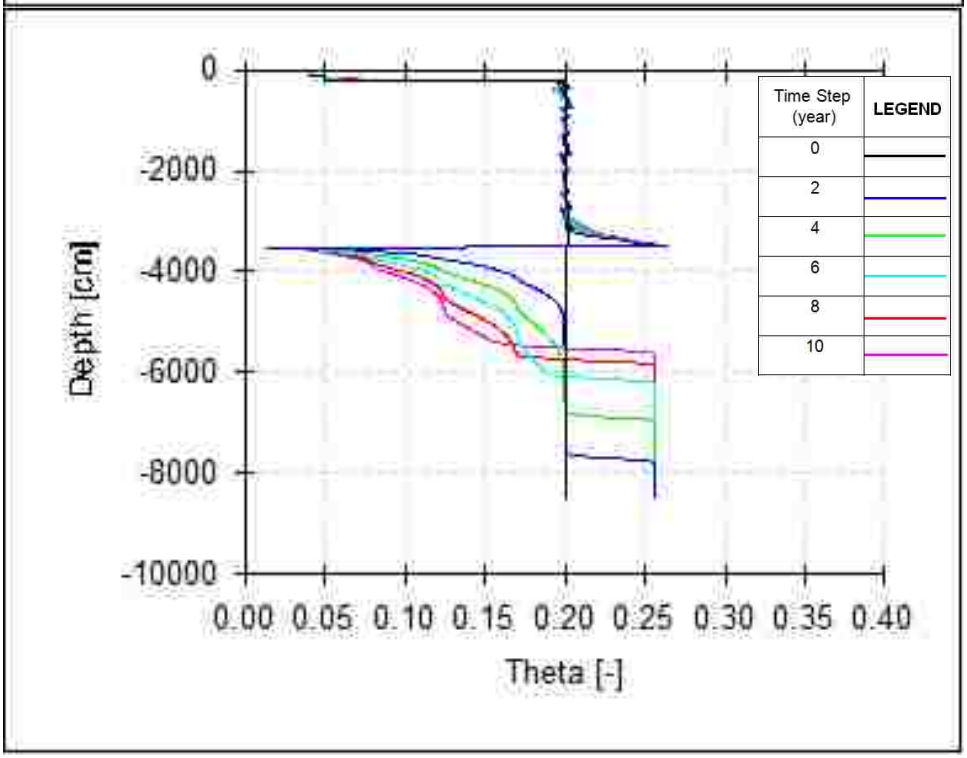

Figure 20: Baseline Results: Flux for Profiles 3 (top) and 8 (bottom)

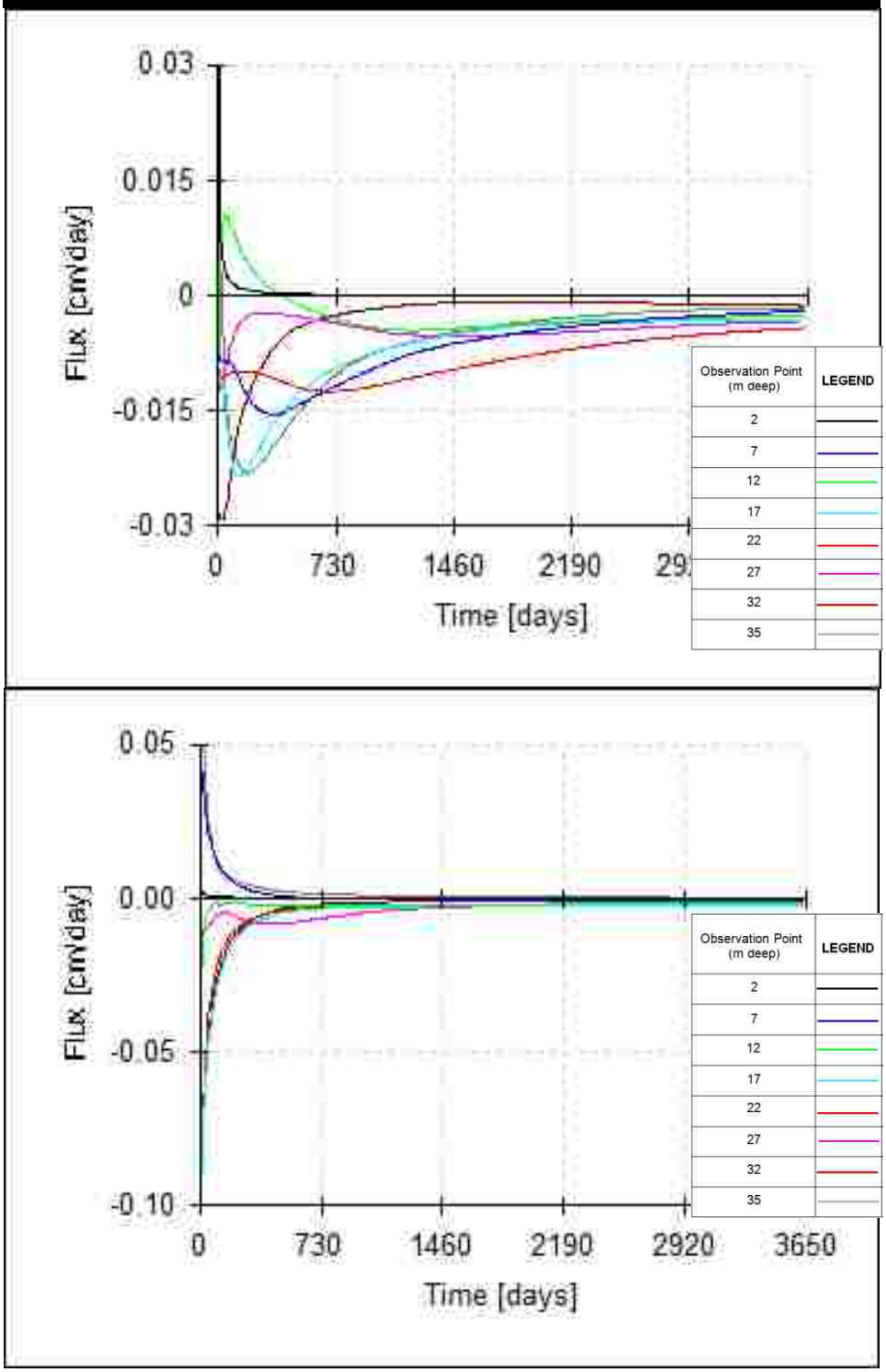

Figure 21: Baseline Results: Water Content vs. Depth for Profiles 3(top) and 8(bottom)

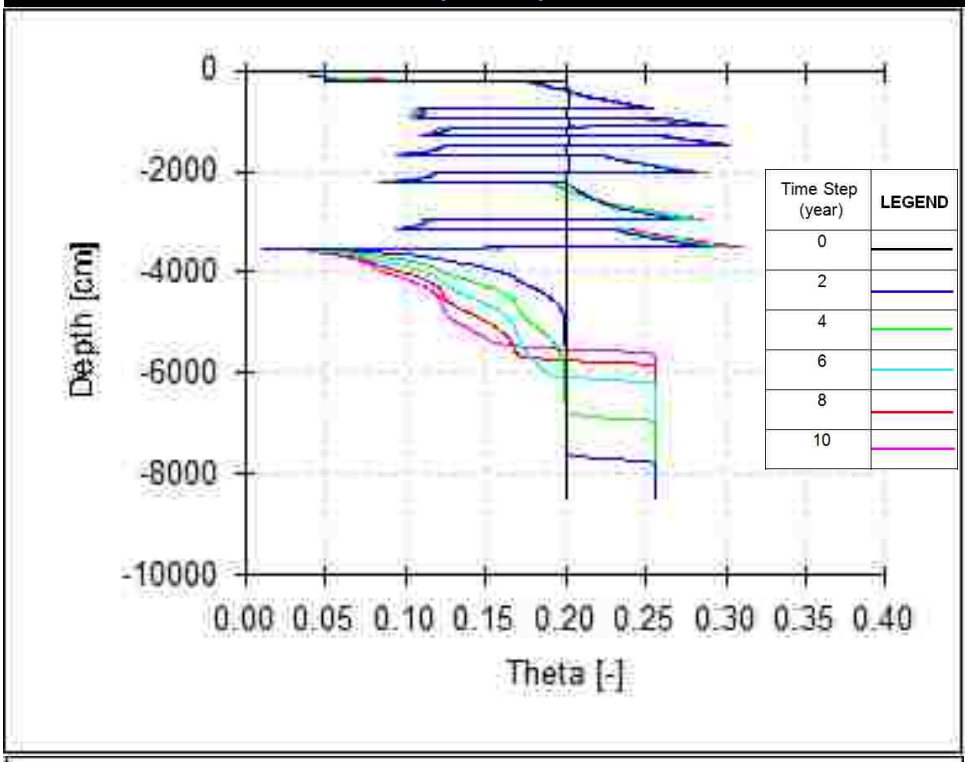

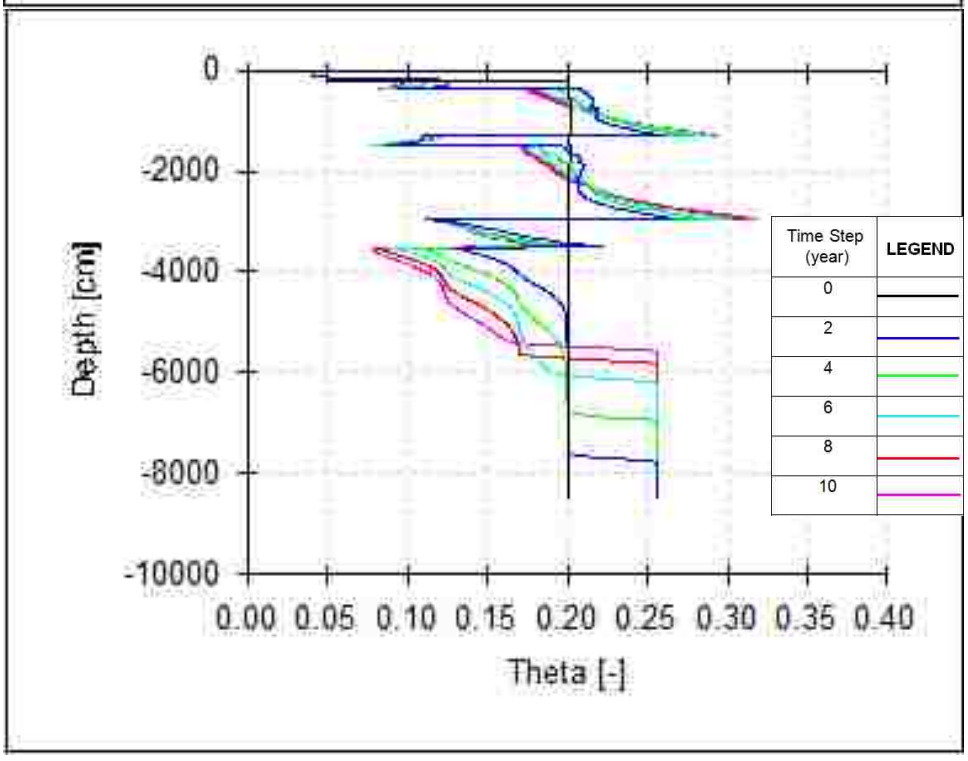

Initial Moisture Content

The fly ash only profile displays downward fluxes at the bottom of the CCB pit at an initial water content of 30 and 40%. The bottom ash only profile displays a downward flux at initial water content of 40% only. Profile 3 shows downward fluxes at the bottom of the CCB pit at initial water contents of 20, 25, 30, and 40%. Profile 8 displays a downward flux at the bottom of the CCB pit at an initial water content of 40% only. The prominent flux vs. initial water content is shown in figure 22. The term 'prominent flux' is defined as the either the maximum upward value if no downward flux is shown or the maximum downward value observed if present. For all simulations, the prominent flux occurred briefly, during the first 1 to 2 years of the simulation.

Figure 22: Flux at Bottom of CCB Pit During Initial Moisture Content Sensitivity Analysis

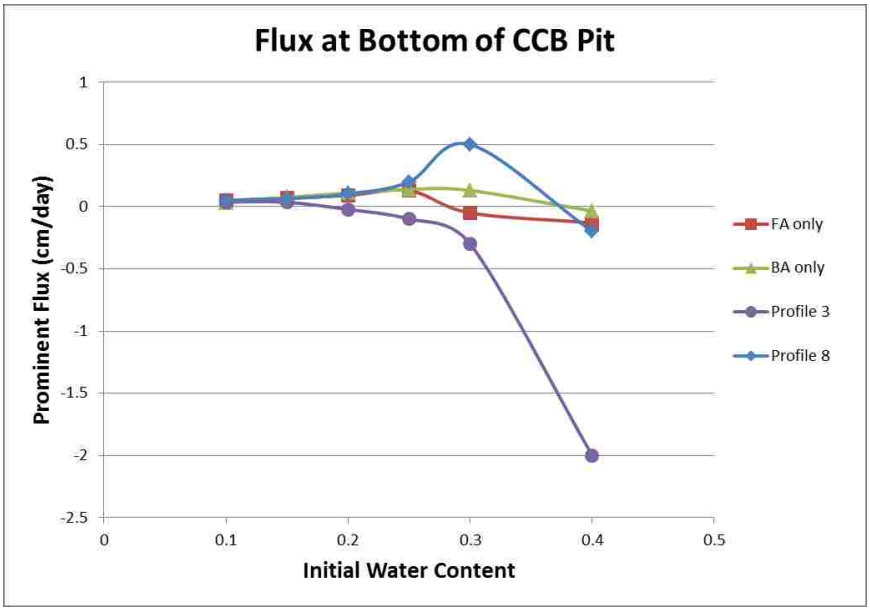

Root Water Uptake

Results of the model without the root water uptake simulation show no significant impact on the flux at the top soil and CCB pit interface for both the fly ash only and bottom ash only profiles during the 10 year duration. About 40 cm of water does not evaporate, but no water moves from the top soil to the CCB pit during the 10 years of the simulation. This indicates that the top soil layer is storing additional moisture. Results of surface infiltration, root water uptake, and evaporation both with and without root water uptake simulation can be seen in figures 23, 24, and 25.

Figure 23: Cumulative Infiltration of Baseline Model

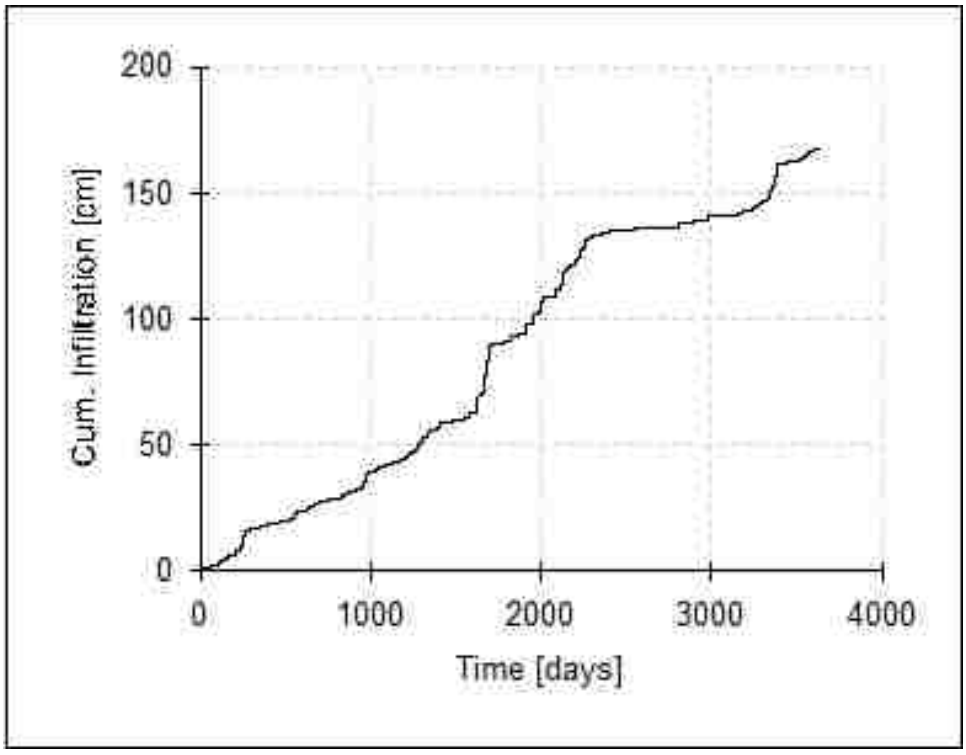

Figure 24: Cumulative Root Water Uptake (top) and Cumulative Evaporation (bottom) for Baseline Model

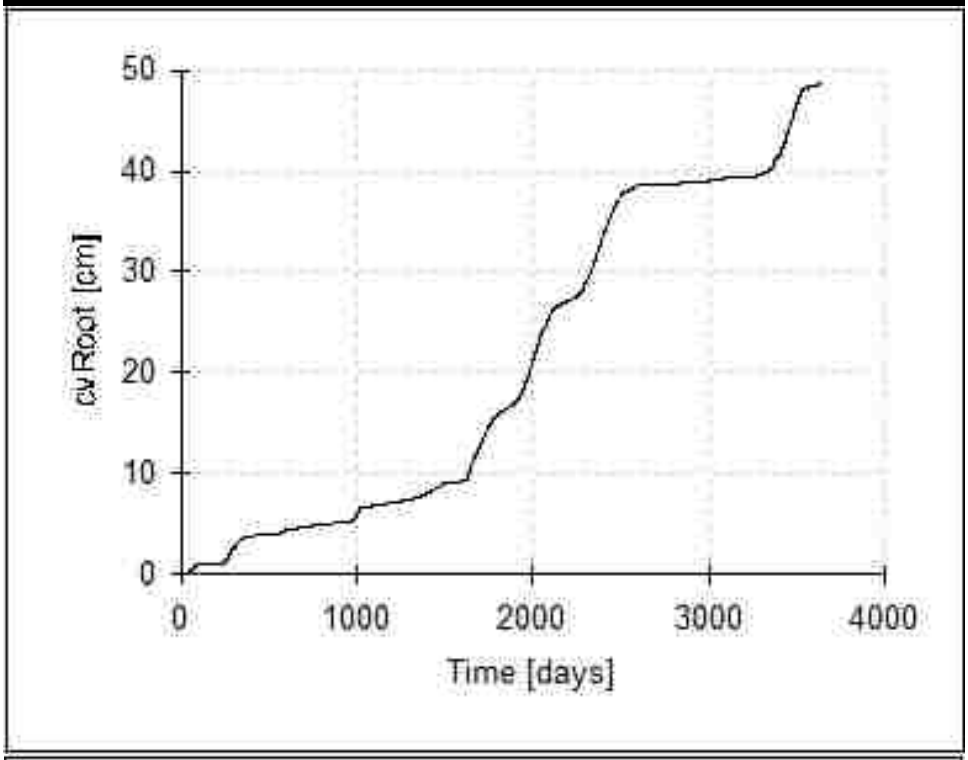

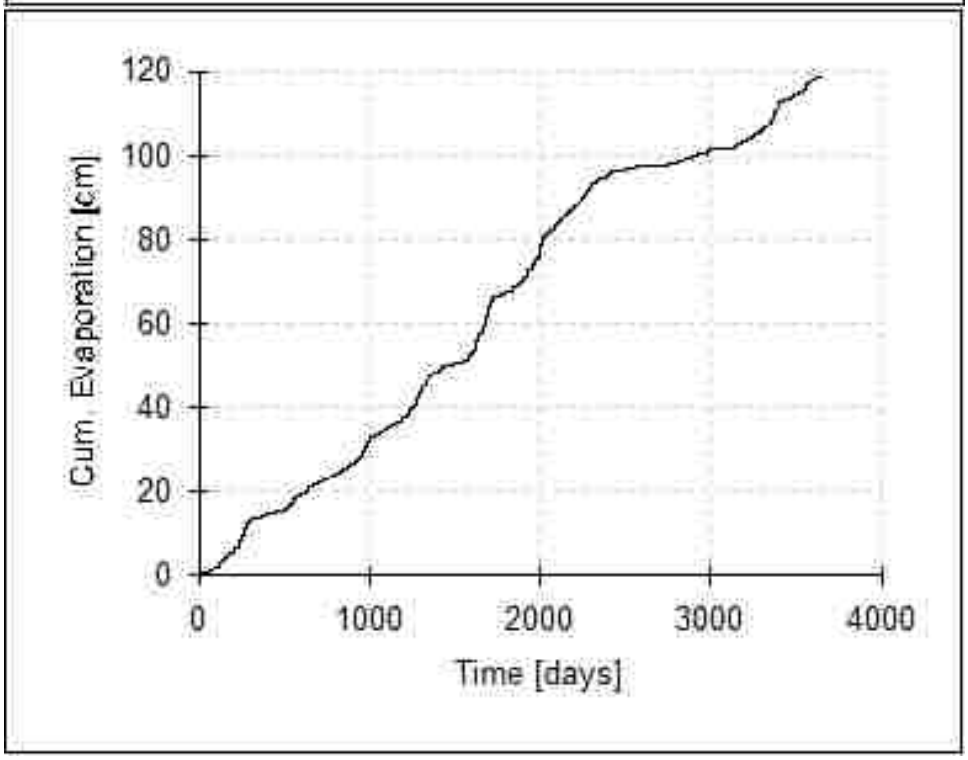

Figure 25: Cumulative Evaporation without Root Water Uptake

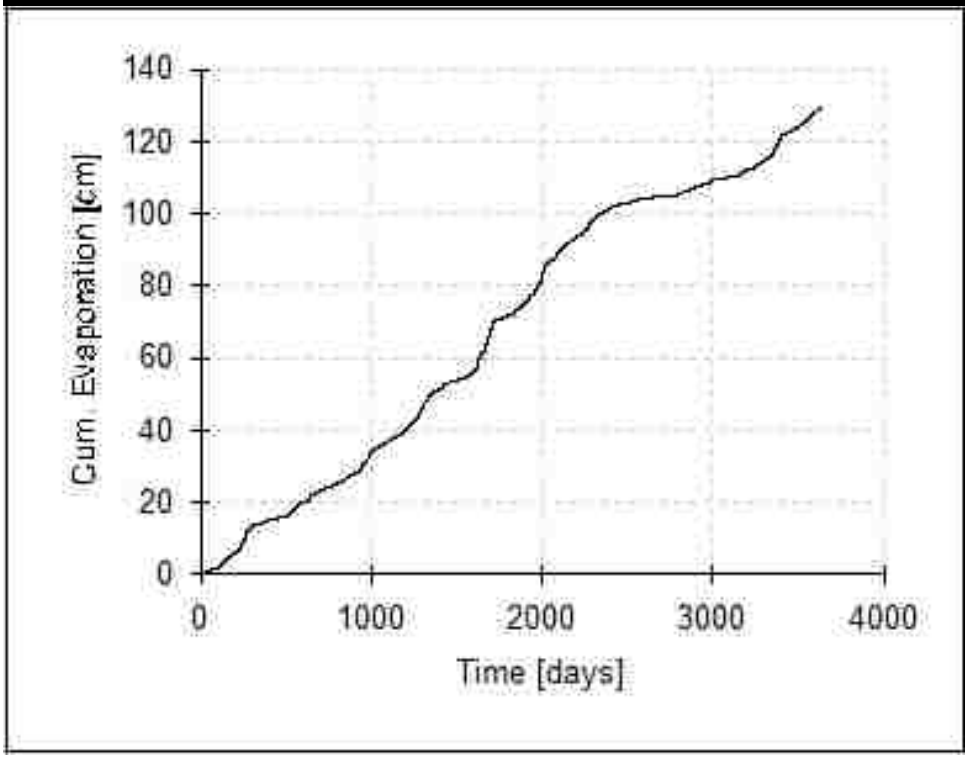

Upper Boundary Condition

Results from the model simulation with the upper boundary condition set to a zero constant flux and no root water uptake simulation showed no significant impact on the movement of water within or below the CCB pit for the fly ash only and bottom ash only profiles, these were the only profiles simulated for this condition.

Extended Simulation Duration

The results for the 100 year simulation indicate equilibrium had not been reached within the extended duration for both fly ash only and bottom ash only profiles. Minimal fluxes (less than 5×10^{-4} cm/day) were still occurring throughout the profiles after the 100 year duration.

Focused Recharge on Surface Scenario

The cumulative surface infiltration results from the focused recharge scenario can be seen in figure 26, showing greater magnitudes of infiltration than the baseline model (figure 23). The surface focused recharge flux vs. time and water content with depth results can be seen in figures 27 and 28. The top soil shows highly varied moisture contents during the focused recharge simulation.

The fly ash only profile simulation results from focused recharge show the CCB pit wetting throughout the entire depth of the pit within the time duration of the simulation. The picture cliffs sandstone material begins to show wetting at the interface with the CCB pit near the end of the simulation. The bottom ash only profile simulation displays the CCB pit wetting at top soil interface at 8 years and continue wetting downward through the pit throughout the extent of the simulation. The bottom ash only profile, however, never experiences wetting at the bottom of the CCB pit throughout the 20 year simulation.

Figure 26: Cumulative Infiltration into Top Soil for Surface Focused recharge Model Simulation

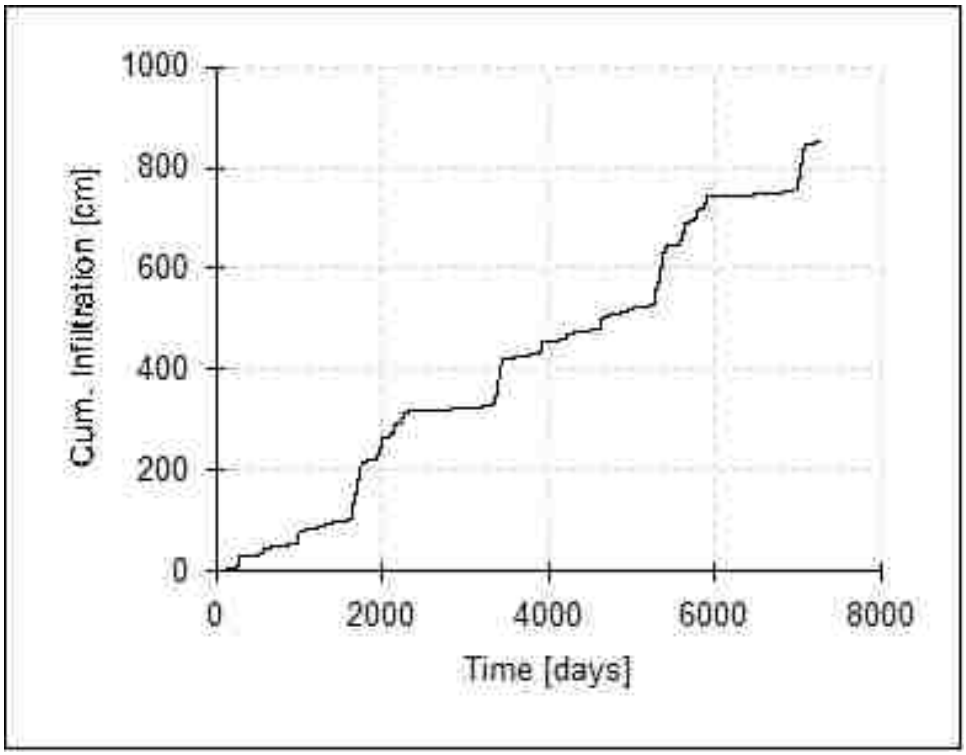

Figure 27: Focused Recharge Flux for Fly Ash Only Profile (top) and Bottom Ash Only Profile (bottom)

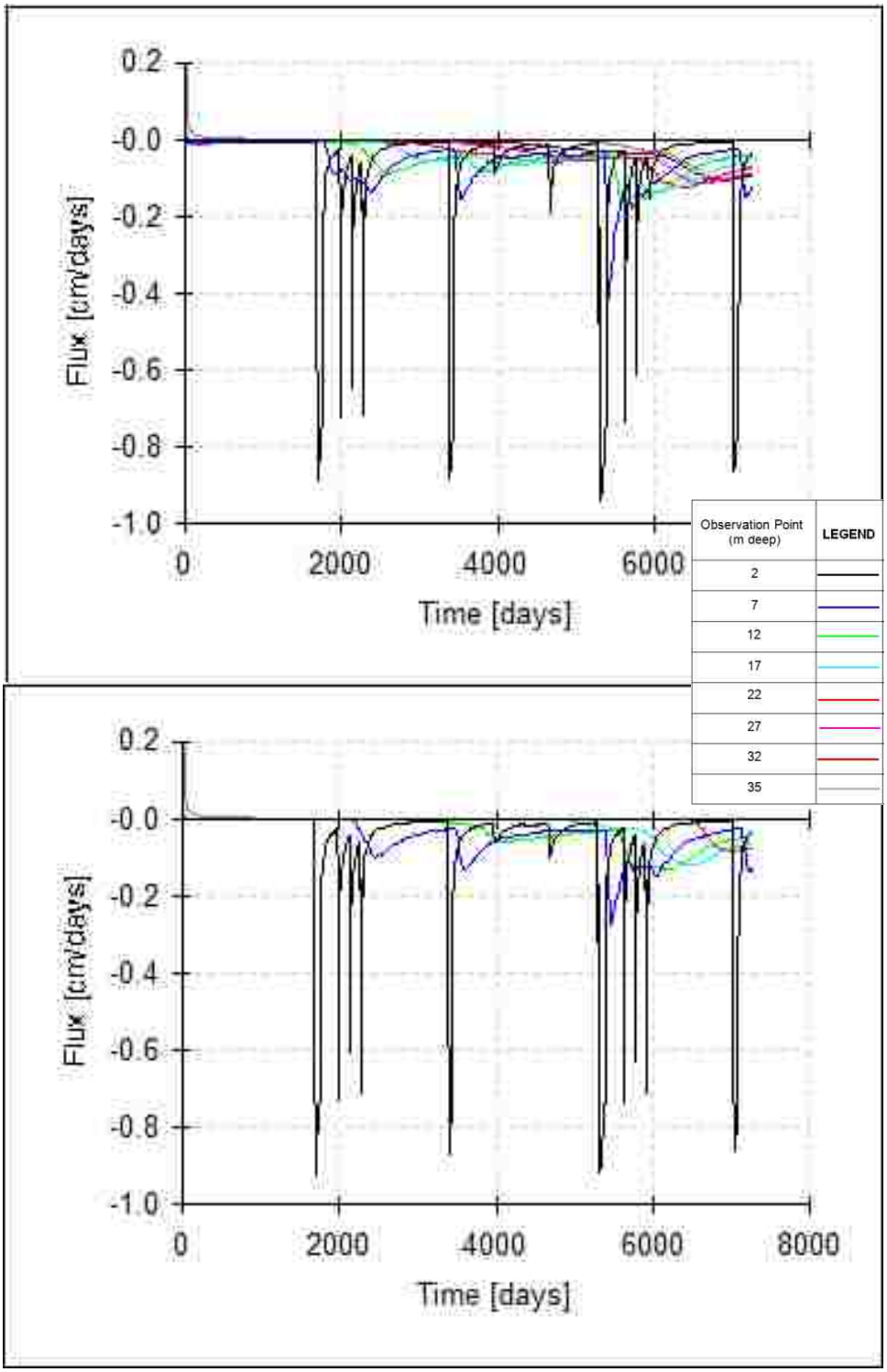

Figure 28: Focused Recharge Water Content vs. Depth for Fly Ash (top) and Bottom Ash (bottom) Only Profiles

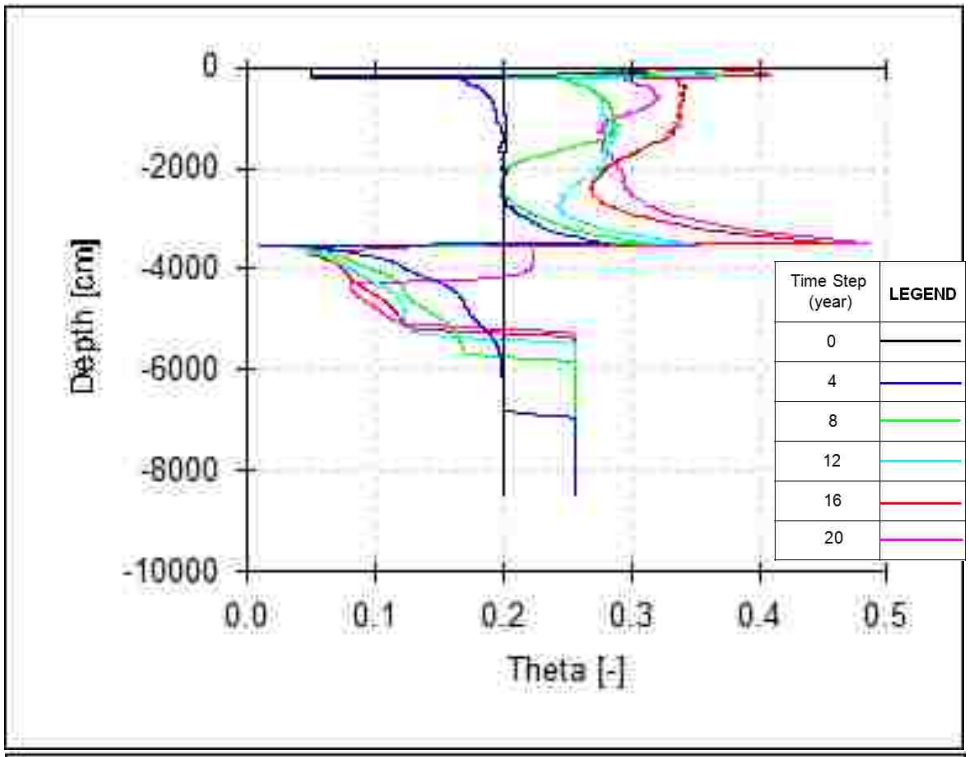

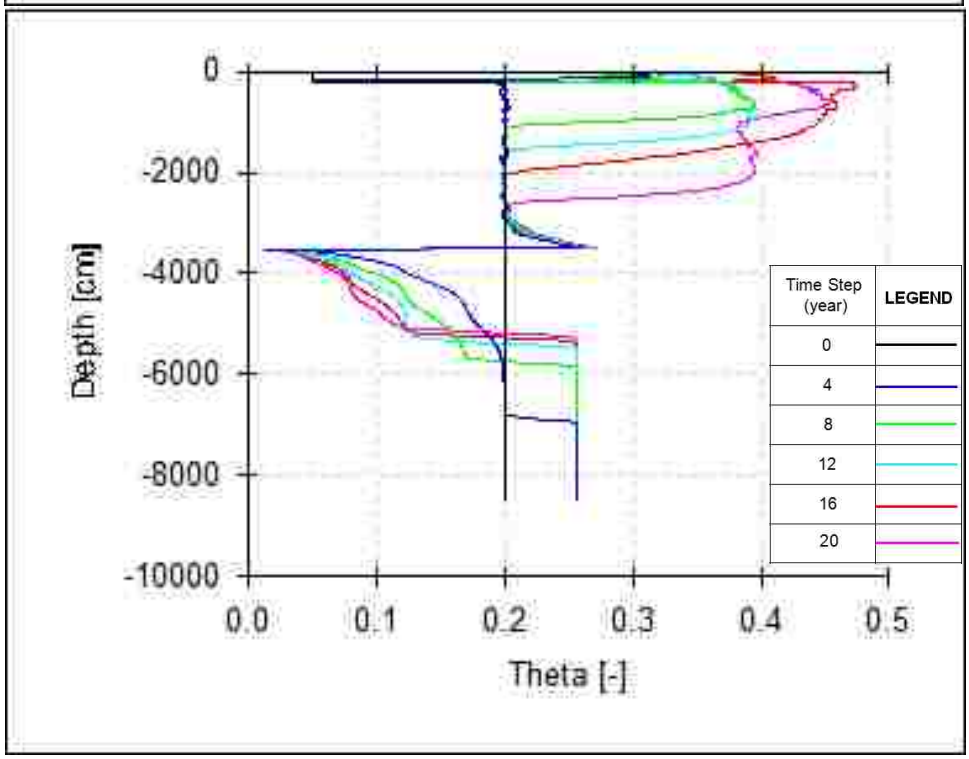

Presence of Water Table

The results of a water table present at the bottom of the CCB pit are shown in figures 29 and 30. It is important to note the difference in the scale of the vertical axis in these figures to previous figures; the depth below the surface shown is only 35 m due to the change in lower boundary condition for this simulation. For both the fly ash only and bottom ash only profiles, there is a large, initial upward flux at the bottom of the pit during the first year of the simulation. The fly ash only profile, throughout the simulation, is drying from the top soil interface downward whereas the bottom ash only profile shows no such behavior.

Lowering of Water Table Scenario

The results for a scenario in which a water table is lowered from a depth of 35 to 85 m can be viewed in figures 31 and 32. The fly ash only and bottom ash only profiles provide similar results to one another, an initial downward flux of approximately 0.2 cm /day at the bottom of the CCB pit. The profiles show a drying of the pictured cliff sandstone as well as the CCB pit, both originating from the interface between the two.

Figure 29: Water Table at Bottom of CCB Pit Flux Results for Fly Ash (top) and Bottom Ash (bottom) Only Profiles

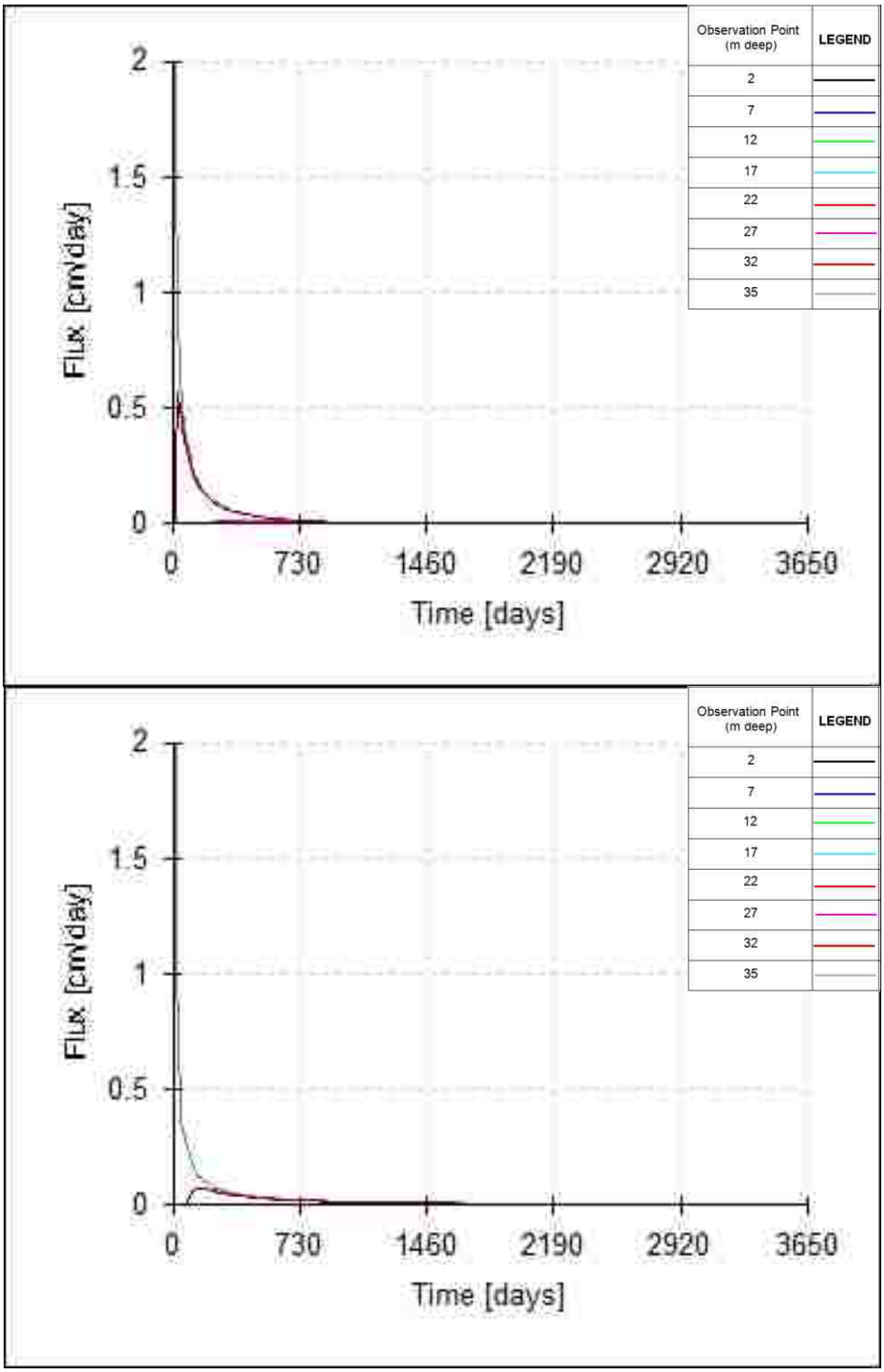

Figure 30: Water Table Present Water Content vs. Depth Results for Fly Ash(top) and Bottom Ash (bottom) Only Profiles

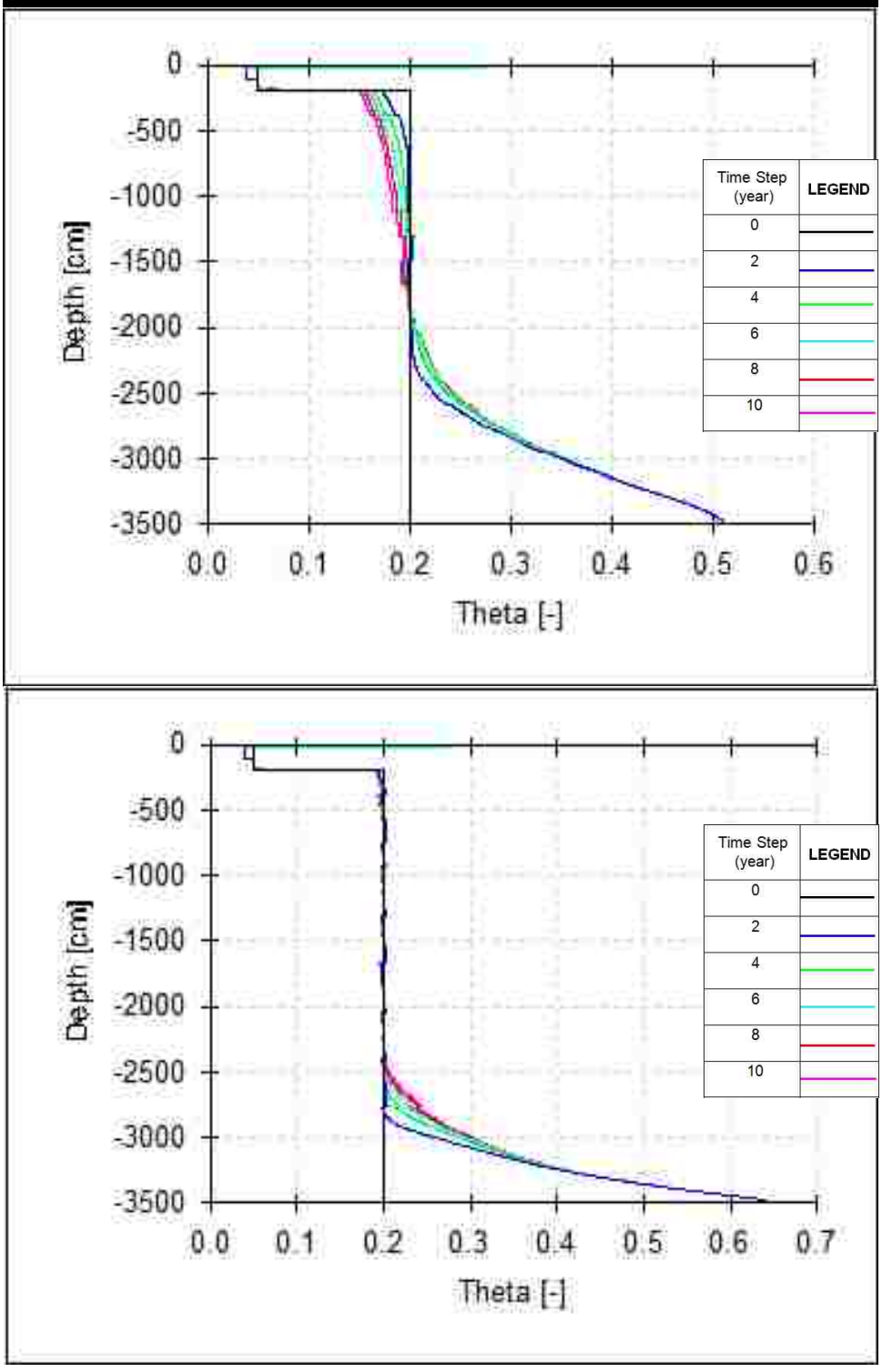

Figure 31: Lowering of Water Table Flux Results for Fly Ash Only Profile (top) and Bottom Ash Only Profile (bottom)

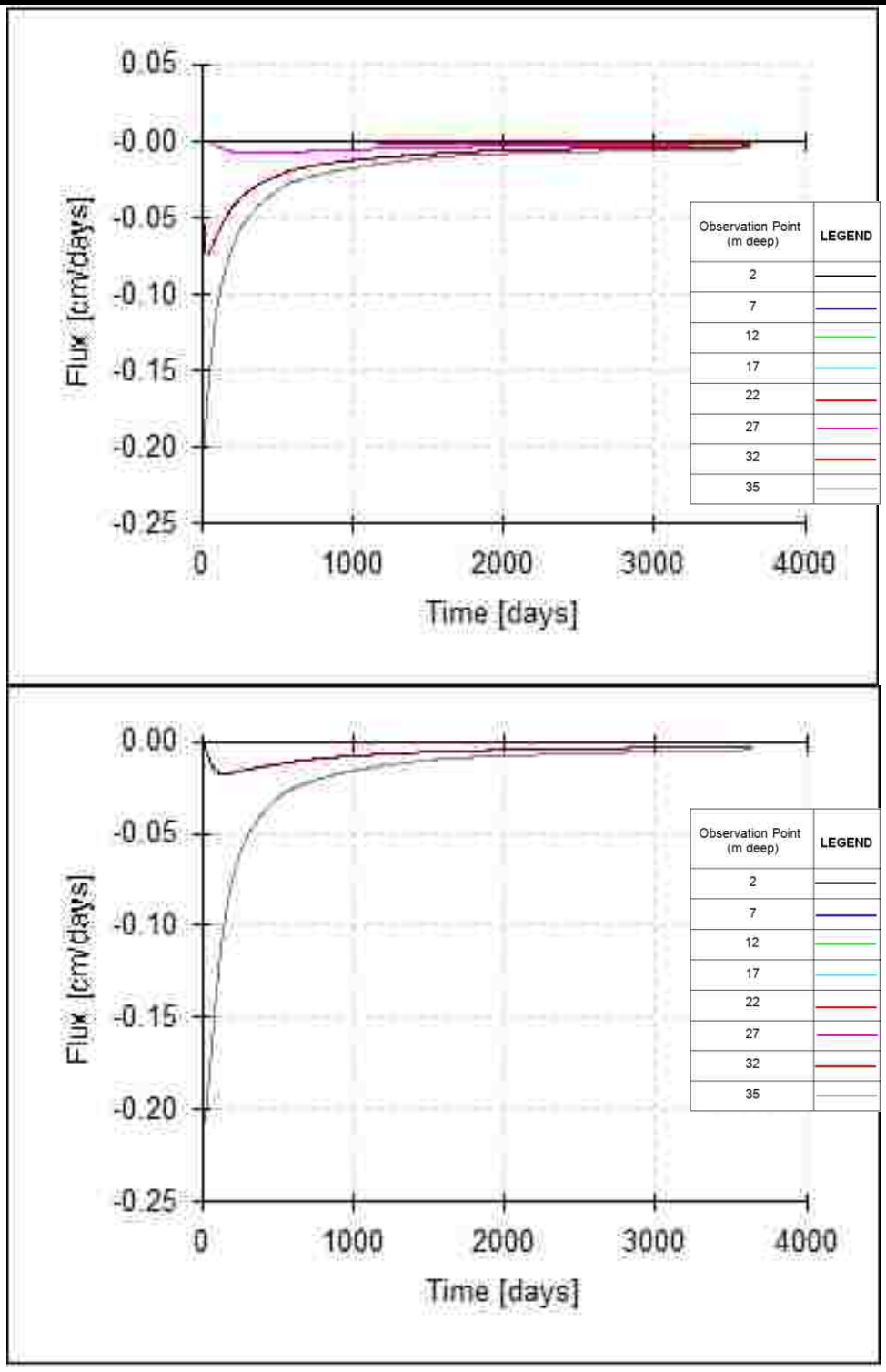

Figure 32: Lowering of Water Table Water Content Results for Fly Ash Only (top) and Bottom Ash Only (bottom) Profiles

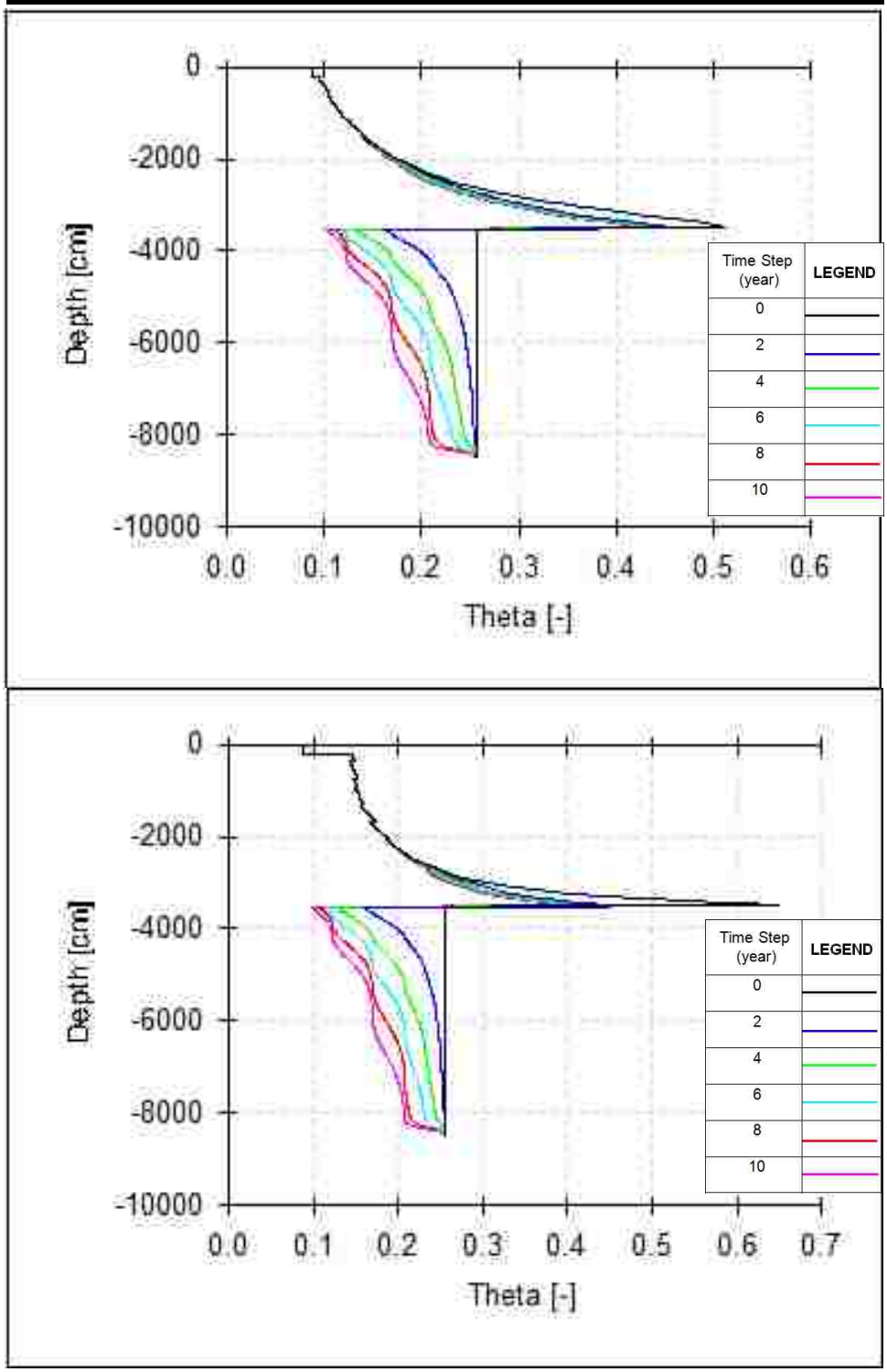

9. MODELING DISCUSSION

The water fluxes observed in the model simulations appear to be primarily resulting from the initial conditions. Differences in total head result in the gradients driving the observed fluxes. Results from the simulations with a zero constant flux upper boundary condition and no root water uptake simulation show that no water infiltrates past the root zone during the 10 year duration of the baseline model and thus fluxes in the CCB pit are primarily due to initial water contents. The movement of water across the bottom of the CCB pit is an upward flux in most simulations; this is a result of initial conditions once again and variations between material properties resulting in an upward gradient driving the movement of water. A summary of the flux of water at the 2 m and 35 m deep observation points, the top and bottom of the CCBs, respectively, are plotted at 1, 5, and 10 years in figures 33 and 34, respectively. The data points represent the average flux for all baseline simulations and the whiskers represent the minimum and maximum fluxes.

Figure 33: Top Soil and CCB Interface Results

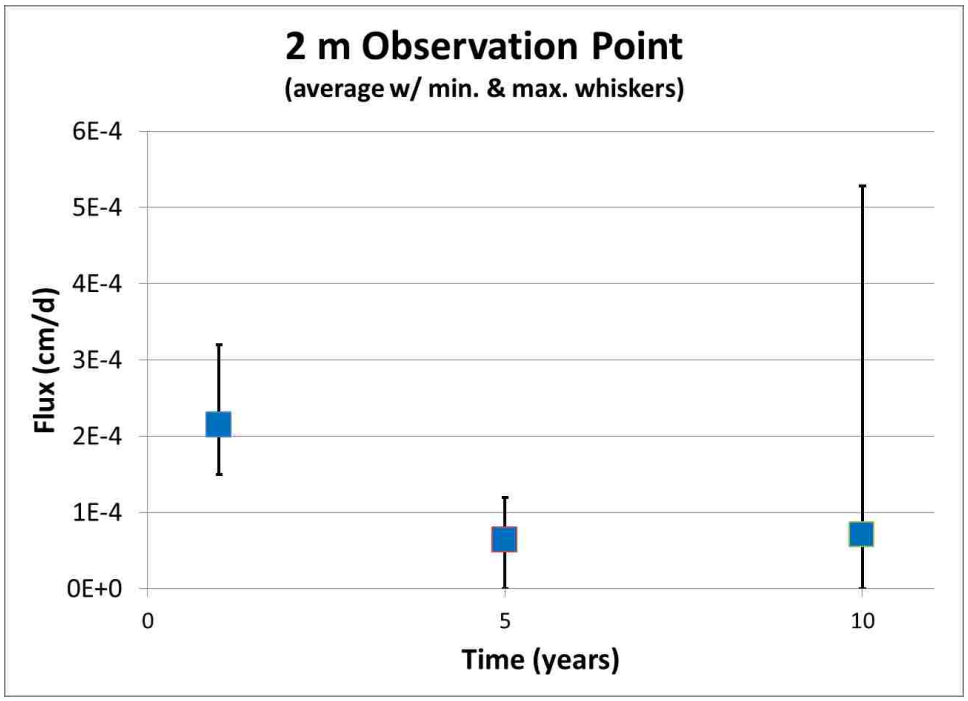

Figure 34: CCB and Pictured Cliff Sandstone Interface Results

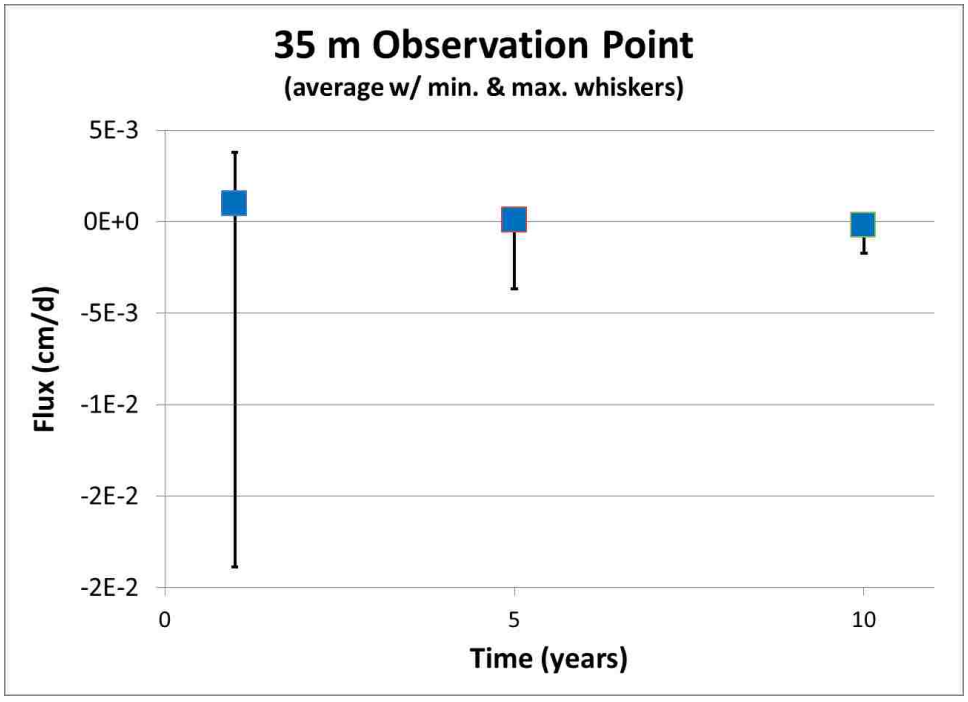

Figures 35, 36, and 37 show the MCCs, K vs. h, and K vs. θ of materials for profile 3, respectively. It can be seen with these MCCs that the initial conditions existing at the interfaces between different materials results in significant pressure head differences which can induce water movement. For example, at the initial moisture content of 0.2, pressure heads of fly ash and bottom ash are approximately 1000 cm and 316 cm, respectively. Thus, water will initially tend to move from bottom ash to fly ash. Water accumulates at the interface between the pictured cliffs sandstone and CCBs because of the initial upward gradient. Also, as water drains towards equilibrium, the K of the pictured cliffs sandstone becomes very low.

Figure 36: MCCs for Materials in Profile 3

Figure 35: log K vs. log h for Materials in Profile 3

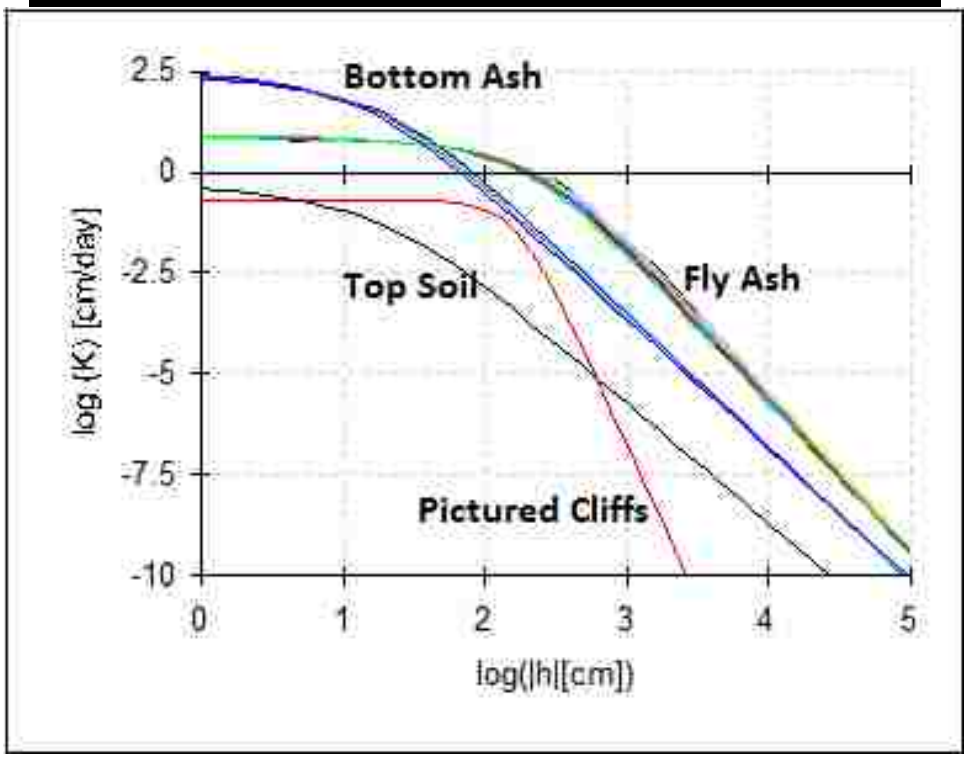

Figure 37: log K vs Water Content for Materials in Profile 3

When ponding is allowed to accumulate on the surface, water is able to infiltrate through the top soil and into the CCB pit. It can be seen in figure 28 that water moves more rapidly through the fly ash only profile than the bottom ash only profile. Water is able to infiltrate through the entire depth of the CCB pit between 8 and 12 years in the fly ash only profile; whereas in the bottom ash only profile, water still has not infiltrated the entire CCB pit at 20 years. This difference in infiltration depth is due to bottom ash requiring a higher moisture content compared to fly ash in order to transmit the water that is moving from the top soil into the CCB pit. Thus, because it wets up more to transmit this flux, water does not move as deep in the bottom ash profile compared to the fly ash profile. The MCCs and K vs. suction head of the top soil and CCBs present

beneath the top soil for these simulations are displayed in figures 38 and 39, respectively.

Figure 38:MCC of Top Soil, Fly Ash, and Bottom Ash at Interface between Top Soil and CCBs for Focused Recharge Simulations

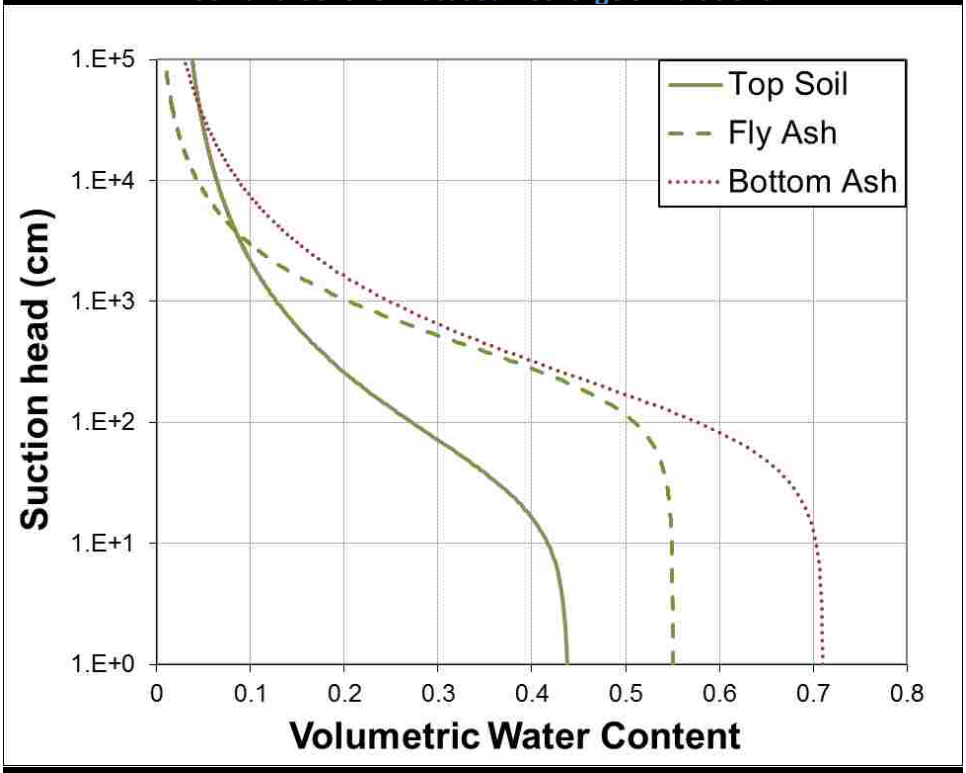

Figure 38: K vs. Suction Head for Top Soil, Fly Ash, and Bottom Ash at Interface between Top Soil and CCBs for Focused Recharge Simulations

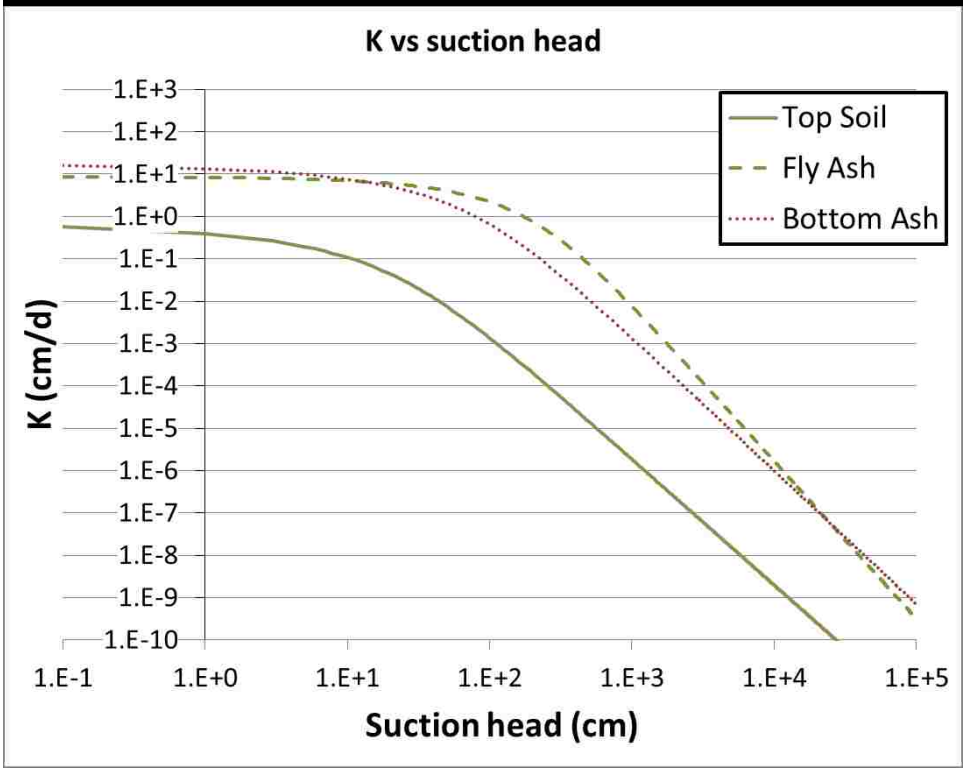

The focused recharge scenario only accounts for one dimensional flow, and therefore does not consider the effect lateral water movement would have on this scenario. It does, however, display the potential for water movement through a CCB pit if substantial ponding is present at the surface causing focused recharge.

Results from the scenario of a water table being present at the bottom of the CCB pit show capillary rise at the water table interface. Within the fly ash only profile, there is also some drying of the CCBs near the top of the CCB pit whereas the bottom ash only profile does not display this behavior.

The simulated lowering of the water table shows little drainage into the picture cliff sandstone. The fly ash only profile shows a downward flux occuring further up from the bottom of the CCB pit than the bottom ash only profile.

Sensitivity Analyses

The initial water content present in the system appears to have a significant impact on the downward flux at the bottom of the CCB pit. At initial water contents in excess of about 25%, downward fluxes in excess of 0.05 cm/day occur around 25% and above. This result suggests that disposal practices may influence the flux at the bottom of the CCB pits. The significant fluxes at the bottom of the pits did not occur for a prolonged period of time, but briefly, once again providing evidence that fluxes are related to equilibration of initial conditions between materials.

The sensitivity of the simulation to the root water uptake is small over the 10 year duration. With no root water uptake being simulated, there was still not enough infiltration to enter the CCB pit after 10 years. The results show that evaporation is the dominant factor in evapotranspiration. With no root water uptake, water may eventually infiltrate into the CCB pits, but root water uptake by vegetation likely to be present in the arid climate would most likely eliminate infiltration moving beyond the root zone under the conditions simulated. This is consistent with literature concerning aquifer recharge in arid environments (Scanlon, 2006).

Controlling Factor

The low permeability of the pictured cliffs sandstone has shown to be the controlling factor within all the simulations. The low permeability relative to CCB materials forms an impediment to flow at the interface. At a pressure head of about -300 cm, the fly ash has a hydraulic conductivity of 0.316 cm/d and Pictured Cliff Sandstone has a conductivity of 0.001 cm/d. This is also the only material in the model for which there were no properties measured in the laboratory. Results could vary with different material properties present beneath the CCB pits.

Properties as a Function of Density

Modeling the CCB hydraulic properties as a function of density did not appreciably affect the amount of water that passed into and out of the CCB pit. This is largely due to the lack of infiltration past the top soil. Water movement within the CCB pits was influenced by the variable hydraulic properties, but not to a significant degree. For the focused recharge simulation, if an average material property would have been used for the CCBs, then exchange of water across the interface between the top soil and CCBs may have been different. For most of the simulations in this study, the modeling of material properties as a function of density did not significantly alter the results.

10. MODELING CONCLUSIONS

Results from this one dimensional numerical modeling have shown that infiltration from the surface into CCB pits has the greatest potential of occurring in situations which focused recharge is allowed to occur. In all other scenarios, evapotranspiration is effective at keeping water from traveling further than the root depth of 1 m under the conditions provided for this model. If a water table is present at the bottom of the CCB pit, simulation results suggest that water movement will be upward into the CCBs. Should the water table be lowered at a

later date, results suggest that little water will drain from the CCBs into the underlying material under conditions of this model. Initial water content impacts the flux at the bottom of the CCB pit above 25% water content. Water movement simulated in this study is primarily due to the redistribution of water between layers due to equilibrating initial conditions. Further studies should include testing of the picture cliff sandstone to include measured properties of this material in order to better predict fluxes from the CCB pits into the underlying material.

11. CONCLUSIONS

Saturated hydraulic properties of both fly ash and bottom ash vary as a function of density. Unsaturated hydraulic properties of fly ash show a trend in variations as a function of density whereas bottom ash unsaturated hydraulic properties show less trend in variations associated with density. Further testing may be needed to better define these variations as a function of density due to the high variability of bottom ash results. The variations that were found as a function of density did not appreciably affect the amount of water that passed into and out of the CCB pit.

The laboratory methods used in this study have shown that methods common to soil testing may be utilized to predict the changes in both saturated

and unsaturated hydraulic properties of fly ash and bottom ash as a function of density.

Infiltration through the top soil and into landfill pits of CCBs is most likely in situations where focused recharge is allowed to occur. Under focused recharge conditions, water infiltrates through a landfill pit of fly ash only faster than a pit of bottom ash only. If focused recharge is not occurring on the surface and desert shrubs are present, it is not likely that surface water will infiltrate past the root zone. Initial water content begins to impact the flux at the bottom of the CCB pit above 25%. Water movement, under conditions simulated, was primarily due to equilibration of initial conditions. The low permeability of the pictured cliffs sandstone have been shown to have a strong impact upon the flux from the bottom of the CCB pit at the SJM. Upward gradients were observed at the interface between CCBs and pictured cliffs sandstone due to the hydraulic properties, providing an impediment to flow. Future studies should provide testing of the pictured cliffs sandstone hydraulic properties.

APPENDIX

Grain Size Distribution

Sieve Analysis (dry)							
Date tested:	6/28/2011						
Project Name:	SJM						
Sample ID:	June Fly Ash						
Wt. of Dry Sample (g):		37.6					

Sieve #	Diameter (mm)	Mass of Empty Sieve (g)	Mass of Sieve + Sample Retained (g)	Sample Retained (g)	Sample Retained - accu (g)	% Retained	% Passing
4	4.750	503.2	503.2	0.0	0.0	0.0	100.0
10	2.000	465.0	465.0	0.0	0.0	0.0	100.0
20	0.840	412.4	412.5	0.1	0.1	0.0	100.0
40	0.425	381.7	381.9	0.2	0.3	0.1	99.9
60	0.250	361.5	362.3	0.8	1.1	0.3	99.6
140	0.106	345.3	364.2	18.9	20.0	7.6	91.9
200	0.075	338.9	355.2	16.3	36.3	6.6	85.4
Pan	--	362.9	364.3	1.4	37.7	0.6	--
			pre-wash total - losses:		248.1		

Hydrometer

Project Name:	San Juan Mine											
Sample ID:	June FA											
Hydrometer type:	ASTM 152H		Zero correction:	4.00		Meniscus:	0.0					
Dispersing agent:	$NaPO_3$ (Calgon)		Amount used:	4% & 125mL								
G_s of sample:	2.00		CF a =	1.25	(EQ 5.8 in lab manS	ample finer than #200			85.4%			
Mass sample (dry), g:	50		% Finer:			Control Sieve #:	200					

Date	Time of reading	Elapsed time, min	Temp, °C	Actual Hyd. Reading, R_a	Corr. Hyd. Reading R_c	Act % Finer	Adj % Finer	Hyd. Corr. Only for meniscus, R	L from table 6-5	L/t	K	D, mm
		0	22	--								
		0.25	22	45.0	41.7	103.7	88.59	45.0	8.9	35.6000	0.0171	0.1021
		0.50	22	43.0	39.7	98.8	84.33	43.0	9.2	18.4000	0.0171	0.0734
		1	22	40.0	36.7	91.3	77.95	40.0	9.7	9.7000	0.0171	0.0533
		2	22	36.0	32.7	81.3	69.44	36.0	10.4	5.2000	0.0171	0.0390
		4	22	30.0	26.7	66.4	56.68	30.0	11.4	2.8500	0.0171	0.0289
		8	22	23.0	19.7	48.9	41.79	23.0	12.5	1.5625	0.0171	0.0214
		15	22	18.0	14.7	36.5	31.16	18.0	13.3	0.8867	0.0171	0.0161
		30	22	15.0	11.7	29.0	24.78	15.0	13.8	0.4600	0.0171	0.0116
		60	22	13.0	9.7	24.0	20.52	13.0	14.2	0.2367	0.0171	0.0083
		120	22	9.0	5.7	14.1	12.02	9.0	14.8	0.1233	0.0171	0.0060
		260	22	8.0	4.7	11.6	9.89	8.0	15.0	0.0577	0.0171	0.0041
		484	22	7.0	3.7	9.1	7.76	7.0	15.2	0.0314	0.0171	0.0030
		1,439	22	7.0	3.7	9.1	7.76	7.0	15.2	0.0106	0.0171	0.0018
		2,877	22	6.0	2.7	6.6	5.6	6.0	15.3	0.0053	0.0171	0.0012
		4,243	22	6.0	2.7	6.6	5.6	6.0	15.3	0.0036	0.0171	0.0010

Sieve Analysis (dry)

Date tested:	6/28/2011		
Project Name:	SJM		
Sample ID:	**June Bottom Ash**		
Wt. of Dry Sample (g):	228.9		

Sieve #	Diameter (mm)	Mass of Empty Sieve (g)	Mass of Sieve + Sample Retained (g)	Sample Retained (g)	Sample Retained - accu (g)	% Retained	% Passing
4	4.750	512.9	541.5	28.6	28.6	9.7	90.3
10	2.000	487.8	517.6	29.8	58.4	10.1	80.2
20	0.840	412.4	472.4	60.0	118.4	20.4	59.8
40	0.425	381.7	419.1	37.4	155.8	12.7	47.2
60	0.250	361.5	387.3	25.8	181.6	8.8	38.4
140	0.106	345.3	383.3	38.0	219.6	12.9	25.5
200	0.075	338.9	348.3	9.4	229.0	3.2	22.3
Pan	--	362.9	363.2	0.3	229.3	0.1	--
			pre-wash total - losses:		294.8		

Hydrometer

Project Name: San Juan Mine
Sample ID: June BA
Hydrometer type: ASTM 152H | Zero correction: 4.00 | Meniscus: 0.0
Dispersing agent: $NaPO_3$ (Calgon) | Amount used: 4% & 125mL
G_s of sample: 2.06 | CF a = 1.21 (EQ 5.8 in lab manS | ample finer than #200 22.3%
Mass sample (dry), g: 50 | % Finer: | Control Sieve #: 200

Date	Time of reading	Elapsed time, min	Temp, °C	Actual Hyd. Reading, R_a	Corr. Hyd. Reading R_c	Act % Finer	Adj % Finer	Hyd. Corr. Only for meniscus, R	L from table 6-5	L/t	K	D, mm
		0	22	--								
		0.25	22	47.0	43.7	105.6	23.56	47.0	8.6	34.4000	0.0166	0.0975
		0.50	22	45.0	41.7	100.8	22.48	45.0	8.9	17.8000	0.0166	0.0701
		1	22	42.0	38.7	93.5	20.86	42.0	9.4	9.4000	0.0166	0.0509
		2	22	36.0	32.7	79.0	17.62	36.0	10.4	5.2000	0.0166	0.0379
		4	22	30.0	26.7	64.5	14.38	30.0	11.4	2.8500	0.0166	0.0281
		8	22	24.0	20.7	50.0	11.14	24.0	12.4	1.5500	0.0166	0.0207
		15	22	19.0	15.7	37.9	8.45	19.0	13.2	0.8800	0.0166	0.0156
		30	22	15.0	11.7	28.2	6.29	15.0	13.8	0.4600	0.0166	0.0113
		60	22	12.0	8.7	20.9	4.67	12.0	14.3	0.2383	0.0166	0.0081
		120	22	10.0	6.7	16.1	3.59	10.0	14.7	0.1225	0.0166	0.0058
		248	22	9.0	5.7	13.7	3.05	9.0	14.8	0.0597	0.0166	0.0041
		473	22	8.0	4.7	11.3	2.51	8.0	15.0	0.0317	0.0166	0.0030
		1,428	22	8.0	4.7	11.3	2.51	8.0	15.0	0.0105	0.0166	0.0017
		2,862	22	7.0	3.7	8.8	2.0	7.0	15.2	0.0053	0.0166	0.0012
		4,293	22	7.0	3.7	8.8	2.0	7.0	15.2	0.0035	0.0166	0.0010

Specific Gravity

	Sample: June Fly Ash (unit 4)			
	Test #	**1**	**2**	**3**
	date	6/30/2011	7/1/2011	7/4/2011
	time vacuum applied (hr)	20	24	6
M_1	mass of flask w/ water	664.9	664.9	664.9
M_2	flask w/ sample post vacuum	713.8	715	715.9
M_S	dry sample mass	97.4	100.3	102.1
M_W	$(M_1 + M_S) - M_2$	48.5	50.2	51.1
G_S initial	M_S/M_W	2.01	2.00	2.00
	Temperature (degees C)	22	22	22
	T correction	0.9996	0.9996	0.9996
G_S Corrected	Corrected Secific Gravity	2.01	2.00	2.00
G_S Final		avg. =	**2.00**	
	notes:			
	all masses in grams			
	difficult to see meniscus with ash in flask			
witnessed ash "climbing" wet walls inside neck of flask				
	vacuum applied roughly 85 kPa			

	Sample: June Bottom Ash (unit 4)			
	Test #	**1**	**2**	**3**
	date	7/5/2011	7/7/2011	7/8/2011
	time vacuum applied (hr)	17	27	20
M_1	mass of flask w/ water	664.9	664.9	664.9
M_2	flask w/ sample post vacuum	713.1	715.7	719.1
M_S	dry sample mass	95.5	97.5	104.9
M_W	$(M_1 + M_S) - M_2$	47.3	46.7	50.7
G_S initial	M_S/M_W	2.02	2.09	2.07
	Temperature (degees C)	22	21	21
	T correction	0.9996	0.9998	0.9998
G_S Corrected	Corrected Secific Gravity	2.02	2.09	2.07
G_S Final		avg. =	**2.06**	

Relative and Clod Density

	Relative Density			
mold diameter	6.00	in		
mold height	4.60	in		
mold Area	28.27	in^2		
mold Volume	130.06	in^3 =	0.08	ft^3

Sample	**FA**	**BA**		
dump weight w/ mold	19.14	17.66	lb	
sample mass	4.73	3.25	lb	
vibration time	8.00	8.00	min	
top of mold to top of plate (avg)	0.45	0.46	in	
change in sample height	0.69	0.70	in	
new sample volume	0.06	0.06	ft^3	
dump dry density	**62.89**	**43.21**	pcf	
"max" dry density	**73.94**	**50.80**	pcf	
dump dry density	**1007.39**	**692.20**	kg/m^3	
"max" dry density	**1184.37**	**813.81**	kg/m^3	

surcharge weight	57.04	lb
pressure	2.02	psi
mold mass	14.41	lb
top plate thickness	0.24	in

Sample	**FA**	**BA**
ΔH1	0.41	0.48
ΔH2	0.46	0.42
ΔH3	0.44	0.44
ΔH4	0.47	0.50

*distances in inches from top of mold to top of plate after vibration

Clod Density

Clod sample: Juniper Pit 04 at 124 ft deep

ring #	d (mm)	L (mm)	mass (g)	Vol. (mm^3)
1	15.88	28.37	11.17	5618.89
2	15.82	28.70	11.38	5641.37
3	15.87	28.63	11.76	5663.24

ring #	1	2	3	
mass ring + can + wet sample	M_1	33.13	33.61	33.55	
mass ring + can + dry sample	M_2	31.43	31.97	31.60	
mass can	M_C	14.57	14.53	14.18	
mass dry sample	M_S	5.69	6.06	5.66	
dry	density	1012.66	1074.21	999.43	kg/m^3
dry density		avg	**1028.76**	kg/m^3	
dry density		=	**64.22**	pcf	

notes:

drying oven 110 degrees C for 48 hrs

water added to sample prior to extraction to ease process. In situ content NOT found

Compressibility

Sample:	June Fly Ash											
H_0 =	0.875	in	diameter =	2.4	in	Volume =	3.958407					
orig. dens. =	62.86	lb/cf										
					trial a	trial a	trial b	trial b	trial c	trial c	trial d	trial d
	Interval	wt of stone	added weight	tot psi	delta H	new dens.	delta H	new dens.	delta H	new dens.	delta H	new dens.
	0	0	0	0	0	62.86	0	62.86	0	62.86	0	62.86
	1	1.141	5.0105	6.897	0.016	64.03253589	0.02	64.3321	0.023	64.55862	0.02	64.3321
	2	1.141	10.493	14.17	0.024	64.63448687	0.026	64.78675	0.032	65.24786	0.028	64.93973
	3	1.141	17.742	23.78	0.044	66.19007019	0.033	65.32535	0.042	66.03115	0.035	65.48089
	4	1.141	24.779	33.12	0.06	67.48950715	0.039	65.7942	0.054	66.99628	0.041	65.95198
	5	1.141	35.9615	47.95	0.081	69.27449411	0.049	66.59074	0.068	68.15855	0.053	66.91478
	6	1.141	44.8105	59.68	0.087	69.80196488	0.053	66.91478	0.074	68.6691	0.06	67.48951
	7	1.141	60.7405	80.81	0.105	71.43369912	0.066	67.99005	0.088	69.89066	0.074	68.6691
	8	1.141	71.5625	95.16	0.124	73.24094318	0.07	68.32789	0.113	72.18366	0.08	69.18736
	9	1.141	96.3415	128	0.129	73.73183422	0.084	69.53723	0.116	72.46897	0.096	70.60841
	10	1.141	107.439	142.7	0.134	74.22934997	0.088	69.89066	0.121	72.94953	0.1	70.97284

Sample:	June Bottom Ash											
H_0 =	0.875	in	diameter =	2.4	in	Volume =	3.958407					
orig. dens. =	43.19	lb/cf										
					trial e	trial e	trial f	trial f	trial g	trial g	trial h	trial h
	Interval	wt of stone	added weight	tot psi	delta H	new dens.	delta H	new dens.	delta H	new dens.	delta H	new dens.
	0	0	0	0	0	43.19	0	43.19	0	43.19	0	43.19
	1	1.141	5.0105	6.897	0.042	45.36890296	0.033	44.88396	0.062	46.48499	0.055	46.08817
	2	1.141	10.493	14.17	0.075	47.2403702	0.061	46.42788	0.097	48.57622	0.089	48.0818
	3	1.141	17.742	23.78	0.104	49.01724535	0.083	47.71755	0.126	50.457	0.118	49.92377
	4	1.141	24.779	33.12	0.123	50.25571298	0.102	48.89042	0.146	51.84128	0.139	51.34823
	5	1.141	35.9615	47.95	0.148	51.98390119	0.124	50.32263	0.17	53.60609	0.162	53.00462
	6	1.141	44.8105	59.68	0.16	52.85635827	0.139	51.34823	0.183	54.61314	0.177	54.14369
	7	1.141	60.7405	80.81	0.181	54.45575816	0.162	53.00462	0.204	56.32235	0.197	55.74085
	8	1.141	71.5625	95.16	0.193	55.41392399	0.186	54.85094	0.215	57.26105	0.207	56.57529
	9	1.141	96.3415	128	0.21	56.83052054	0.192	55.33279	0.235	59.05046	0.226	58.23158
	10	1.141	107.439	142.7	0.217	57.43510055	0.201	56.07166	0.241	59.6093	0.235	59.05046

Falling Head

Sample #:	June Fly Ash								
Diameter:	3"	Area:	7.0686	Density:	64.2	(lb/ft^3)	Length of	2.54	cm
Height(in)	1.0000	Volume:	7.0686	(in^3)					
Mass									
no soil		(g)	Date	7/7/2011					
with soil		(g)	Time						
soil	118.5	(g)							
			Area of standpipe:		5.0670	cm^2			

Test no.	h1	h2	t, s	Q (out) cm^3	T, °C	α (table 6-1)	K_T	K_{20} (cm/s)	K_{20} (cm/d)
1	56.4	45.5	900.16	55.23	22.0	0.9530	6.73E-05	6.42E-05	5.5
2	56.4	31.0	1,574.47	128.70	22.0	0.9530	1.07E-04	1.02E-04	8.8
3	61.8	54.7	484.57	35.98	22.0	0.9530	7.11E-05	6.77E-05	5.9
								7.81E-05	6.7

Sample #:	June Fly Ash								
Diameter:	3"	Area:	7.0686	Density:	64.2	(lb/ft^3)	Length of	2.54	cm
Height(in)	1.0000	Volume:	7.0686	(in^3)					
Mass									
no soil		(g)	Date	11/29/2011					
with soil		(g)	Time						
soil	118.5	(g)							
			Area of standpipe:		5.0670	cm^2			

Test no.	h1	h2	t, s	Q (out) cm^3	T, °C	α (table 6-1)	K_T	K_{20} (cm/s)	K_{20} (cm/d)
1	35.1	21.5	925.78	68.91	22.0	0.9530	1.49E-04	1.42E-04	12.3
2	21.5	18.6	345.03	14.69	22.0	0.9530	1.19E-04	1.13E-04	9.8
3	49.8	25.4	1,350.38	123.63	22.0	0.9530	1.41E-04	1.34E-04	11.6
								1.30E-04	11.2

Sample #:	June Fly Ash								
Diameter:	3"	Area:	7.0686	Density:	69.5	(lb/ft^3)			
Height(in)	1.0000	Volume:	7.0686	(in^3)					
Mass									
no soil		(g)	Date	7/20/2011					
with soil		(g)	Time						
soil	128.4	(g)							
			Area of standpipe:		5.0670	cm^2			

Test no.	h1	h2	t, s	Q (out) cm^3	T, °C	α (table 6-1)	K_T	K_{20} (cm/s)	K_{20} (cm/d)
1	41.3	33.9	797.78	37.50	22.0	0.9530	6.99E-05	6.66E-05	5.8
2	33.9	25.8	1,124.43	41.04	22.0	0.9530	6.85E-05	6.53E-05	5.6
3	41.2	38.1	315.22	15.71	22.0	0.9530	7.00E-05	6.68E-05	5.8
								6.62E-05	5.7

Sample #:	June Fly Ash								
Diameter:	3"	Area:	7.0686	Density:	69.5	(lb/ft^3)			
Height(in)	1.0000	Volume:	7.0686	(in^3)					
Mass									
no soil		(g)	Date	11/30/2011					
with soil		(g)	Time						
soil	128.4	(g)							
			Area of standpipe:		5.0670	cm^2			

Test no.	h1	h2	t, s	Q (out) cm^3	T, °C	α (table 6-1)	K_T	K_{20} (cm/s)	K_{20} (cm/d)
1	33.3	28.7	504.56	23.31	22.0	0.9530	8.32E-05	7.93E-05	6.8
2	39.3	26.7	1,269.94	63.84	22.0	0.9530	8.59E-05	8.19E-05	7.1
3	48.3	33.3	1,222.13	76.01	22.0	0.9530	8.59E-05	8.19E-05	7.1
								8.10E-05	7.0

Sample #:	June Fly Ash								
Diameter:	3"	Area:	7.0686	Density:	73	(lb/ft^3)			
Height(in)	1.0000	Volume:	7.0686	(in^3)					
Mass									
no soil		(g)	Date	7/29/2011					
with soil		(g)	Time						
soil	134.7	(g)							
			Area of standpipe:		5.0670	cm^2			

Test no.	h1	h2	t, s	Q (out) cm^3	T, °C	α (table 6-1)	K_T	K_{20} (cm/s)	K_{20} (cm/d)
1	70.6	43.1	2,497.00	139.34	22.0	0.9530	5.58E-05	5.32E-05	4.6
2	43.1	33.8	1,166.12	47.12	22.0	0.9530	5.88E-05	5.61E-05	4.8
3	45.9	31.4	1,885.00	73.47	22.0	0.9530	5.69E-05	5.42E-05	4.7
								5.45E-05	4.7

Sample #:	June Fly Ash								
Diameter:	3"	Area:	7.0686	Density:	73	(lb/ft^3)			
Height(in)	1.0000	Volume:	7.0686	(in^3)					
Mass									
no soil		(g)	Date	12/3/2011					
with soil		(g)	Time						
soil	134.7	(g)							
			Area of standpipe:		5.0670	cm^2			

Test no.	h1	h2	t, s	Q (out) cm^3	T, °C	α (table 6-1)	K_T	K_{20} (cm/s)	K_{20} (cm/d)
1	51.0	33.8	1,862.00	87.15	22.0	0.9530	6.24E-05	5.94E-05	5.1
2	33.8	28.1	952.78	28.88	22.0	0.9530	5.47E-05	5.21E-05	4.5
3	27.5	23.4	644.72	20.77	22.0	0.9530	7.07E-05	6.74E-05	5.8
								5.96E-05	5.2

Sample #:	June Bottom Ash								
Diameter:	3"	Area:	7.0686	Density:	45.4	(lb/ft^3)	Length of	2.54	cm
Height(in)	1.0000	Volume:	7.0686	(in^3)					
Mass									
no soil		(g)	Date	7/21/2011					
with soil		(g)	Time						
soil	83.9	(g)							
			Area of standpipe:		5.0670	cm^2			

Test no.	h1	h2	t, s	Q (out) cm^3	T, °C	α (table 6-1)	K_T	K_{20} (cm/s)	K_{20} (cm/d)
1	60.9	20.9	80.84	202.68	22.0	0.9530	3.73E-03	3.56E-03	307.5
2	41.6	18.9	60.78	115.02	22.0	0.9530	3.66E-03	3.49E-03	301.7
3	69.7	18.4	101.03	259.94	22.0	0.9530	3.72E-03	3.55E-03	306.4
								3.53E-03	305.2

Sample #:	June Bottom Ash								
Diameter:	3"	Area:	7.0686	Density:	45.4	(lb/ft^3)	Length of	2.54	cm
Height(in)	1.0000	Volume:	7.0686	(in^3)					
Mass									
no soil		(g)	Date	12/4/2011					
with soil		(g)	Time						
soil	83.9	(g)							
			Area of standpipe:		5.0670	cm^2			

Test no.	h1	h2	t, s	Q (out) cm^3	T, °C	α (table 6-1)	K_T	K_{20} (cm/s)	K_{20} (cm/d)
1	39.5	18.1	30.29	108.43	22.0	0.9530	7.27E-03	6.93E-03	598.8
2	57.1	15.9	72.84	208.76	22.0	0.9530	4.95E-03	4.72E-03	407.9
3	39.0	13.1	38.19	131.24	22.0	0.9530	8.06E-03	7.68E-03	663.9
								6.45E-03	556.9

Sample #:	June Bottom Ash								
Diameter:	3"	Area:	7.0686	Density:	50	(lb/ft^3)			
Height(in)	1.0000	Volume:	7.0686	(in^3)					
Mass									
no soil		(g)	Date	7/24/2011					
with soil		(g)	Time						
soil	92.3	(g)							
			Area of standpipe:		5.0670	cm^2			

Test no.	h1	h2	t, s	Q (out) cm^3	T, °C	α (table 6-1)	K_T	K_{20} (cm/s)	K_{20} (cm/d)
1	68.5	23.0	130.63	230.55	22.0	0.9530	2.36E-03	2.25E-03	194.2
2	42.6	19.5	88.91	117.05	22.0	0.9530	2.48E-03	2.36E-03	204.3
3	60.3	19.8	136.85	205.21	22.0	0.9530	2.30E-03	2.19E-03	189.1
4	42.2	20.7	79.69	108.94	22.0	0.9530	2.52E-03	2.40E-03	207.7
								2.27E-03	195.9

Sample #:	June Bottom Ash								
Diameter:	3"	Area:	7.0686	Density:	50	(lb/ft^3)			
Height(in)	1.0000	Volume:	7.0686	(in^3)					
Mass									
no soil		(g)	Date	12/6/2011					
with soil		(g)	Time						
soil	92.3	(g)							
			Area of standpipe:		5.0670	cm^2			

Test no.	h1	h2	t, s	Q (out) cm^3	T, °C	α (table 6-1)	K_T	K_{20} (cm/s)	K_{20} (cm/d)
1	60.4	15.8	50.28	225.99	22.0	0.9530	7.53E-03	7.17E-03	619.9
2	36.1	14.8	32.06	107.93	22.0	0.9530	7.85E-03	7.48E-03	646.4
3	56.2	20.6	65.47	180.39	22.0	0.9530	4.33E-03	4.12E-03	356.3
4	20.6	14.4	12.19	31.42	22.0	0.9530	8.29E-03	7.90E-03	682.7
								6.26E-03	540.9

Sample #:	June Bottom Ash								
Diameter:	3"	Area:	7.0686	Density:	57	(lb/ft^3)			
Height(in)	1.0000	Volume:	7.0686	(in^3)					
Mass									
no soil		(g)	Date	11/11/2011					
with soil		(g)	Time						
soil	98.9	(g)							
			Area of standpipe:		5.0670	cm^2			

Test no.	h1	h2	t, s	Q (out) cm^3	T, °C	α (table 6-1)	K_T	K_{20} (cm/s)	K_{20} (cm/d)
1	39.5	18.0	135.44	108.94	22.0	0.9530	1.64E-03	1.56E-03	134.9
2	52.1	19.0	190.97	167.72	22.0	0.9530	1.49E-03	1.42E-03	122.8
3	37.5	19.0	124.59	93.74	22.0	0.9530	1.54E-03	1.47E-03	126.8
								1.48E-03	128.2

Sample #:	June Bottom Ash								
Diameter:	3"	Area:	7.0686	Density:	57	(lb/ft^3)			
Height(in)	1.0000	Volume:	7.0686	(in^3)					
Mass									
no soil		(g)	Date	12/8/2011					
with soil		(g)	Time						
soil	98.9	(g)							
			Area of standpipe:		5.0670	cm^2			

Test no.	h1	h2	t, s	Q (out) cm^3	T, °C	α (table 6-1)	K_T	K_{20} (cm/s)	K_{20} (cm/d)
1	53.0	14.8	99.03	193.56	22.0	0.9530	3.64E-03	3.47E-03	299.4
2	36.8	14.9	60.56	110.97	22.0	0.9530	4.21E-03	4.02E-03	347.0
3	35.8	21.2	33.40	73.98	22.0	0.9530	4.43E-03	4.22E-03	364.6
								3.90E-03	337.0

WP4

				gravimetric		
	M can (g)	M wet (g)	M dry (g)	w (%)	WP (Mpa)	h (cm)
FA	24.3	27.9232	27.6	8.93	-0.980	9993.2
FA	24.5	28.2906	27.9	12.54	-0.790	8055.8
FA	24.8	28.3866	27.9	15.73	-0.760	7749.8
FA	24.4631	28.3817	27.7323	19.86	-0.660	6730.1
FA	24.7461	28.7739	28.0306	22.63	-0.650	6628.2
FA	24.3984	28.9784	28.0685	24.79	-0.550	5608.4
FA	24.2426	28.6793	27.7147	27.78	-0.530	5404.5
FA	24.4648	29.0854	27.9604	32.18	-0.520	5302.5
FA	24.2594	30.6265	28.9306	36.31	-0.560	5710.4
FA	24.3981	28.8391	28.8021	0.84	-13.100	133582.8
FA	24.1643	27.8937	27.7872	2.94	-1.420	14480.0
FA	24.4527	27.9061	27.792	3.42	-1.470	14989.8
FA	24.2425	28.0677	27.8733	5.35	-1.050	10707.0
FA	24.3137	28.5504	28.2563	7.46	-0.780	7953.8
FA	24.736	28.5416	28.1479	11.54	-0.650	6628.2
FA	24.2596	28.3099	27.8203	13.75	-0.640	6526.2
FA	24.7576	29.0105	28.3759	17.54	-0.540	5506.5
FA	24.462	28.9818	28.2036	20.80	-0.470	4792.7
FA	24.5403	28.9257	28.0609	24.56	-0.450	4588.7

	M can (g)	M wet (g)	M dry (g)	w (%)	WP (Mpa)	h (cm)
BA	24.5	27.7266	27.6	3.00	-1.600	16315.5
BA	24.3	27.5792	27.4	4.20	-0.910	9279.4
BA	24.7	28.4523	28.2	6.05	-0.750	7647.9
BA	24.2428	27.5528	27.3397	6.88	-0.680	6934.1
BA	24.7575	28.4109	28.1002	9.29	-0.640	6526.2
BA	24.5409	28.0702	27.709	11.40	-0.790	8055.8
BA	24.3967	28.0535	27.664	11.92	-0.570	5812.4
BA	24.3112	28.1732	27.6696	15.00	-0.580	5914.4
BA	24.4532	28.2791	27.748	16.12	-0.560	5710.4
BA	24.1645	28.4999	27.8154	18.75	-0.490	4996.6

	M can (g)	M wet (g)	M dry (g)	w (%)	WP (Mpa)	h (cm)
top soil	24.5	28.1916	27.9	7.69	-0.700	7138.0
top soil	24.7	29.5738	29.3	6.40	-0.770	7851.8
top soil	24.8	29.4794	29.3	4.21	-1.750	17845.0

RH Box

					gravimetric	
	h(cm)	**FA lid (g)**	**FA w/lid (**	**FA dry (g)**	**Final (g)**	**w (%)**
NaCl	400983	5.885	17.0318	11.1468	17.067	0.316
LiCl	3053224	5.8851	17.0318	11.1467	17.0803	0.435

				gravimetric	
h(cm)	**BA lid (g)**	**BA w/lid (**	**BA dry (g)**	**Final (g)**	**w (%)**
400983	6.0326	15.0416	9.009	15.0813	0.441
3053224	6.0326	15.0416	9.009	15.0533	0.130

					gravimetric	
	h(cm)	**TS lid (g)**	**TS w/lid (g)**	**TS dry (g)**	**Final (g)**	**w (%)**
NaCl	400983	5.9929	12.7113	6.7184	12.8159	1.557
LiCl	3053224	5.9929	12.7113	6.7184	12.7484	0.552

Hanging Column & Pressure Plate

sample:	Fly Ash A		Fly Ash B		Fly Ash C	
metal ring (g)		92.8		91.3		93.7
metal ring + dry soil (g)		169.1		167.6		169.9
dry sample (g)		76.3		76.3		76.3
height (in)		1		1		1
diameter (in)		2.400		2.400		2.400
volume (in^3)		4.524		4.524		4.524
dry density (lb/ft^3)		64.2		64.2		64.2
porosity				0.486		
post testing density (mass/density)	169.22	1,030.8	167.92	1,033.1	170.38	1,034.7
		target	1028.4	kg/m^3		
	h (cm)	**mass (g)**	**h (cm)**	**mass (g)**	**h (cm)**	**mass (g)**
Hanging Column						
	5	208.1	4	209.3	7	211.3
	25	207.3	25	209.0	25	211.1
	50	206.5	50	208.4	50	210.6
	80	205.5	80	207.5	80	210.0
	115	204.6	115	206.2	115	209.1
	155	203.5	155	204.3	155	207.1
Pressure Plate						
	560	188.0	560	186.43	560	185.9
	1275	185.4	1275	185.9	1275	180.3
WP4						

Fly Ash D		Fly Ash E		Fly Ash F				Fly Ash G		Fly Ash H		Fly Ash I	
	90.0		94.6		91.6				93.8		91.1		95.8
	172.5		177.2		174.1				180.5		177.8		182.5
	82.5		82.5		82.5				86.7		86.7		86.7
	1		1		1				1		1		1
	2.400		2.400		2.400				2.400		2.400		2.400
	4.524		4.524		4.524				4.524		4.524		4.524
	69.5		69.5		69.5				73.0		73.0		73.0
			0.443								0.415		
172.23	1,109.7	176.74	1,107.7	174.55	1,118.8			180.67	1,172.2	178.10	1,173.4	182.93	1,175.2
		1113.3	kg/m^3							1169.3	kg/m^3		
h (cm)	**mass (g)**	**h (cm)**	**mass (g)**	**h (cm)**	**mass (g)**			**h (cm)**	**mass (g)**	**h (cm)**	**mass (g)**	**h (cm)**	**mass (g)**
0	211.5	0	215.39	5	217.65			5	217.1	5	214.3	5	221.1
12	211.0	12	213.9	25	216.33			25	215.9	25	212.5	25	219.3
55	209.2	55	212.07	50	215.18			50	215.1	50	211.9	50	218.4
100	207.6	100	211.36	80	214.2			80	214.5	80	211.5	80	217.8
160	206.4	160	210.55	115	212.99			115	214.2	115	211.3	115	217.3
				155	211.97			155	213.9	155	211.0	155	216.7
917.7	193.9	917.7	197.29	560	198.99			510	207.3	510	205.9	510	210.2
				1275	197.39			1275	205.4	1275	205.3	1275	208.7

sample:	Bottom Ash A		Bottom Ash B		Bottom Ash C			Bottom Ash D		Bottom Ash E		Bottom Ash F	
metal ring (g)		91.6		92.5		93.8			94.5		91.6		93.7
metal ring + dry soil (g)		145.5		146.4		147.7			153.9		151.0		153.1
dry soil (g)		53.9		53.9		53.9			59.4		59.4		59.4
height (in)		0.97		0.97		0.97			1		1		1
diameter (in)		2.400		2.400		2.400			2.400		2.400		2.400
volume (in^3)		4.388		4.388		4.388			4.524		4.524		4.524
dry density (lb/ft^3)		46.8		46.8		46.8			50.0		50.0		50.0
porosity				0.647							0.611		
	145.62	751.8	146.33	749.0	147.45	746.6		153.44	795.2	150.73	797.1	152.90	798.7
			727.2	kg/m^3						800.9	kg/m^3	797.0	
	h (cm)	**mass (g)**	**h (cm)**	**mass (g)**	**h (cm)**	**mass (g)**		**h (cm)**	**mass (g)**	**h (cm)**	**mass (g)**	**h (cm)**	**mass (g)**
Hanging Column													
	5	182.6	5	188.4	5	190.4		5	201.8	5	199.3	5	199.6
	25	177.6	25	179.0	25	179.7		25	186.9	25	194.3	25	185.8
	50	172.9	50	174.1	50	174.6		50	183.1	50	179.7	50	182.0
	80	169.1	80	170.1	80	170.7		80	179.4	80	175.9	80	178.1
	115	165.8	115	166.6	115	167.2		115	175.7	115	172.0	115	174.2
	155	162.9	155	163.5	155	164.5		155	172.4	155	169.0	155	171.0
Pressure Plate													
	510	154.5	510	155.6	510	156.5		510	163.6	510	160.4	510	162.5
	1275	152.0	1275	154.2	1275	155.7		1275	162.9	1275	158.0	1275	160.1

Bottom Ash G		Bottom Ash H		Bottom Ash I	
	94.0		91.6		93.8
	161.7		159.3		161.5
	67.7		67.7		67.7
	1		1		1
	2.400		2.400		2.400
	4.524		4.524		4.524
	57.0		57.0		57.0
			0.557		
161.66	912.3	159.32	913.5	161.80	916.8
		913.1	kg/m^3	914.2	
h (cm)	**mass (g)**	**h (cm)**	**mass (g)**	**h (cm)**	**mass (g)**
5	212.4	5	203.4	5	206.2
35	198.4	35	194.3	35	199.4
65	193.2	65	189.3	65	194.3
120	186.4	120	183.0	120	187.4
160	183.0	160	179.9	160	184.0
917.7	173.4	917.7	170.9	917.7	174.1

sample ID	Top Soil SJM YR1 01 01 T02	
metal ring (g)		97.5
metal ring + dry soil (g)		215.3
dry soil (g)		117.8
height (in)		1
diameter (in)		2.375
volume (in^3)		4.430
dry density (lb/ft^3)		101.3
	215.3	1622.6308
Hanging Column	**h (cm)**	**mass (g)**
11/5 12:53pm	9:30	11/5/2010
11/9 11:45am	5	245.4
11/12 9am	20	244.3
11/15 8:15am	40	242.3
11/17 9:40am	60	239.3
11/19 10:20am	80	236.5
11/22 8:15am	100	234.7
11/24 12:10pm	120	233.3
11/27 8:10am	140	232.2
11/29 8:40am	160	231.4
12/1 9:15am	180	230.8
12/7 8:30am	200	230.2
Pressure Plate		
	356.9	227.8
	1121.7	227.7

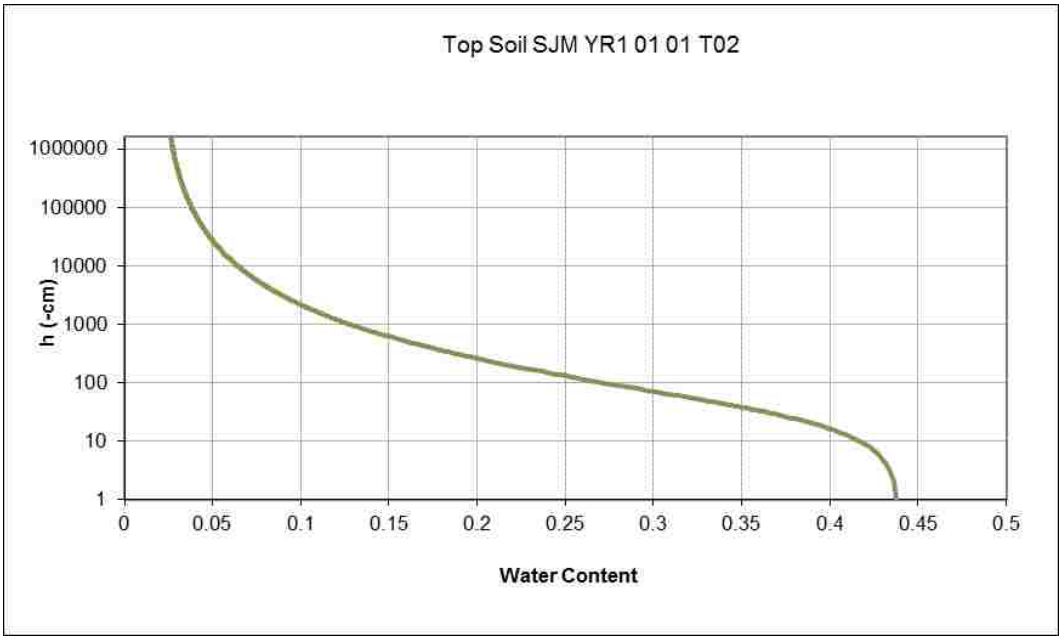

Correction Factors

Correction Factor A	Gs
0.96	2.85
0.97	2.80
0.98	2.75
0.99	2.70
1.00	2.65
1.01	2.60
1.02	2.55
1.04	2.50
1.05	2.45
1.07	2.40
1.08	2.35
1.10	2.30
1.12	2.25
1.13	2.20
1.15	2.15
1.17	2.10
1.19	2.05
1.22	2.00

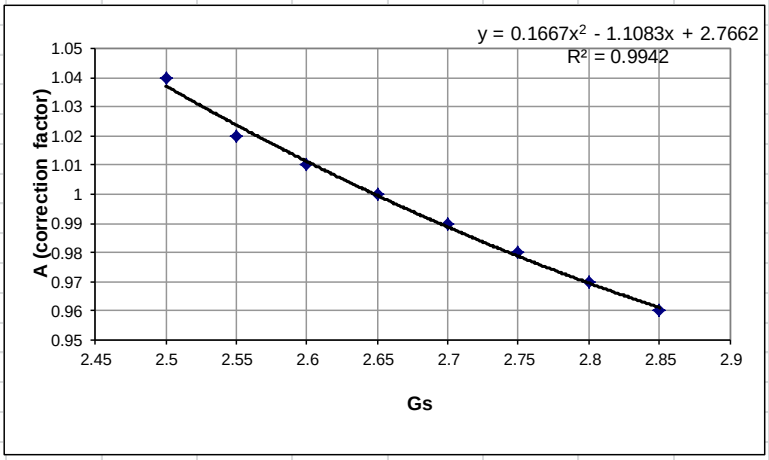

Table 6-4

Correction Factor K	Gs
0.0127	2.85
0.0129	2.80
0.0131	2.75
0.0133	2.70
0.0135	2.65
0.0137	2.60
0.0139	2.55
0.0141	2.50
0.0143	2.45
0.0145	2.40
0.0147	2.35
0.0149	2.30
0.0151	2.25
0.0153	2.20
0.0155	2.15
0.0157	2.10
0.0159	2.05
0.0161	2.00

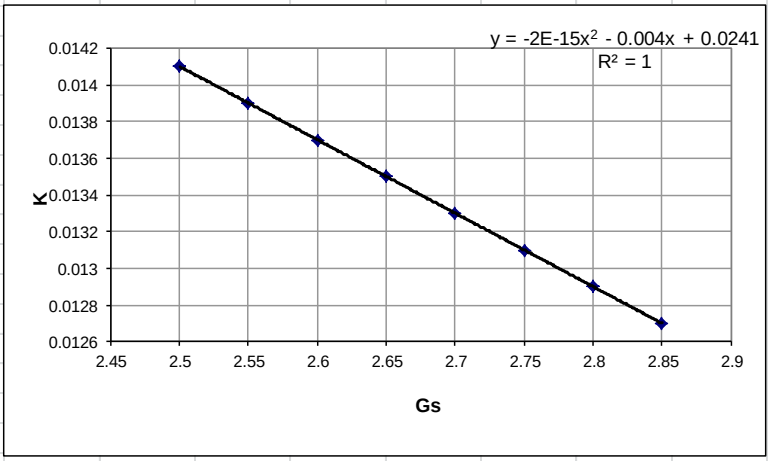

REFERENCES

ACAA. 2010.2010 CCP Production Use Survey. ACAA http://acaa.affiniscape.com/associations/8003/files/2010_CCP_Survey_FINAL_102011.pdf

Adrano, D.C., Page, A.L., Elseewi, A.A., Chang, A.C., and Straughan, I., 1980. "Utilization and Disposal of Fly Ash and Other Coal Residues in Terrestrial Ecosystems:A Review." *J. of Environ. Qual.* 9:333-344.

Assouline, S., Tavares-Filho, J., and Tessier, D., 1997. "Effect of Compaction on Soil Physical and Hydraulic Properties: Experimental Results and Modeling." *Soil Sci. Soc. Of American Jour. 61:390-398*

ASTM D2216, 2010, "Standard Test Method for Laboratory Determination of Water (Moisture) Content of Soil and Rock by Mass." Annual Book of ASTM Standard, Vol. 04.08, ASTM International, West Conshohocken, PA.

ASTM D5856, 2007, "Standard Test Method for Measurement of Hydraulic Conductivity of Porous Material Using a Rigid-Wall, Compaction-Mold Permeameter." Annual Book of ASTM Standard, Vol. 04.08, ASTM International, West Conshohocken, PA.

ASTM D7263, 2009, "Standard Test Method for Laboratory Determination of Density (unit Weight) of Soil Specimens." Annual Book of ASTM Standard, Vol. 04.09, ASTM International, West Conshohocken, PA.

ASTM D6836, 2008, "Standard Test Methods for Determination of the Soil Water Characteristic Curve for Desorption Using a Hanging Column, Pressure Head Extractor, Chilled Mirror Hygrometer, and/or Centrifuge," Annual Book of ASTM Standard, Vol. 04.09, ASTM International, West Conshohocken, PA.

ASTM D422, 2007, "Standard Test Method for Particle-Size Analysis of Soils," Annual Book of ASTM Standard, Vol. 04.08, ASTM International, West Conshohocken, PA.

ASTM D854, 2009, "Standard Test Method for Specific Gravity of Soil Solids by Water Pycnometer," Annual Book of ASTM Standard, Vol. 04.08, ASTM International, West Conshohocken, PA.

Campbell, D. J., Fox, W.E., Aitken, R.L, and Bell, L.C., 1983. “Physical Characteristics of Sands Amended with Fly Ash.” *Aut. J. Soil Res.* 21:147-154.

Chakrabarti, S., Mudd, G.M., Kodikara, J.K., 2005. “Coupled Atmospheric-Unsaturated Flow Modelling of Leached Ash Disposal in the Latrobe Valley, Australia.” *International Conference of Engineering for Waste Treatment.*

Chan, M., 2010. “Site Visit and Sample Test Results of San Juan Mine CCBs”. University of New Mexico

Decagon Devices, Inc. (2010). *Generating a Soil Moisture Characteristic Using the WP4C.* http://www.decagon.com/assets/Uploads/AN-Generating-a-Soil-Moisture-Characteristic-using-the-WP4C.pdf

Department of the Army Office of the Chief of Engineers. (1970). Engineering and Design: Laboratory Soils Testing. Washington, DC: U.S. Government Printing Office.

El-Mogazi, D., Lisk, D.J., and Weinstein, L.H., 1988. “A Review of Physical, Chemical, and Biological Properties of Fly Ash and Effects on Agricultural Ecosystems.” *Science of Total Environment* 74:1-37.

Ferraiolo, G., Zilli, M., and Converti, A., 1990. “Fly Ash Disposal and Utilization.” *J. of Chemical Technology and Biotechnology* 47:281-305.

Hill, J.N.A., and Sumner, M.E., 1967. “Effect of Bulk Density on Moisture Characteristics of Soils.” *Soil Sci.* 103:234-238.

Huang, C., Lu, C., and Tzeng, J., 1998. “Model of Leaching Behavior from Fly Ash Landfills with Different Age Refuses.” *J. of Environ. Eng.* August, 1998:767-775.

Joshi, R.C., Hettiaratchi, J.P.A., and Achari, G., 1994. “Properties of Modified Alberta Fly Ash in Relation to Utilization in Waste Management Applications.” *Canadian J. of Civ. Eng.* 21:419-426.

Kernodle, J.M., 1996. “Hydrogeology and Steady-State Simulation of Ground-Water Flow in the San Juan Basin, New Mexico, Colorado, Arizona, and Utah. USGS Water-Resources Investigations Report 95-4187

Kiteley, L.W., 1977. “Shallow Marine Deposits in the Upper Cretaceous Pierre Shale of the Northern Denver Basin and their Relation to Hydrocarbon

Accumulation." *Rocky Mountain Association of Geologists.* 1977 Sympsium,

Klute, A., 1986, "Physical and Mineralogical Methods, " *Methods of Soil Analysis*, 2nd ed., American Society of Agronomy, Inc., Madison, WI, Part 1.

Kumar, S., and Stewart, J., 2003. "Utilization of Illinois PCC Dry Bottom Ash for Compacted Landfill Barriers." *Soil and Sediment Contamination* 12:401-415.

Lu, N., and Likos, W., 2004. *Unsaturated Soil Mechanic*. Hoboken, NJ: John Wiley & Sons Inc.

Luther, J., Musslewhite, B., and Brown, C. The Relationship Between Water Quality and Coal Combustion By- Product Placement in an Arid Western Coal Mine. San Juan Coal Co.

Martin, J., Collins, R., Browning, J., and Biehl, T., 1990. "Properties and Use of Fly Ashes for Embankments." *J. of Energy Eng.* 116:71-86.

Miller, C., 2007. "What is FGD Gypsum?" http://www.google.com/url?sa=t&rct=j&q=&esrc=s&source=web&cd=3&ved=0CC4QFjAC&url=http%3A%2F%2Flibrary.acaa-usa.org%2F2-what_is_FGD_Gypsum.pdf&ei=G7UpT5qdF6qjiAKf5O3GCg&usg=AFQjCNHXJif1RaPPrVJTnaMaTKPQPYyvrQ&sig2=Nf_y9fFD2lplJ4LQEaoVCw

Mudd, G., and Kodikara, J., 2000. "Field Studies of the Leachability of Aged Brown Coal Ash." *J. of Hazardous Materials* 76:159-192.

New Mexico Mining and Minerals Division. 2009. Annual Evaluation Summary Report for the Regulatory Program Administered by the State of New Mexico for Evaluation Year 2009. Office of Surface Mining Reclamation and Enforcement..

New Mexico Mining and Minerals Division. 2011. Quarterly Ash Quanitity Report San Juan Coal Company: First Quarter 2011 and Third Quarter 2010 Office of Surface Mining Reclamation and Enforcement.

NMCC, 2011. New Mexico Climate Center Climate Data for Farmington Agricultural Science Center, 1992-2011. http://weather.nmsu.edu/data/data.html

Palmer, B., Edil, T., and Benson, C., 2000. "Liners for Waste Containment Constructed with Class F and C Fly Ashes." *J. of Hazardous Materials* 76:193-216.

Pathan, S., Aylmore, L., and Colmer, T., 2003. “Properties of Several Fly Ash Materials in Relation to Use as Soil Amendments.” *J. Environ. Qual.* 32:687-693.

Prashanth, J., Sivapullaiah, P., and Sridharan, A., 1998. “Compaction Curves on Volume Basis.” *Geotechnical Testing Journal* 21:58-65.

Prashanth, J., Sivapullaiah, P., Sridharan, A., 2001. “Pozzolanic Fly Ash as a Hydraulic Barrier in Land Fills.” *Eng. Geology* 60:245-252.

Richard, G., Cousin, I., Sillon, J., Bruand, A., and Guerif, J., 2001. “Effect of Compaction on the Porosity of Silty Soil: Influence on Unsaturated Hydraulic Properties.” *European Jour. of Soil Sci.* 52:49-58.

Scanlon, B., Keese, K., Flint, A., Flint, L., Gaye, C., Edmunds,W., and Simmers, I., 2006. “Global synthesis of groundwater recharge in semiarid and arid regions.” Hydrological Processes 20:3335-3370.

Steinwand, A., Harrington, R., and Groeneveld, D., 2001. “Transpiration coefficients for three Grat Basin shrubs.” *Journal of Arid Environments* 49:555-567.

Seals, R., Moulton, L., and Ruth, B., 1972. “Bottom Ash: An Engineering Material.” *J. of the Soil Mechanics and Foundations Div.* 98:311-325.

Simunek, J, M. Sejna, H. Saito, M. Sakai, and M. Th. Van Genuchten, 2008. The HYDRUS-1D software package for simulating the movement of water, heat, and multiple solutes in variably saturated media, Version 4.0. HYDRUS Softw. Ser. 3. Dep. Of Environ. Sci., Univ. of California, Riverside.

Sivapullaiah, P., and Lakshmikantha, H., 2004. “Properties of Fly Ash as Hydraulic Barrier.” *International J. of Geomechanics* 13:391-406.

Truman, C.C., R.C. Nuti, L.R. Truman, J.D. Dean, 2010. “Feasibility of Using FGD Gypsum to Conserve Water and Reduce Erosion from an Agricultural Soil in Georgia.” *Catena* 81:234-239

van Genuchten, M. T., 1980, “A Closed-Form Equation for Predicting the Hydraulic Conductivity of Unsaturated Soils,” *Soil Sci. Soc. Am. J.*, Vol. 44, pp. 892-898.

van Genuchten, M., and Leij, F., 1989. “Indirect Methods for Estimating the Hydraulic Properties of Unsaturated Soils” Proceedings of the International Workshop on Indirect Methods for Estimating Hydraulic

Properties of Unsaturated Soils. Riverside, California, October 11-13, 1989.

van Genuchten, M. T., Leji, F. J., and Yates, S. R., 1991, “The RETC Code for Quantifying the Hydraulic Functions of Unsaturated Soils,” *Report No.* EPA/600/2091/065, Robert S.Kerr Environmental Research Laboratory, Office of Research andDevelopment, U.S. Environmental Protection Agency, Ada, OK

Yeboah, N., and S. Burns, 2011. “Geological disposal of energy-related waste.” *KSCE Journal of Civil Engineering* 15 (4) (April 1): 697-705. doi:10.1007/s12205-011-0010-x.

Zeng, L., Hong, Z., Cai, Y., and Han, J., 2011. “Change of Hydraulic Conductivity During Compression of Undisturbed and Remolded Clays.” *Applied Clay Science* 51:86-93.